MAJORANA MEDIATED NON-LOCAL CHARGE DYNAMICS IN TOPOLOGICAL SUPERCONDUCTORS

Ian J. van Beek

A Thesis Submitted for the Degree of PhD
at the
University of St Andrews

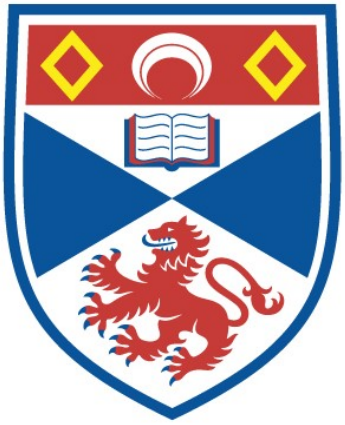

2019

Majorana Mediated Non-Local Charge Dynamics in Topological Superconductors

Ian J. van Beek

University of
St Andrews

This thesis is submitted in partial fulfilment for the degree of
Doctor of Philosophy (PhD)
at the University of St Andrews

June 2019

Candidate's declaration

I, Ian van Beek, do hereby certify that this thesis, submitted for the degree of PhD, which is approximately 22,500 words in length, has been written by me, and that it is the record of work carried out by me, or principally by myself in collaboration with others as acknowledged, and that it has not been submitted in any previous application for any degree.

I was admitted as a research student at the University of St Andrews in August 2014.

I received funding from an organisation or institution and have acknowledged the funder(s) in the full text of my thesis.

Date Signature of candidate

Supervisor's declaration

I, Bernd Braunecker, do hereby certify that the candidate has fulfilled the conditions of the Resolution and Regulations appropriate for the degree of PhD in the University of St Andrews and that the candidate is qualified to submit this thesis in application for that degree.

Date Signature of supervisor

Permission for publication

In submitting this thesis to the University of St Andrews we understand that we are giving permission for it to be made available for use in accordance with the regulations of the University Library for the time being in force, subject to any copyright vested in the work not being affected thereby. We also understand, unless exempt by an award of an embargo as requested below, that the title and the abstract will be published, and that a copy of the work may be made and supplied to any bona fide library or research worker, that this thesis will be electronically accessible for personal or research use and that the library has the right to migrate this thesis

into new electronic forms as required to ensure continued access to the thesis.

I, Ian van Beek, have obtained, or am in the process of obtaining, third-party copyright permissions that are required or have requested the appropriate embargo below. The following is an agreed request by candidate and supervisor regarding the publication of this thesis:

Printed copy

No embargo on print copy.

Electronic copy

No embargo on electronic copy.

Date Signature of candidate

Date Signature of supervisor

Underpinning Research Data or Digital Outputs

Candidate's declaration

I, Ian van Beek, hereby certify that no requirements to deposit original research data or digital outputs apply to this thesis and that, where appropriate, secondary data used have been referenced in the full text of my thesis.

Date Signature of candidate

Abstract

Topology has enjoyed great success as a paradigm for the classification and understanding of condensed matter outside the framework of spontaneously broken symmetry. This success is all the more remarkable considering that the impact of interactions, in particular the Coulomb interaction between electrons, has been neglected in most analyses. Experience in topologically trivial systems demonstrates that, beyond simply leading to quantitative modifications, interactions can give rise to qualitatively new physics in condensed matter. This thesis explores the interplay between interaction effects and topologically non-trivial states and demonstrates how this interplay can lead to novel physics which is fundamentally contingent upon both a system's topological character and interactions.

The prototypical example of a topological state in condensed matter is the Majorana bound state (MBS). In the work presented here, MBSs are significant because they lead to non-local fermionic states in superconductors that are bound to near-zero energy, inside the superconducting gap. The new physics arising from the synergy of MBSs and electron-electron interactions is illustrated by two examples. A Majorana-based analogue of the Kondo system is found to exhibit signs of a delocalised many-body state consisting of electrons from both metallic leads and a superconducting condensate. The presence of MBSs in a current driven capacitive Josephson junction enables excitation of the system to a non-equilibrium state and profoundly affects the overall charge dynamics of the junction.

This thesis offers compelling evidence for the importance of interactions in the context of topologically non-trivial systems, not only with regard to determining the topology of the system *per se*, but also as the means by which new physics is realised.

Acknowledgements

I must first thank Bernd for all the support and advice he has given me since the start of my time at St Andrews. His vision provided the initial impetus for my research and he has always been pleased to offer his input when it was required, whilst still allowing me to make the work my own. I am grateful to him for his patience with my shortcomings and enthusiasm for my successes. It was my honour to be his first PhD student (to start, if not to finish!) and I'm sure there will be many more.

Although too numerous to mention by name, I am also indebted to my friends and colleagues, both in St Andrews and further afield, for their camaraderie and insight, which made no small contribution to the eventual completion of this thesis. In particular, a dishonourable mention goes to my officemates in Room 120, without whom I would probably have had a more productive, but certainly less enjoyable, start to my PhD studies.

Science is a collaborative, international, effort and so I am pleased to acknowledge the hospitality of the physics department at Universidad Autónoma de Madrid, especially Alfredo Levy Yeyati, who hosted me during the sultry summer of 2017.

Beyond researchers themselves, scientific progress is contingent upon administrative and material backing from the wider community. For the former, I thank all the support staff in the St Andrews physics department, particularly those in the CM-CDT office who never failed to impress with their efficiency. For the latter, I am grateful to the British taxpayers whose insatiable appetite for knowledge led them to fund this work via EPSRC Grant No. EP/I007002/1.

I will finish by thanking my parents, without whom I would not be in this position today. This is true not only in the obvious material sense, but also because their help and encouragement over the course of my PhD studies, as well as the preceding twenty-two years, has had a profound influence on who I have become.

Contents

Chapter 1

Introduction

Perhaps the greatest achievement of Condensed Matter Physics in the Twentieth Century has been the classification of matter according to the principle of spontaneous symmetry breaking [1–3], which has proved to be a widely applicable paradigm that explains the existence of many different phenomena. Despite this success, it has long been apparent that symmetry alone does not constitute a complete description of the phases of condensed matter and that there exists physics beyond this scheme. Early indications that this might be the case were studies of the A-phase of ^{3}He [4–6] and the theoretical discovery of the Berezinskii–Kosterlitz–Thouless transition in the 1970s [7, 8], which were explained in terms of not only symmetry, but also *topology*. The experimental discovery, and theoretical explanation, of the Quantum Hall Effect in the 1980s [9–14] further emphasised the role that topology plays in determining the properties of condensed matter systems, but the rather special nature of these cases caused many to feel that, whilst important, topology was not of general significance in condensed matter. This attitude has had to be reconsidered with the growth in the study of topologically non-trivial systems over the last decade, as an increasingly wide variety of systems have been found to exhibit topological character and the theoretical understanding of topology in condensed matter has also improved significantly. The emergence of topological insulators [15–17], topological superconductors [18–21], Weyl semimetals [22–24] and other topologically non-trivial systems has been a source of great interest from both a physics and engineering perspective [25, 26]. By employing the idea of topology, it becomes possible to describe a wide variety of complex many-body quantum systems in a unified and systematic manner, thereby allowing us to make predictions about their physical properties on the basis of very general considerations.

A particularly prominent manifestation of topology in condensed matter systems is the Majorana bound state (MBS), or Majorana zero mode, as it is also known [27]. The MBS is based on the idea of a Majorana fermion, first proposed by Ettore Majorana in 1937 as a neutral solution to the Dirac equation [28, 29]. The defining feature of the Majorana fermion is often taken to be the Hermiticity of its corresponding operator [30],

$$\gamma\left(E,p\right)=\gamma^{\dagger}\left(-E,-p\right), \tag{1.1}$$

where E and p are the energy and momentum of the Majorana fermion, respectively. This relation demonstrates that the Majorana fermion is its own antiparticle, from which it immediately follows that it has no charge. Furthermore, Eq. (1.1) leads to the idea that a Dirac fermion, which corresponds to an electron or hole in the context of condensed matter, may be represented in terms of two Majorana fermions, with perhaps the most natural choice of normalization being,

$$d^{\dagger}=\frac{1}{\sqrt{2}}\left(\gamma_{1}-i\gamma_{2}\right), \quad d=\frac{1}{\sqrt{2}}\left(\gamma_{1}+i\gamma_{2}\right). \tag{1.2}$$

Note that, despite the charge neutrality of γ, a linear superposition of Majorana fermions can still have a charge and is therefore a suitable way in which to represent electrons and holes. One can, in principle, always choose to represent Dirac fermions in this manner, but under most circumstances such a representation is rather unhelpful as it does not reflect any underlying physical reality. However, as we shall see below, in some condensed matter systems, a description in terms of Majorana fermions has proven to be useful.

It is important to emphasise that the above discussion is concerned with *elementary* Majorana fermions, but the remainder of this thesis will consider Majorana fermions in condensed matter. Whilst superficially similar, in so much as Eq. (1.1) and Eq. (1.2) still apply, condensed matter Majorana fermions are a fundamentally many-body phenomenon, arising from the interplay of a number of electrons. A description of condensed matter systems in terms of Majorana fermions is useful if conditions are such that, with reference to Eq. (1.2), $\gamma_{1,2}$ are isolated and γ_1 is spatially separated from γ_2. It then follows from Eq. (1.2) that, taken together, the two Majorana fermions make up a single fermion state, that is delocalised over some finite region of space. If we now consider the consequences of imposing particle-hole symmetry on the system hosting the Majorana fermions, we see that, since $\gamma_{1,2}$ have an equal weighting of particle and hole components, they must be pinned to zero energy, i.e. the Fermi energy of the system. We refer to this special case of a Majorana fermion in condensed matter as a Majorana bound state, or Majorana zero

mode. It is these MBSs that have generated so much interest over the last decade, in large part due to their potential utility in the field of quantum computing [31]. This utility is a result of two properties of the MBS. Firstly, the delocalised nature of the electronic state corresponding to the MBSs means that computing operations which utilise the MBSs are resistant to local perturbations of electronic states by the environment [32]. Secondly, whilst we have not shown it here, it turns out that the MBSs obey non-Abelian exchange statistics [33], which increases the number of useful operations that can be carried out by exchanging MBSs [34], although the set of operations accessible by MBS exchange alone is not sufficient for universal computation and so must be supplemented by other operations [35]. Whilst the potential of MBSs in quantum computing applications is noteworthy, this is far from the only appeal that they hold for physicists. As we shall see over the course of this thesis, MBSs also offer the possibility of realising novel physics in condensed matter systems. The two essential properties of the MBSs described above, namely that they are pinned to zero energy and, when considered in pairs, constitute spatially delocalised single particle states, can interface with other phenomena to give rise to a variety of exotic effects.

There are several straightforward experimental signatures associated directly with MBSs themselves in condensed matter systems, most notably a zero bias peak in the conductance properties of these systems [36]. However, to explore how the presence of MBSs might give rise to qualitatively new physics, we shall go beyond the non-interacting paradigm that has been the basis for much of the work on MBSs up to now, and instead consider what impact interactions, in particular the Coulomb interaction between electrons, might have on the behaviour of condensed matter systems that host MBSs. An obvious source of inspiration for where to start searching for such new physics is provided by the interaction effects that were first investigated in topologically trivial condensed matter over fifty years ago and have proved to be a fruitful object of study ever since. It seems reasonable to believe that there will be a strong interplay between these interaction effects and MBSs since the MBSs are, ultimately, comprised of many electrons.

A good example of interactions qualitatively changing the behaviour of a system is the Anderson Impurity model [37] and associated Kondo effect [38] which, whilst in many ways conceptually simple, has played an important role in elucidating the role of interactions in condensed matter and the theoretical techniques required to understand the phenomena that they give rise to [39]. In general, the Kondo effect occurs as a result of a single, localised, spin-degenerate, fermionic state with a charg-

ing energy, interacting with a continuum of spinful fermions. The original example of such a scenario was a magnetic impurity in a metal [40], but since then much of the work around Kondo physics has considered a quantum dot in a mesoscopic system [41, 42], which is effectively equivalent to a magnetic impurity but is much more amenable to controlled experiment. This paradigm can be straightforwardly extended to incorporate MBSs. A pair of MBSs comprise a single fermionic state which is similar to the impurity state in a Kondo system, albeit not spin-degenerate and spatially delocalised. It therefore seems plausible, if not necessarily obvious, that a pair of MBSs, in an environment with a significant charging energy and able to couple to a fermionic continuum, will give rise to an effect that is somewhat analogous to the Kondo effect. We shall explore the nature of this effect and how it comes about in greater detail in Chapter 3, but a brief summary of the salient points is as follows. By carefully taking into account the tunnelling properties of MBSs, it is possible to write down the Hamiltonian for a one dimensional topological superconductor (TSC) hosting MBSs at its ends, which are in turn coupled to two separate metallic leads. From this Hamiltonian it is apparent that the system exhibits two distinct tunnelling processes, both of which are mediated by the MBSs, but only one of which entails a change in the number of Cooper pairs in the superconducting condensate. If a charging energy of the form $H_C = E_C \left(n - n_g\right)^2$ is also introduced, where n is the operator for the number of electrons on the TSC and n_g is a number corresponding to a gating voltage, then the effect is to split the Hilbert space of the system into sectors, separated by an energy of order E_C. Transitions between and within these energy sectors are facilitated by tunnelling between the metallic leads and TSC. This model is the Majorana analogue to the Anderson Impurity model and may be dealt with in a similar fashion. In particular, by applying a Schrieffer-Wolff transformation [43] the high energy sector can be reduced to an effective interaction. The resulting effective Hamiltonian is somewhat reminiscent of the Kondo Hamiltonian but with three significant differences. Firstly, the role of spin degeneracy in the Kondo model is taken over by "lead degeneracy" in the Majorana case, i.e. the fact that the isolated fermionic state is coupled to two different reservoirs, thanks to its delocalised nature, results in a degeneracy that is similar to the spin degeneracy in the Kondo case. Secondly, in contrast to the Kondo model, the effective Hamiltonian in the Majorana case cannot be written as a pure spin-spin interaction. Thirdly, and of crucial importance for the system's behaviour under renormalization, the non-local nature of the single particle state associated with the MBSs results in the spin-spin part of the effective Hamiltonian having "cross" terms of the form $s^y S^z$, where s and S are pseudospins corresponding to the leads and

MBSs, respectively. The combined effect of these three differences is to cause the Majorana version of the Anderson impurity model to behave very differently under renormalization and, instead of going to a strong or weak coupling limit, tend to an intermediate exchange coupling which is observable in the conductance properties of the system. The key point is that, whilst the system appears very similar to the scenarios which give rise to the Kondo effect, the unusual properties of the MBSs result in qualitatively different physics. Since this new physics has Kondo aspects but is dependent upon the Majorana bound states, it might concisely be referred to as *Kondorana* physics.

A further scenario which makes clear the importance of interactions in condensed matter, but has received relatively little attention compared to the Kondo effect is the case of a current biased capacitive Josephson junction. This system, which was first studied theoretically by Likharev and Zorin in 1985 [44], is interesting because interactions lead to the possibility of observing quantum phase coherence on a macroscopic scale. In contrast to the case of Kondo physics, MBSs may be added to this system, rather than substituted for one of its elements, to produce novel physics. In the case of the Josephson junction, the MBSs take on a somewhat more specialised role than in the previously described Kondo analogue, with their importance coming from the fact that they constitute a fermionic state that both exists within the superconducting gap, and is spatially delocalised. We shall see in Chapter 4 exactly what impact the presence of MBSs in this system has on its charge dynamics, but the essentials of the discussion are as follows. The capacitive Josephson junction exhibits charge dynamics which are $2e$ periodic, corresponding to tunnelling of Cooper pairs across the junction. The MBSs are, in part, significant because they enable single electrons to tunnel into and out of the junction, thereby permitting perturbations of the system that are non-periodic and which can therefore induce excitation or relaxation. The delocalised nature of the fermionic state associated with the MBSs is also important, in that it allows a current to be established transverse to the bias current across the Josephson junction. Taken together, these two attributes of the MBSs have the potential to greatly change the charge dynamics of the *Majorana-Josephson* device, and the experimental signatures associated with them, compared to a topologically trivial capacitive Josephson junction. The Majorana-Josephson device exhibits several different regimes, in both the static and time-varying bias current driving modes, which depend upon various system parameters and are a result of the presence of the MBSs in the system.

The work on Kondorana physics described in Chapter 3 has been published in Ref. [45], and the study of the Majorana-Josephson device described in Chapter 4 has been published in Ref. [46].

The overall message that the reader should take from this thesis is that topologically non-trivial systems, as well as being of great interest in their own right, can also play host to a variety of exciting new physics. This claim is substantiated by the two examples described above, which feature the interplay of Majorana bound states and interactions, but these cases are not unique and it seems likely that a wide variety of other phenomena will emerge in the future.

Chapter 2

Literature Review

The description and understanding of condensed matter systems in terms of topology is not new, but in the past decade this field has witnessed rapid progress with respect to both the diversity of systems recognised to be topologically non-trivial, and also our understanding of the precise role that topology plays and how best to study it. Nevertheless, much work still remains to be done, in particular in relation to how topological systems are influenced by interaction effects and many-body physics. Whilst a fair amount of research has been carried out to determine how interactions can impact the topological classification of a system [47–51], there has been comparatively little interest in the novel physics that might arise from the interplay of topological states and many-body physics and it is this subject that will be the focus of this thesis. Of the many different manifestations of non-trivial topology, perhaps one of the most promising candidates for realising new physics is the Majorana bound state, on account of the fact that it is amenable to a simple theoretical treatment, can be achieved relatively easily in experiments, and yet still embodies distinctly topological characteristics. Before we embark upon an investigation of this topic, it is worth briefly discussing the nature and origin of Majoranas, as well as providing a more detailed description of the topologically trivial many-body effects that we will be taking as the basis for new Majorana-mediated physics. In particular, we consider Kondo physics and macroscopic quantum phenomena in capacitive Josephson junctions.

2.1 Majorana Bound States

Over eighty years ago it was shown that the Dirac equation admits real solutions consisting of two particles, each of which is its own antiparticle [28, 29]. There has long been interest in these solutions, so-called *Majorana fermions*, as candidates for

the neutrino, but to date there remains no confirmed case of a fundamental particle which is a Majorana fermion. In condensed matter, essentially the only fundamental particles are electrons, but from this homogeneous starting point a remarkably rich variety of phenomena can emerge. It is the case of Majorana fermions as *emergent* quasiparticles, based on many-body electron correlations, that we study in this thesis.

2.1.1 Properties of Majoranas

The Majorana fermion is, in essence, a very simple state, defined by the condition,

$$\gamma = \gamma^\dagger, \tag{2.1}$$

where, for clarity, we suppress energy and momentum labels which do not influence our discussion. As their name suggests, Majorana fermions also obey the fermionic commutation relation,

$$\gamma_n \gamma_m + \gamma_m \gamma_n = \delta_{n,m}. \tag{2.2}$$

It follows that Majorana fermions may be written as a superposition of electron and hole operators,

$$\gamma_1 = \frac{1}{\sqrt{2}}\left(d + d^\dagger\right), \quad \gamma_2 = \frac{i}{\sqrt{2}}\left(d^\dagger - d\right), \tag{2.3}$$

which obey the standard commutation relation $\left\{d, d^\dagger\right\} = 1$. Any system of electrons and holes may be written in terms of Majorana fermions, but Eq. (2.3) suggests that, for the γ operators to have any physical meaning, the system must be capable of supporting a superposition of particles and holes. The most prominent example of such a system is a superconductor, in which Bogoliubov quasiparticles bear a striking resemblance to the Majorana fermions of Eq. (2.3). Equivalently, we can see that $\gamma_{1,2}$ are only meaningful operators when acting on a state that consists of a superposition of different particle number-states, which again is the case for a superconductor in the Bardeen-Cooper-Schrieffer (BCS) model. This insight offers our first clue as to where we might hope to find Majorana fermions in condensed matter. Unfortunately, the Bogoliubov quasiparticles of the BCS model are a result of s-wave paired electrons with opposite spins, such that their operators are of the form [52],

$$b = u d_\uparrow^\dagger + v d_\downarrow, \tag{2.4}$$

and so we immediately see that $b \neq b^\dagger$ due to the presence of spin. Hence, we conclude that Majorana fermions will be observable only in a superconductor that lacks spin-degeneracy which, by the Pauli exclusion principle, must therefore have an odd orbital pairing between electrons [4], of which the most prominent example

is p-wave pairing. Some of these p-wave superconductors are known to have a non-trivial topology and therefore will exhibit topological defects and boundary states corresponding to the topology of the bulk. If a Majorana fermion is bound to one of these defects, and by extension zero energy, then it is referred to as a Majorana bound state or Majorana zero mode. It is these MBSs that have excited so much interest, in large part due to their associated non-Abelian exchange statistics, which are attributed to the Ising anyon that results from binding a Majorana fermion to a topological defect [25]. Although we do not exploit these exchange statistics through braiding in this thesis, we shall see that the non-locality of the electron and hole states associated with the MBS can have profound consequences.

Having established the essential conditions for a Majorana bound state to arise, we now turn to how such conditions can be achieved in condensed matter systems.

2.1.2 The Creation of Majorana Bound States

Many systems have been proposed as theatres for the observation of MBSs. The reason for this diversity is that the conditions required to create MBSs are, in principle, rather generic, which is perhaps unsurprising given their simplicity. The above comments on their nature make clear that superconducting pairing is intimately associated with MBSs. In addition, it is expedient to remove degeneracies by breaking both spin and time-reversal symmetries. We anticipate that a pair, or more generally even number, of MBSs bound to topological defects will be present when these conditions are satisfied. In terms of topology, the MBSs may be thought of as the boundary states corresponding to the topologically non-trivial bulk of a system with Altland-Zirnbauer symmetry class D [53], but this idea is inessential to our discussion. Below, we provide a brief outline of two of the systems in which MBSs are thought to be present.

P-Wave Superconductors and Superfluids The earliest proposals for the creation of MBSs suggested using the bound states associated with vortices in superconductors or superfluids. For s-wave superconductors, it has long been known that these bound states are fermionic and have an energy given by [54],

$$E_n = \left(n + \frac{1}{2}\right)\hbar\omega, \quad n = 0, 1, 2, ..., \tag{2.5}$$

for which the level spacing is small compared to the superconducting gap, Δ, since $\hbar\omega \sim \Delta^2/E_F$, with E_F the Fermi energy. However, extending the microscopic theory of Kopnin and Salomaa [55], Volovik showed [56] that the energy of the vortex bound

states in a p-wave superconductor or superfluid is,

$$E_n = n\hbar\omega. \tag{2.6}$$

From our previous discussion, we identify the $n = 0$ bound state of the vortex as a MBS. These states were explicitly found to be non-Abelian by Read and Green [57] and Ivanov [33]. Unfortunately, p-wave superconductors and superfluids are, to say the least, something of a rarity with ^{3}He-A being the only confirmed example, although Sr_2RuO_4 [58] and UPt_3 [59] are also strong, if controversial [60], candidates. Even in these systems, the superconductivity is easily destroyed by disorder. For these reasons, it seems unlikely that observing MBSs in p-wave superconductors or superfluids will be possible in practice and so we consider alternative experimental implementations.

Quantum Wires The quantum wire is a well known geometry amongst semiconductor physicists and offers a real world realisation of a one dimensional system. To understand in detail how such a system might host MBSs, we begin by looking at a toy model suggested by Alexei Kitaev in 2001 [18] and shown in Fig. 2.1.

Consider spinless fermions, on a one dimensional lattice with N sites, having the Hamiltonian,

$$H = \sum_j \left\{ -t\left(c_j^\dagger c_{j+1} + h.c.\right) - \mu\left(c_j^\dagger c_j - \frac{1}{2}\right) + \Delta\left(c_j^\dagger c_{j+1}^\dagger + h.c.\right) \right\}, \tag{2.7}$$

where j is an index running over the lattice sites, c_j are spinless fermion operators, t is the hopping integral, μ is the chemical potential and Δ is the superconducting gap. Notice that this situation already has the ingredients previously determined to be necessary for MBSs. Namely, superconductivity and manifest lack of spin degeneracy, since the fermions are spinless. Decomposing the ordinary fermionic operators in to pairs of Majorana operators, γ_1 and γ_2, as in Eq. (1.2), the Hamiltonian becomes,

$$H = i\sum_j \left\{ -\mu\gamma_{j,1}\gamma_{j,2} + (\Delta + t)\,\gamma_{j,2}\gamma_{j+1,1} + (\Delta - t)\,\gamma_{j,1}\gamma_{j+1,2} \right\}. \tag{2.8}$$

It is instructive to consider two sets of parameters. Firstly, the case $t = \Delta = 0$ which results in a Hamiltonian,

$$H = -\mu\sum_j \left(c_j^\dagger c_j - \frac{1}{2}\right). \tag{2.9}$$

We see that all sites are occupied (empty) for $\mu > 0$ ($\mu < 0$) and this is clearly a topologically trivial phase. On the other hand, for the case $\mu = 0, t = \Delta$, the

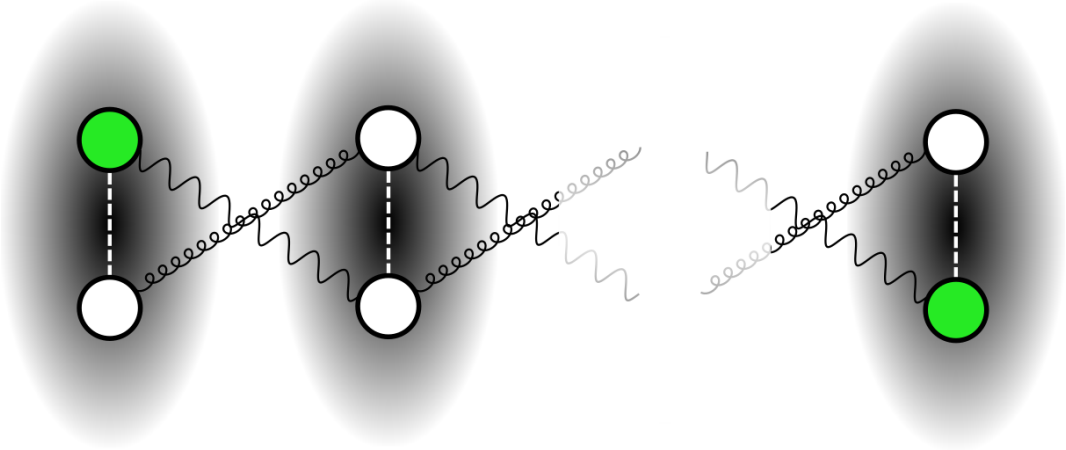

Figure 2.1: Cartoon of the Kitaev chain, with two ends and one intermediate site shown. Large ellipses represent fermionic states each of which consists of two Majorana states represented by circles. With reference to Eq. (2.8), dashed lines correspond to the chemical potential, μ, whilst wavy and curly curves represent the couplings $(\Delta - t)$ and $(\Delta + t)$, respectively. For the case $\Delta = t$ and $\mu = 0$, the two Majorana states in green are unpaired, and together comprise a zero-energy fermionic state.

Hamiltonian becomes,

$$H = 2it \sum_{j=1}^{N-1} \gamma_{j,2}\gamma_{j+1,1}. \tag{2.10}$$

We now pair up the Majorana fermion operators on adjacent sites to write this Hamiltonian in terms of the auxiliary fermion operator, $d_j = (\gamma_{j,2} + i\gamma_{j+1,1})$ which gives the result,

$$H = t \sum_{j=1}^{N-1} \left(d_j^\dagger d_j - 2 \right). \tag{2.11}$$

Remarkably, (2.10) does not include the two Majorana fermions $\gamma_{1,1}$ and $\gamma_{N,2}$ and similarly (2.11) does not include the ordinary fermion d_N which is formed from them. Thus, the "Kitaev Chain" hosts two Majorana fermions with zero energy, i.e. Majorana bound states. Furthermore, we see that the MBSs, $\gamma_{1,1}$ and $\gamma_{N,2}$, are located on opposite ends of the wire, meaning that their corresponding auxiliary fermion d_N is highly non-local in nature. In terms of topology, we can think of the system undergoing a topological phase transition from the trivial state with Hamiltonian (2.9) to the non-trivial state with Hamiltonian (2.10), as the system parameters are tuned from the point $t = \Delta = 0$ to the point $\mu = 0, t = \Delta$. The emergence of the MBSs at the boundary of the system as the topology of the bulk changes is a clear example of the so-called bulk-boundary correspondence. It is a historical curiosity that an essentially identical result, including the existence of zero energy modes, was found forty years earlier by Elliott Lieb and co-workers in the

context of a one dimensional XY spin chain [61].

The above model is appealingly simple, but its relevance to real systems is rather dubious. Therefore, to understand how MBSs might be created in practice, we change tack slightly and turn to a more heuristic argument.

In 1939, William Shockley's theoretical study of electrons in finite crystals, revealed the existence of distinct surface states [62]. These Shockley states exist at energies "forbidden" by the bare band structure, and were shown to arise due to a crossing of energy bands, or what one might think of as a closing and reopening of the band gap. In reality, these states have proven very difficult to observe since they can easily be pushed out of the band gap by local perturbations. However, if Shockley states were to occur in a superconductor at $E = 0$, then particle-hole symmetry would constrain them to $E = 0$ in spite of perturbations. We conclude, admittedly without giving a rigorous justification here, that these superconducting Shockley states are none other than Majorana bound states. This connection, which offers a pleasingly intuitive way of thinking about MBSs, was first pointed out by Wimmer et al. in 2010 [63].

The question which we are now inclined to ask is how one might achieve the closing and reopening of the superconducting energy gap. The first process is straightforward: a sufficiently large applied magnetic field will cause the superconducting gap to close. The reopening of the gap is more difficult, but one possible method of achieving this is through a Rashba spin-orbit coupling which cancels out the applied magnetic field. Two studies in particular [64, 65] demonstrated the specifics of how such a scheme might be realised in a quantum wire. We will now briefly discuss the key points of their arguments.

We begin by considering a one dimensional semiconductor, with chemical potential $\mu(y)$, aligned along the y axis, with a strong spin-orbit coupling of magnitude u in the z direction. Examples of suitable semiconductors include InAs and InSb. Let this be in proximity to an s-wave superconductor with order parameter Δ, such that superconductivity is induced in the semiconductor. Imagine, also, that a magnetic field B is applied in the x direction. The corresponding Hamiltonian is [64, 65],

$$\begin{aligned} H &= \int \Psi^\dagger(y)\mathcal{H}\Psi(y)\mathrm{d}y, \qquad \Psi^\dagger = \left(\psi_\uparrow^\dagger, \psi_\downarrow^\dagger, \psi_\downarrow, -\psi_\uparrow\right) \\ \mathcal{H} &= \left(\frac{p^2}{2m} - \mu(y)\right)\tau_z + pu\sigma_z\tau_z + B(y)\sigma_x + \Delta_{\text{eff}}(y)\tau_x, \end{aligned} \tag{2.12}$$

where $\psi^\dagger$ are electron creation operators, Δ_{eff} is the effective superconducting gap, σ_i are the Pauli Matrices in spin space and τ_i are the Pauli Matrices in Nambu

space. Assuming spatially constant parameters, we can simply square $\mathcal{H}$ to find the energies of the eigenstates,

$$E_{\pm}^2 = B^2 + \Delta^2 + \xi_p^2 + (pu)^2 \pm \sqrt{B^2\Delta^2 + B^2\xi_p^2 + \xi_p^2(pu)^2}, \tag{2.13}$$

where we have defined $\xi_p = p^2/(2m) - \mu$. Considering E_- at the $p = 0$ point, we see that the energy gap is given by,

$$E_g = 2\left|B - \sqrt{\Delta^2 + \mu^2}\right| \tag{2.14}$$

The gap can therefore be closed and reopened by varying the parameters B, Δ and μ. Of these three, μ will most likely be the easiest to control on short length scales in experiments, since it can be manipulated directly using gate voltages. We note in passing that, whilst Eq. (2.14) contains no reference to u, the spin-orbit coupling is still essential to observe the topological transition described here. Having established what Majorana bound states are, and how they might be generated, we next conduct a brief survey of experimental efforts to probe their existence.

2.1.3 The Observation of Majorana Bound States

The quantum wire scheme is significantly more experimentally accessible than other proposals, and so thus far has attracted by far the most experimental interest. In all cases, experiments have relied on transport measurements to probe the existence of the MBSs. If the superconducting gap is sufficiently large, then tunnelling into the bulk states of the wire is greatly inhibited. But, if MBSs are present within the gap, then these allow tunnelling by contributing a term of the form [36, 66],

$$H_T = \sum_{k,\sigma,j} t_{j,k,\sigma} c_{j,k,\sigma} \gamma_j + h.c., \tag{2.15}$$

to the system Hamiltonian, where $t_{j,k,\sigma}$ is a tunnelling coefficient, j is the lead index and $c_{j,k,\sigma}$ are lead electron annihilation operators. A detailed analysis shows that this results in a conductance of $G_{MBS} = \frac{2e^2}{h}$ [36]. Although there will also be a contribution due to Andreev reflection, this is proportional to $(e^2/h)\left(\frac{\Gamma}{\Delta}\right)^2$ [67], where Γ is the tunnelling broadening and so in the large Δ limit the MBS mediated conductance dominates. On the basis of this result, the experimental signature of the MBS was thought to be a so-called *zero bias peak* in the conductance of the system. There was therefore great interest when this was reported by several groups studying semiconductor nanowires in 2012 and 2013 [21, 68–70], with representative results shown in Fig. 2.2. In the interests of completeness, we note that other experiments have used a chain of Fe atoms deposited on the surface of a Pb superconductor [71–73]. There is evidence [74] that Pb has significant intrinsic spin-orbit

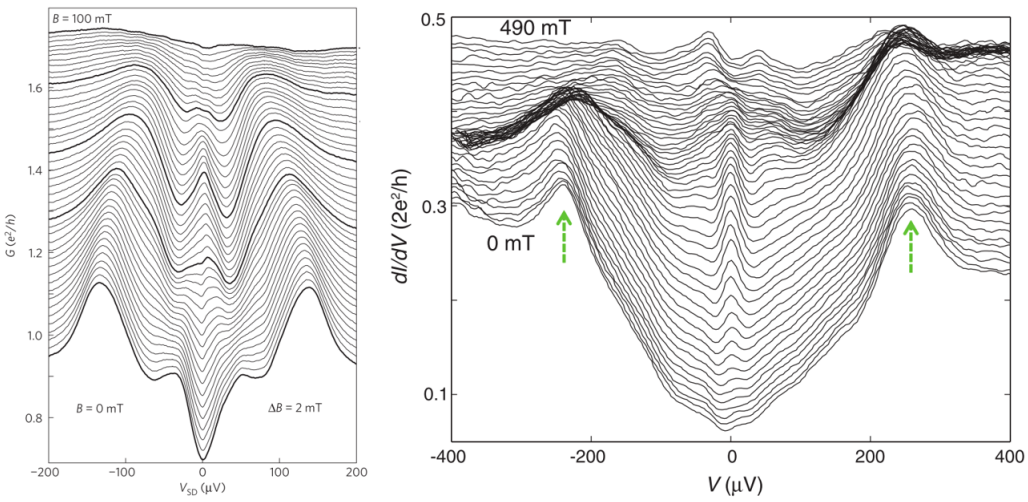

Figure 2.2: Typical zero bias conduction peaks observed in measurements on topologically superconducting quantum wires. Traces are offset for clarity. Adapted from Ref. [68] (left) and [21] (right), reprinted with permission from Springer Nature and AAAS.

coupling which, in concert with its superconductivity and the helical ordering of the Fe magnetic moments [75, 76] recreates the essential elements of the semiconductor implementation discussed above. The advantage of the Fe chain approach is that it more easily allows spatial probing of the system using a Scanning Tunnelling Microscope tip. Using this method, it was claimed that MBSs were observed at the ends of the chain. However, there was some scepticism surrounding this claim due to the ferromagnetic coupling of the Fe atoms compromising the superconductivity of the Pb in its vicinity, rendering any zero bias peak indistinct and potentially resulting in strong Majorana hybridisation [77]. The latter of these issues may be nullified by an unusual renormalization of the superconducting coherence length [78], but measurements at lower temperatures are still desirable to come to a more definitive conclusion as to the presence of MBSs in this system [79]. Nonetheless, it is still possible that similar set-ups will provide a useful theatre in which to perform experiments with MBSs in the future.

Soon after results indicating the presence of a zero bias conductance peak were released, it was quickly pointed out that several other effects could also give a very similar signal. For example, it has been shown that weak antilocalization due to the superconductor's particle-hole symmetry can contribute a conductance $\frac{e^2}{h}$, even in the topologically trivial case [80]. Similarly, it has been suggested [70] that the observed signals might be due to a Kondo Resonance [81–83]. Typically, one would expect this effect to be suppressed provided Δ is much larger than the Kondo Temperature. However, the "soft" gap present in early experiments [84] has

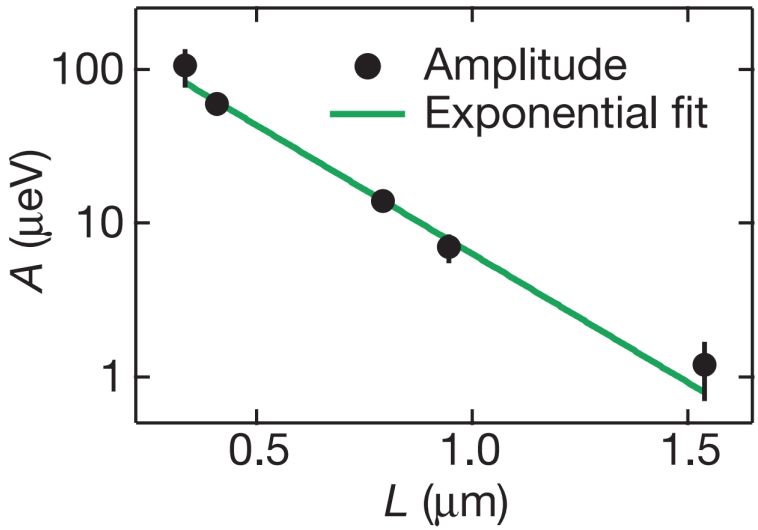

Figure 2.3: Plot of Majorana bound state hybridisation energy as a function of MBS separation in quantum wires. Five devices (black points) with different lengths, L, were measured. The green line is the theoretical prediction given by Eq. 2.16 with $\xi_{\text{eff}} = 260\text{nm}$. Adapted from Ref. [86], reprinted with permission from Springer Nature.

been shown to provide a sufficient density of quasiparticle states to enable a Kondo Resonance [85].

In light of the alternative explanations offered above, it is apparent that a zero-bias conductance peak does not represent an absolute proof of the presence of MBSs. These initial experiments were therefore followed by further attempts to produce still more evidence for the existence of MBSs. Amongst these, perhaps the most convincing was an experiment performed by Albrecht et al. in 2016 which probed not only the energy of the MBSs, i.e. the fact that they exist at $E = 0$, but also their exponentially localised spatial characteristics [86]. This work relied on the fact that two MBSs spatially separated by some distance, L, have an overlap energy given by,

$$E_\gamma \propto \exp\left(-\frac{L}{\xi_{\text{eff}}}\right), \tag{2.16}$$

where $\xi_{\text{eff}} = \hbar v_{\text{F}}/\pi\Delta_{\text{eff}}$ is the effective coherence length [18, 87]. It is possible to measure E_γ by using a quantum wire with a charging energy and measuring the linear conductance of the wire as a function of its gate voltage. By carrying out this measurement on multiple wires with different lengths, Albrecht et al. were able to experimentally test the relation (2.16). Their results are shown in Fig. 2.3 and offer compelling evidence for the existence of exponentially localised states at the ends of the quantum wires, which it is reasonable to identify as Majorana bound states.

The work of Albrecht at al. [86] constituted convincing evidence for the existence of MBSs in quantum wires [88], and also highlighted the significance of interactions. In this instance, the interactions were an experimentally useful tool, but as we will

see over the course of the next few chapters, they can also allow a topologically non-trivial system to host qualitatively distinct physics.

2.1.4 Beyond Majoranas: Parafermions

We might imagine that Majorana fermions are a special case of a more general class of excitations whose operators, α obey the relations,

$$\begin{aligned} \alpha^n &= 1, \\ \alpha_1\alpha_2 &= \alpha_2\alpha_1 \exp\left(\frac{2\pi i}{n}\right), \end{aligned} \tag{2.17}$$

where n is an integer greater than 1 and the Majorana relations, up to some normalisation, are recovered for the case $n = 2$. It turns out that such excitations emerge as non-local mappings of "clock models" with $\mathbb{Z}_n$ symmetry [89], which constitute a natural extension of the $\mathbb{Z}_2$ symmetric XY Spin chain and its associated Majorana fermions [18, 61]. On the basis that these excitations are many-body phenomena arising from fermionic systems, but do not themselves exhibit fermionic statistics, they have been dubbed *parafermions*. Just as Majorana fermions exhibit a two-fold degeneracy, so too do parafermions exhibit an n-fold degeneracy.

In contrast to Majorana fermions, which can naturally be thought of as a superposition of electron and hole states, it is not immediately clear if there is any prospect of observing parafermions, as they are contingent upon fractionalised charges, which do not appear as elementary particles in condensed matter. Fortunately, quasiparticles with the necessary properties can be found in strongly correlated systems. In particular, it has been suggested [90–92] that several systems based on the Fractional Quantum Hall State could support parafermions and, remarkably, even a system without explicit fractionalisation has been proposed has a potential host [93,94]. Having said this, there is currently no known experimental confirmation of parafermions with $n > 2$.

Much of the interest surrounding parafermions has been in relation to their potential applications in quantum computing, specifically the superior topological protection and more complete set of computational operations that they enable compared to Majorana fermions [95]. However, in keeping with the theme of this thesis, we imagine that a union of parafermions and other many-body effects might give rise to exciting new physics, although these are beyond the scope of our discussion here.

2.2 Kondo Physics

A subject of great importance within condensed matter physics is the role played by the interaction of many electrons over an extended region. These so-called Many-Body effects give rise to striking new observable phenomena, that cannot be explained in terms of a single particle model. It seems reasonable to speculate that, since these many-body phenomena play such a prominent role in topologically trivial systems, they may also give rise to novel effects in topologically non-trivial systems. Perhaps one of the most well studied and influential of all the systems in which many-body physics plays a decisive role is that associated with the Kondo effect. The generality and prototypical simplicity of this system suggests that it is a promising subject for a first investigation into the interplay of many-body physics and topology. With this in mind, we undertake a brief overview of the topologically non-trivial physics, so that we might stand better equipped to address its topological analogue.

2.2.1 The Kondo Effect

Study of Kondo physics began in 1934 when measurements on low purity gold wires revealed a resistance minimum at low temperatures [40]. In particular, it was later established that the resistivity exhibits a dependence on temperature of the form $\rho \propto -\ln(T)$ [96]. Furthermore, experiments found that, below some threshold temperature, T_K, the logarithmic dependence of the resistivity disappears [97]. These results for the electrical properties were complemented by magnetic studies which revealed that, whilst the samples exhibited a magnetic susceptibility $\propto 1/T$ at temperatures greater than T_K, in accordance with the Curie Law for free magnetic moments, at temperatures below T_K the magnetic susceptibility tends to a constant, indicating that the magnetic impurities are in a spin singlet state [98]. These results were wholly unexpected at the time and remained unexplained for thirty years, with existing theories predicting only a monotonically decreasing resistivity with decreasing temperature and a consistent $1/T$ dependence of the magnetic susceptibility. It was not until the 1960s that research began to shed light on the underlying mechanism of these effects, when it was recognised that they are contingent upon the presence of magnetic impurities in the otherwise non-magnetic metallic samples [99]. Shortly after this realisation, Jun Kondo was able to show, using a minimal model, how these magnetic impurities could give rise to a resistivity with a logarithmic temperature dependence [38]. Subsequently, this toy model has been reproduced experimentally through the use of quantum dots, which allow a di-

rect investigation of Kondo physics without the complications inherent in magnetic impurity systems [41, 42].

2.2.2 The Anderson-Kondo Model

Kondo considered a simple Hamiltonian modelling the interaction between a single magnetic impurity and a sea of itinerant conduction electrons [38],

$$H_K = \sum_k \epsilon_k c_k^\dagger c_k + J \sum_{k',k''} \left[S_d^z \left(c_{k'\uparrow}^\dagger c_{k''\uparrow} - c_{k'\downarrow}^\dagger c_{k''\downarrow} \right) + S_d^+ c_{k'\downarrow}^\dagger c_{k''\uparrow} + S_d^- c_{k'\uparrow}^\dagger c_{k''\downarrow} \right], \tag{2.18}$$

where c_k are the itinerant electron operators, ϵ_k is their dispersion, $S_d^{z,+,-}$ are the impurity spin components and J is the Kondo coupling. The sign of J depends upon the sign of the on-site energy of the magnetic impurity and the magnitude of this energy relative to the Coulomb interaction between electrons on the impurity, but for typical systems $J > 0$. The electron scattering, and hence resistivity, corresponding to this Hamiltonian can be found by summing the various different scattering processes. Here, we outline the process in sufficient depth to understand the pertinent physics, without going into all of the various technical details. This exposition will provide the necessary background to contextualise the work described in Chapter 3.

We begin by noting that first order estimates of the scattering rate are independent of the temperature of the system, T, which is at odds with the experimentally observed $\ln(T)$ dependence. At progressively higher orders, the scattering rate will decrease by a factor of J and so we might naively expect such higher order processes to have no qualitative effect on the scattering. Nonetheless, let us calculate their influence explicitly, looking in particular at the process in which an electron is scattered into an intermediate state with a flipped spin and then this intermediate state is in turn scattered to a final state with the same spin as the original electron. This path consists of two coherent processes, shown in Fig. 2.4, and it is the superposition of these two processes that yields the overall amplitude. Considering, first the process with a particle-like intermediate state, the amplitude for this is given by,

$$T_{k,\sigma\to k',\sigma}^{(2)p} = J^2 \left| \langle s, m_s + 1 | \, S_d^+ \, | s, m_s \rangle \right|^2 \alpha = J^2 \left(s(s+1) - m_s(m_s+1) \right) \alpha, \tag{2.19}$$

where,

$$\alpha = \sum_q \frac{1 - f_q}{\epsilon_k - \epsilon_q + i\eta}, \tag{2.20}$$

is a factor that takes into account the requirement that the intermediate state be unoccupied prior to the scattering event. Similarly, if the intermediate state is

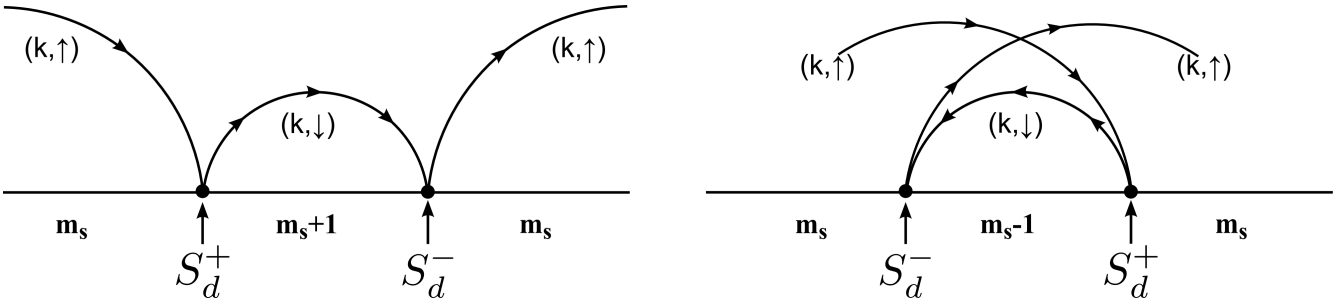

Figure 2.4: Representation of the particle (left) and hole (right) mediated channels contributing to the scattering amplitude $T^{(2)}_{k,\sigma\to k',\sigma}$. The upper line with arrows denotes an itinerant conduction electron, whilst the straight lower line corresponds to the magnetic impurity with spin S. Based on the approach described in Ref. [100].

hole-like, then we find the scattering amplitude,

$$T^{(2)h}_{k,\sigma\to k',\sigma} = J^2 \left|\langle s, m_s - 1| \, S^-_d \, |s, m_s\rangle\right|^2 \beta = J^2 \left(s(s+1) - m_s(m_s-1)\right)\beta, \tag{2.21}$$

where,

$$\beta = -\sum_q \frac{f_q}{\epsilon_q - \epsilon_k + i\eta}, \tag{2.22}$$

is a factor accounting for the requirement that the intermediate state be occupied prior to scattering. Computing the sum of (2.19) and (2.21) gives the overall scattering amplitude,

$$T^{(2)}_{k,\sigma\to k',\sigma} = J^2 \left((s(s+1) - m_s(m_s+1))(\alpha+\beta) + 2m_s\beta\right). \tag{2.23}$$

Examining (2.23), we note that the factors of f_q in $(\alpha+\beta)$ cancel and so the only term with any temperature dependence is that proportional to $2m_s\beta$. We therefore make the approximation,

$$T^{(2)}_{k,\sigma\to k',\sigma} \simeq 2J^2 m_s \beta, \tag{2.24}$$

where we have neglected the temperature independent term on the grounds that it is smaller than $T^{(1)}$, which is also temperature independent, by a factor J and so makes no significant contribution to the scattering. Note that the expression in Eq. (2.24) is also smaller than $T^{(1)}$ by a factor J, but may not be neglected since, as we shall now see, its temperature dependence can lead it to be comparable in size to $T^{(1)}$ at some temperature. Evaluating β using the fact that only those electrons within k_BT of the Fermi energy are appreciably excited, we arrive at the result,

$$T^{(2)}_{k,\sigma\to k',\sigma} \simeq J^2 m_s \ln\left(\frac{T_F}{T}\right), \tag{2.25}$$

where $T_F = \frac{\hbar^2 k_F^2}{2mk_B}$ is the Fermi temperature, and so the overall scattering rate, given by the square of the sum of the scattering amplitudes, taking into account the

first-order scattering amplitude, is found to be,

$$\Gamma \propto J^2 + J^3 \ln\left(\frac{T_F}{T}\right) + \mathcal{O}\left(J^4\right). \tag{2.26}$$

Since $J > 0$, this expression reproduces the experimentally observed result that the resistivity exhibits a minimum with logarithmic dependence at low temperatures. The key point, which had been overlooked in many other analyses but which Kondo realised, is that, although one might naively expect higher order terms to make no meaningful contribution to the scattering rate, the fact that the magnetic impurity has a spin degree of freedom and, more explicitly, that S_d^+ and S_d^- do not commute, leads to an imperfect cancellation between particle and hole scattering channels, which in turn results in a temperature dependent scattering rate. This logarithmic scattering term is comparatively small at high temperatures, as its coefficient is a factor of J smaller than that of the first-order scattering, but at low temperatures the logarithm diverges, leading to its influence becoming visible in experiments.

2.2.3 Poor Man's Scaling

As successful as Kondo's perturbative approach was for explaining the existence of a resistivity minimum at low temperatures, the result given by Eq. (2.26) presents an immediate issue: As $T \to 0$, logarithmic terms diverge and so we anticipate the total resistance of the system growing logarithmically large. This expectation is not substantiated by experiment and so we are faced with the prospect that the approach described above ceases to be valid at low temperatures, a turn of events known as the Kondo Problem [101, 102]. To be explicit, the perturbation analysis is no longer valid below a so-called Kondo temperature, T_K, for which the first and second terms in Eq. (2.26) are comparable, which implies,

$$T_K \sim T_F \exp\left(-\frac{1}{J}\right). \tag{2.27}$$

Finding a solution to this Kondo Problem became a matter of urgency for condensed matter theorists and their efforts led to many lasting innovations in the study of many-body phenomena. Here, we will briefly review one of the early attempts to deal with the Kondo problem, namely the so-called "Poor Man's Scaling" approach of Anderson [103]. This method, whilst not totally rigorous, reveals the salient features of Kondo physics in a straightforward manner and forms the basis for the complete renormalization approach later employed by Wilson [104, 105]. The basic approach of Anderson's technique is to consider all possible processes permitted by the system Hamiltonian and then "integrate out" those processes corresponding to

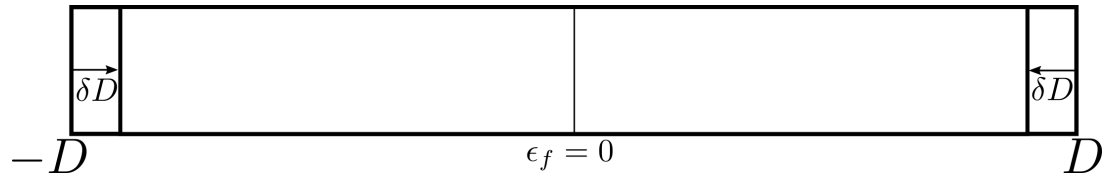

Figure 2.5: Scaling iteratively reduces the total energy space of states considered. Shown is the reduction of a bandwidth D by and increment δD.

excursions to high energy states. That is to say, the influence of these high energy processes is accounted for by changing the coefficients in the low energy space, without the high energy terms appearing explicitly. A visualisation of the method is shown in Fig. 2.5. This technique is applied iteratively such that it becomes apparent how the coefficients of the Hamiltonian "flow" under scaling. The question, then, is how to accurately account for the impact of high energy processes on the low energy sector? Poor Man's scaling is approximate in that it achieves this only by considering high energy excitations to second order, which nevertheless gives the qualitatively correct result.

We begin by considering an asymmetric form of the Kondo Hamiltonian (2.18), with high energy terms given by,

$$H' = \sum_{k',k''} \left[J_z S_d^z \left(c_{k'\uparrow}^\dagger c_{k''\uparrow} - c_{k'\downarrow}^\dagger c_{k''\downarrow} \right) + J_\pm \left(S_d^+ c_{k'\downarrow}^\dagger c_{k''\uparrow} + S_d^- c_{k'\uparrow}^\dagger c_{k''\downarrow} \right) \right]. \tag{2.28}$$

For the sake of simplicity we assume that the impurity has spin $S = 1/2$. Now, the corrections to the J_z terms are given by processes of the form shown in Fig. 2.6. We see that the particle-mediated second order processes, shown in the left half of the figure, make a correction of the form,

$$J_\pm^2 \sum_q S_d^- c_{k'\uparrow}^\dagger c_{q\downarrow} \frac{1}{(E - H_0)} \sum_{q'} S_d^+ c_{q'\downarrow}^\dagger c_{k\uparrow}. \tag{2.29}$$

Substituting $H_0 = \sum_k \epsilon_k c_k^\dagger c_k$, evaluating $S_d^- S_d^+$ and converting the sums over q and q' to an integral using the density of states at the Fermi surface, ρ, and size of the high energy space, δD, this becomes,

$$J_\pm^2 \rho |\delta D| \left(\frac{\hbar}{2} - S_d^z \right) c_{k'\uparrow}^\dagger c_{k\uparrow} \frac{1}{(E - D + \epsilon_k)}. \tag{2.30}$$

Similarly, the hole-mediated process, shown in the right half of Fig. 2.6, make a contribution,

$$J_\pm^2 \rho |\delta D| \left(\frac{\hbar}{2} + S_d^z \right) c_{k\uparrow} c_{k'\uparrow}^\dagger \frac{1}{(E - D - \epsilon_{k'})}. \tag{2.31}$$

If we assume that the final and initial states are close in energy to the Fermi energy, such that $\epsilon = \epsilon_{k'} = 0$, then by comparing Eq. (2.30) and (2.31) to Eq. (2.28) we see that the net effect of the second order processes shown in Fig. 2.6 is to change the coupling constant J_z by an amount,

$$\delta J_z = -\frac{2\rho J_\pm^2 |\delta D|}{E - D}. \tag{2.32}$$

Now, if the excitations are low in energy relative to D, such that $E - D \simeq -D$, then it follows immediately that,

$$\frac{\mathrm{d}J_z}{\mathrm{d}\ln D} = -2\rho J_\pm^2, \tag{2.33}$$

where we have used the fact that δD is negative (see Fig. 2.5) to write $|\delta D| = -\delta D$. A similar calculation of the corrections to the spin flip terms in Eq. (2.28) gives the corresponding result for $J_\pm$,

$$\frac{\mathrm{d}J_\pm}{\mathrm{d}\ln D} = -\rho J_z J_\pm. \tag{2.34}$$

Solving Eq. (2.33) and (2.34) to find and expression for J_z in terms of $J_\pm$ and then substituting this back into Eq. (2.34), we finally arrive at a useful scaling equation for $J_\pm$,

$$\frac{\mathrm{d}J_\pm}{\mathrm{d}\ln D} = \pm\rho J_\pm \sqrt{k + J_\pm^2}, \tag{2.35}$$

where k is some constant. Here, the $+$ solution corresponds to the ferromagnetic case, $J_z < 0$, whilst the $-$ solution corresponds to the antiferromagnetic case $J_z > 0$. Hence, we see that, as the bandwidth decreases, $J_\pm \to 0$ in the ferromagnetic case, whilst in the antiferromagnetic case $J_\pm \to \infty$. If we make the identification $D \sim k_B T$, on the basis that the bandwidth can never be less than the thermally acessible energy regime, then this result demonstrates that, as the system temperature decreases, an antiferromagnetic impurity scales to strong exchange coupling. It is this increase in the strength of the exchange coupling that accounts for the breakdown of the perturbative Kondo model at low temperatures. As we shall see in Chapter 3, this Poor Man's scaling, although simple, is a powerful tool for establishing the behaviour of a system with strong interactions at low temperatures. It is, perhaps, worth pointing out that, whilst the above calculation for determining scaling relations appears very similar to the second order perturbation theory used to derive the logarithmic temperature dependence of the scattering, the method is, in fact, conceptually very different. Whilst the latter involves an unapologetic approximation and requires the acceptance of singularities in the resulting scattering rates, the Poor Man's scaling approach involves no *essential* approximation and avoids a singularity, by simply characterising the evolution of coupling constants.

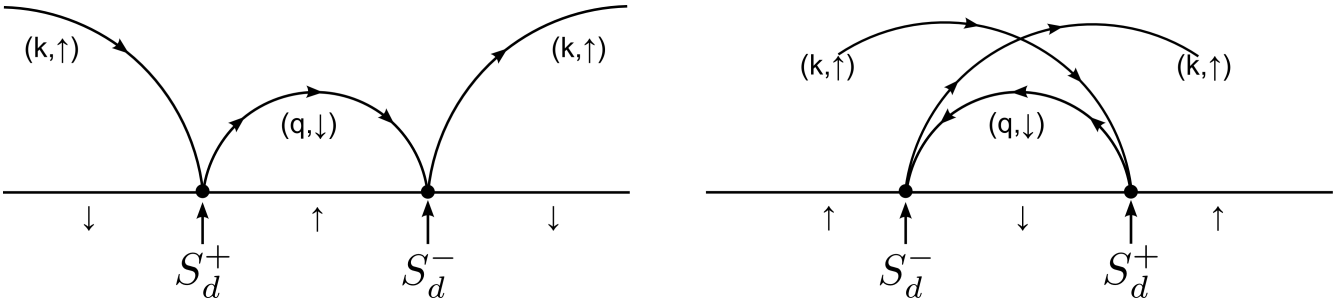

Figure 2.6: Diagrammatic representation of second order processes giving rise to corrections to J_z in scaling analysis. Note that, whilst these diagrams appear almost identical to those in Fig. 2.4, they are part of a very different physical context. Nonetheless, the similarity between this figure and Fig. 2.4 does make clear that Poor Man's scaling is a second order approximation to a true renormalization group analysis.

2.3 Mesoscopic Josephson Junctions

In 1962, the prediction and subsequent experimental observation of the Josephson effect offered a striking manifestation of a macroscopic quantum phenomenon in superconductors [106–108]. However, although the Josephson effect is macroscopic in its results, the underlying origin is fundamentally microscopic in nature, namely the quantum properties of Cooper Pairs. In contrast to this *primary* effect, as early as 1964 interest began to grow in exploring *secondary* effects [44, 109], which result from the fundamentally macroscopic quantum properties of Josephson junctions. The key distinction, then, is that although primary effects are contingent upon microscopic quantum objects, the observables involved are nonetheless classical in nature, whilst secondary effects are not only dependent on quantum objects, but also feature observables whose quantum nature must be taken into account. We anticipate that, if the energies of processes in the junction are greater than both the Josephson coupling, E_J and the temperature k_BT, then such secondary effects will be apparent. A theoretical treatment of such a scenario requires that the quantities associated with the junction are treated as operators. In particular, we demand that the junction charge and phase obey the commutation relation [110],

$$[\phi, Q] = 2ie, \tag{2.36}$$

where e is the electron charge, which is a general property of a Cooper pair condensate. The uncertainty relation implied by Eq. (2.36) indicates how a standard Josephson junction might be modified to exhibit secondary quantum effects. By imposing some restriction on the variation of either ϕ or Q, the fact that the commutator is non-zero becomes important. Of these two variables, it is Q which may be readily influenced by experimental design. A traditional Josephson junction is

sufficiently large that adding a single electron to the junction has no significant impact on the overall charge and so, in effect, the variation of Q is unconstrained and it is no longer necessary to treat ϕ as a quantum variable. However, for a mesoscopic Josephson junction, a single electron constitutes a significant fraction of the total junction charge and so our analysis must respect Eq. (2.36). Equivalently, if the charging energy of a single electron, $E_C = \frac{e^2}{2C}$, with e and C the electronic charge and junction capacitance respectively, is comparable to or greater than both the Josephson coupling, E_J and the temperature $k_B T$, we might expect secondary quantum effects to be apparent.

We may write the junction charge, Q, as an operator in terms of ϕ, by using the commutation relation (2.36),

$$Q = \frac{2e}{i}\frac{\partial}{\partial \phi}. \tag{2.37}$$

The essential Hamiltonian of the mesoscopic Josephson junction then becomes,

$$H_{\text{sc}} = -E_C \frac{\partial^2}{\partial \left(\phi/2\right)^2} - E_J \cos\left(\phi\right), \tag{2.38}$$

where the first term corresponds to the charging energy and the second to the Josephson coupling and we have used an adiabatic approximation to the full Hamiltonian, subject to the condition $\left|\frac{eQ}{C}\right| \ll \Delta$. The Hamiltonian given by Eq. (2.38) also applies to two other well known physical systems: a simple quantum pendulum in a uniform field of strength E_J with moment of inertia $\left(\hbar/2e\right)^2 C$ and angular deflection ϕ from equilibrium; a one-dimensional quantum particle with mass $\left(\hbar/2e\right)^2 C$ moving along the ϕ axis in a field of the form $E_J \cos\left(\phi\right)$. Although these two systems have similar Hamiltonians, their properties are very different, essentially due to their distinct behaviours under a translation,

$$\phi \rightarrow \phi + 2\pi. \tag{2.39}$$

This transformation leaves the pendulum in an indistinguishable state, and so the corresponding wave functions must be 2π periodic, ultimately leading to discrete energy levels. In contrast, the states of the one-dimensional particle before and after the transformation (2.39) are distinguishable and so the wave functions in this case must be comprised of a superposition of Bloch waves, which in turn leads to an energy spectrum consisting of bands.

Hence, at first sight, it seems that the mesoscopic Josephson junction could be accurately modelled as either a quantum pendulum or a one-dimensional quantum particle and, indeed, if we believe that the Josephson junction is represented in its

entirety by Eq. (2.38) then this is true. However, there is a further term in the Josephson Hamiltonian, namely the current-phase coupling [111],

$$V_I = \frac{\hbar}{2e} I(t)\phi, \tag{2.40}$$

where $I(t)$ is the, in general time dependent, current through the junction and, once again, we make the adiabatic approximation under the assumption $\left|\frac{eQ}{C}\right| \ll \Delta$. This coupling is required for $I(t)$ to affect the charge on the junction and, more importantly for the present discussion, breaks the invariance of the system under the transformation (2.39), provided that $I(t) \neq 0$ (any concerns about the case $I(t) = 0$ can be addressed by an appeal to continuity). We therefore conclude that, since two Josephson junction states with a difference in ϕ of 2π are distinguishable, the system is most closely analogous to a one-dimensional quantum particle. This allows us to immediately write down the wave functions of the junction, since they simply take the standard Bloch form,

$$\begin{gathered}\psi(\phi) = \sum_s \int dk C_k^{(s)} \psi_k^{(s)}, \quad \psi_k^{(s)} = u_k^{(s)}(\phi) \exp(ik\phi) \\ u_k^{(s)}(\phi) = u_k^{(s)}(\phi + 2\pi), \quad E^{(s)}(k) = E^{(s)}(k+1), \\ s = 0, 1, 2, .., \quad -\infty < k < \infty,\end{gathered} \tag{2.41}$$

where k is the continuous wave number, s is the band index, $C_K^{(s)}$ are Fourier coefficients, $u_k^{(s)}$ are periodic functions of the superconductor's phase and $E^{(s)}(k)$ is the energy of the state with wave number k in band s. To allow for better interpretation of the theory in terms of observables, we introduce the further variable,

$$q = 2ek, \tag{2.42}$$

which, in direct analogy with the quaismomentum of a crystal lattice, is known as the *quasicharge* of the junction. The energy of the junction can then be written as a function of the quasicharge and band index, $E = E^{(s)}(q)$ which exhibits a periodicity $E^{(s)}(q) = E^{(s)}(q+2e)$. The resulting band structure is shown in Fig. 2.7.

The first experimentally observable consequence of the band structure shown in Fig. 2.7 to be proposed was Bloch oscillations [44]. In direct analogy with electrons in a crystal lattice [112], we anticipate that by driving q at a constant rate, such as by imposing a fixed current across the junction, the value of the junction charge, and therefore voltage, will exhibit oscillations. The driving current, made possible by

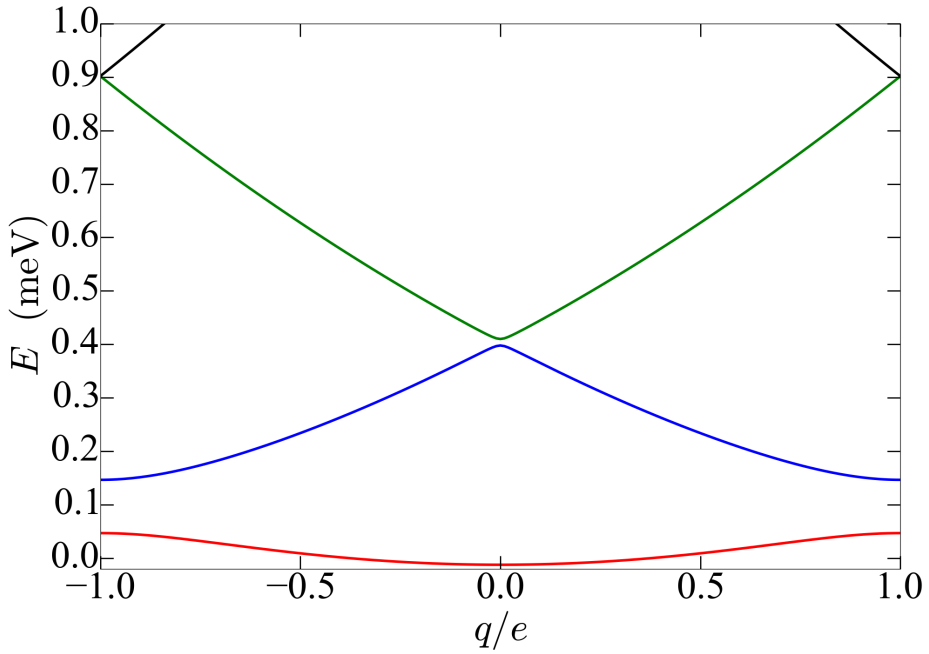

Figure 2.7: The band structure corresponding to Eq. (2.38), plotted in quasicharge space, for system parameters $E_C = E_J = 0.1$meV. Three bands are shown in their entirety , with the lower part of the fourth band also visible. Note that the energy gap between the first (red) and second (blue) bands is approximately equal to E_J.

the presence of a non-zero density of quasiparticle states within the junction, will result in q evolving slowly between $q > -e$ and $q < e$. However, if q is driven across one of the Brillouin Zone boundaries, then it will exhibit a discontinuous jump of $2e$. Physically, this corresponds to a Cooper pair tunnelling across the junction and will manifest as a periodic variation in the junction voltage. To a first approximation, we can model the quasicharge evolution within the Brillouin Zone as being solely a result of the bias current, ignoring the "back-action" of the junction voltage. It then follows immediately that the frequency of the associated Bloch oscillations will be,

$$f_B = \frac{I}{2e}. \tag{2.43}$$

This apparently straightforward result, which attracted a fair amount of controversy following its publication [113–115], is a clear manifestation of a secondary quantum effect in Josephson junctions. Early attempts to observe Bloch oscillations experimentally were hindered by the difficulty of screening the junction from lead capacitances, which effectively result in a reduction of E_C to such an extent that the requirement $E_C \gtrsim E_J$ is no longer satisfied. Nevertheless, by 1991 a carefully designed experiment provided the first indication that Bloch oscillations in Josephson junctions might be a real phenomenon [116]. Rather than looking directly for oscillations in junction voltage, which were not detectable using the techniques of the

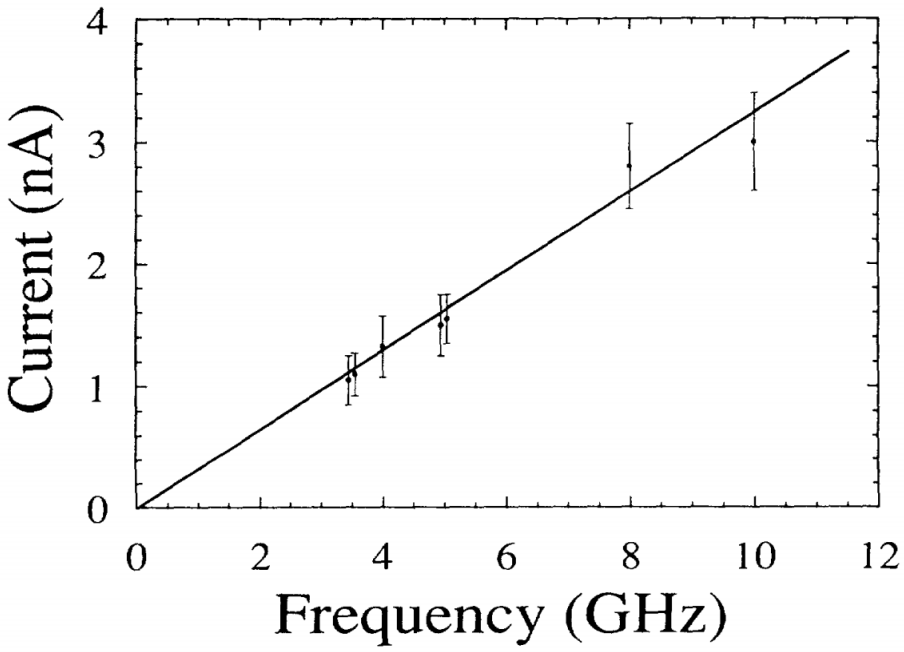

Figure 2.8: Measurement of differential resistance as a function of driving current, for constant driving frequency, reveals broad peaks evenly spaced about zero current. The points shown here are the half-distance between these peaks at a given driving frequency. The solid line is the theoretical prediction, $I = 2ef$. From Ref. [116], reprinted with permission from APS.

time, this experiment instead measured the differential resistance of the junction, $\mathrm{d}V/\mathrm{d}I$ as a function of the magnitude of the driving current and the frequency of its AC component. The result, shown in Fig. 2.8, although not totally conclusive, was in accordance with theoretical predictions and provided tentative evidence for the existence of Bloch oscillations.

Whilst early experiments suggested the existence of Bloch oscillations, they were unavoidably limited by the fabrication and measurement techniques available at the time. As a result, it was not until 2007 that convincing evidence was found for Bloch oscillations in Josephson junctions [117]. In addition to general improvements in electronics, this experiment differed from earlier efforts in two key ways. Firstly, rather than attempting to impose a constant bias current on the junction, which is complicated by the requirement to embed the junction in a high impedance environment, the experiment instead achieved an effective current bias by imposing a triangle-wave gate voltage, N_g, with amplitude ΔN and frequency f_g, on a capacitor in series with the junction. Secondly, the experiment probed the properties of the junction using microwave reflectometry, allowing a much lower noise signal than with a direct measurement. Such techniques enabled the observation of clear Bloch oscillations, both directly in the demodulated microwave signal, shown in Fig. 2.9,

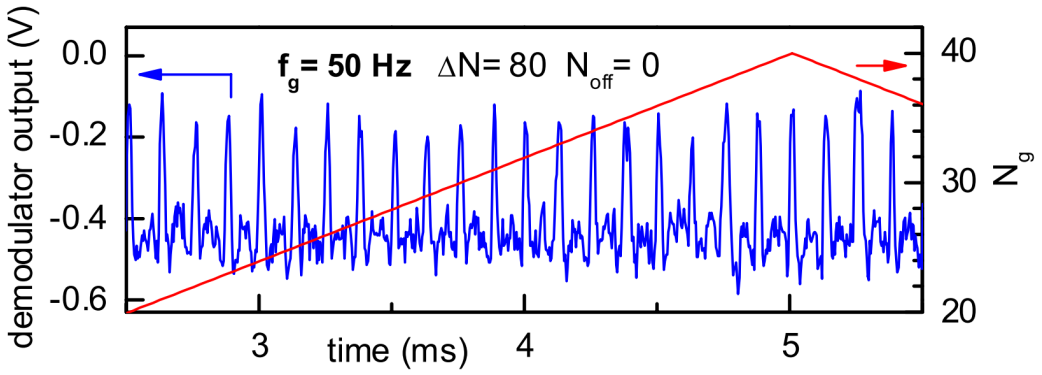

Figure 2.9: Output signal (blue) of a Josephson junction, measured with microwave reflectometry. The red plot is the triangle-wave gate voltage, N_g. There is close agreement between the theoretical result, $f_B = 2\Delta N f_g = 8$kHz and the observed frequency of the output signal. From Ref. [117], reprinted with permission from APS.

and in the power spectrum of the signal, not shown here.

The theoretical discussion and experimental results presented in this section should serve to reinforce one of the main reasons why mesoscopic systems can be of fundamental interest and give rise to qualitatively distinct physics in superconducting systems. Namely, whilst the traditional Josephson junction is, from a quantum perspective, unrestricted with regards to the junction charge, or equivalently number of electrons, the mesoscopic junction, by virtue of its charging energy, limits charge variations and so, by charge-phase conjugation, enables significant variation in superconducting phase. This transition, from a $\Delta\phi \sim 0$ to a $\Delta Q \sim 0$ regime, results in a striking change in the behaviour of the system. As we shall see in Chapter 4, this system is also of interest in the context of Majorana bound states in condensed matter.

Chapter 3

Kondorana

In this chapter we consider the nanowire setup depicted in Fig. 3.1, in which Majorana modes appear at the wire ends as a result of, for example, spin-orbit interaction in the wire, an applied magnetic field and superconductivity induced through contact to an s-wave superconductor [64, 65, 118]. Furthermore, we consider a floating superconductor so that there is a charging energy E_C associated with the tunnelling of electrons to and from the nanowire. Several studies have been performed on the low energy behaviour of such a system, predicting distinctive non-local transport and Coulomb blockade phenomena [119–127]. The latter of these appears to have been confirmed experimentally [86]. A coupling of several such Majorana wires through a common floating superconductor gives rise to the topological Kondo effect [128–136]. This is a result of the existence of Majorana modes in combination with constrained fluctuations due to a charging energy E_C. A Majorana mode may also be coupled to a quantum dot to explore the competition between Kondo and Majorana physics [137–140]. However, these works do not fully explore the potential of the Majorana modes as a novel interface between the topological superconductor and its environment.

Over the course of this chapter, we shall see that such an exploration reveals fundamentally new physics in which the Kondo and Majorana aspects combine and leads to a new type of many-body state. This marriage of traditionally distinct physics leads us to call the result the *Kondorana* model.

We consider a single Majorana wire as shown in Fig. 3.1 and tune it to degeneracy of two different charging states, such that tunnelling into the Majorana states can make a transition between the degenerate states or lead to a high energy ($2E_C$) excitation. By integrating out the latter, we obtain an effective Kondo like low energy theory, in which the two degenerate charging states take the role of the Kondo

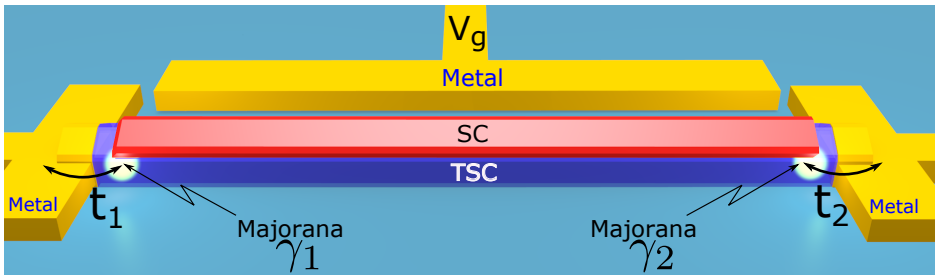

Figure 3.1: A Majorana system with a floating superconductor. An s-wave superconductor (red) is grown on a nanowire with strong spin-orbit coupling (blue). For sufficiently large applied magnetic field and appropriate chemical potential the nanowire becomes a topological superconductor (TSC) with Majorana bound states $\gamma_{1,2}$ at each end. A gate at voltage V_g is used to tune the ground state occupation number, which is dictated by the capacitive charging energy E_C. The nanowire couples to leads at either end with tunnelling coefficients t_1 and t_2 between lead electrons and $\gamma_{1,2}$.

spin S. However, the situation differs from the Kondo model in two essential ways. Firstly, a Kondorana spin flip is induced by electron tunnelling and not by an electron spin flip type process. Secondly, the effective S^z interaction couples not to the electron spin but to a pseudo-spin s constructed from the electron operators for the left and right leads. Indeed, the absence of an electronic spin degree of freedom for the Majorana states, due to the spin polarization induced by the applied magnetic field and spin-orbit coupling, is an important condition for the results found in this chapter, as we shall discuss later. In addition to the regular $S^z s^z$ coupling, the teleportation property of the Majorana states [119] leads to a further $S^z s^y$ coupling. Due to the latter, the renormalization group flow for the interaction strength has a zero eigenvalue and hence the fixed point of this Kondorana model is finite and does not lie at zero or infinity as for the Kondo model. Nevertheless, this fixed point describes a many-body state extending across the metallic leads, superconducting condensate, and Majoranas. It is important to note that the Kondorana fixed point is distinct from that found in the Two Channel Kondo Model, [39] despite superficial similarities arising from the invocation of Majorana modes to solve the latter scenario [141, 142]. Finally, we determine how the conductance of the nanowire scales with the ratio of tunnelling couplings and with the temperature, and we suggest signatures of this state, that should be observable with current experimental techniques.

Subsequent to completion of the research described in this chapter, Bao and Zhang published work [143] in which a similar setup was investigated in a time reversal invariant topological superconductor with two Majorana states at each end of the

Parameter	Symbol	Value
Lead Bandwidth	D_0	0.4meV
Charging Energy	E_C	0.2meV
Left Lead-TSC Tunnelling Coefficient	t_1	0.1meV
Righ Lead-TSC Tunnelling Coefficient	t_2	0.01meV

Table 3.1: Representative parameters for the floating TSC, with a superconducting gap $\Delta > E_C$, based on values reported in Ref. [86].

wire. Remarkably, instead of Kondorana physics, a two channel Kondo model is obtained in this system.

3.1 Model

Our analysis is based on the Majorana Single Charge Transistor (MSCT) [120, 121], which results from the usual Majorana setup of a quantum wire with strong spin-orbit interaction in a magnetic field, but where the coupled superconductor is mesoscopic and floating, with a charging energy E_C, where $4E_C \lesssim \Delta_{TS}$, with Δ_{TS} the proximity induced gap of the topological superconductor. We furthermore assume that E_C is large compared with all other energy scales, notably the tunnel couplings $t_{1,2}$ to the leads, temperature T and applied voltage bias V. A representative experimental setup is shown in Fig. 3.1 and typical parameter values are given in Table 3.1.

3.1.1 Full Hamiltonian

This system is described by the Hamiltonian $H = H_{el} + H_T + H_C$. The leads are treated as non-interacting reservoirs, $H_{el} = \sum_{j,k,\sigma} \epsilon_{jk} c^\dagger_{jk\sigma} c_{jk\sigma}$, where $c_{jk\sigma}$ are electron operators for leads $j = 1, 2$, momenta k and spins $\sigma =\uparrow, \downarrow$, with the dispersion ϵ_{jk}. The coupling between the leads and the superconductor is restricted to tunnelling into the Majorana states $\gamma_{1,2}$, and we explicitly exclude the possibility of exciting quasiparticles [127]. The tunnelling Hamiltonian can then be written as [121],

$$H_T = \sum_k (t_1 c^\dagger_{1k\downarrow} \eta_1 + i t_2 c^\dagger_{2k\uparrow} \eta_2) + \text{h.c.}, \tag{3.1}$$

where $t_{1,2}$ are the tunnelling amplitudes and $\eta_{1,2} = d \pm \mathrm{e}^{-i\phi} d^\dagger$, with $d = (\gamma_1 + i\gamma_2)/\sqrt{2}$. We note that tunnelling through the Majoranas is spin polarised [64, 144], for in-

stance, with opposite spins for both Majoranas if the magnetic field is applied perpendicular to the spin-orbit polarization direction, as written here. The spin polarization may also be non-antiparallel, if the magnetic field is tilted or if there exists a mixture of Rashba and Dresselhaus spin orbit coupling [144]. For our purposes here, it is only important that the coupling to the leads no longer has the spin degree of freedom. This allows us to effectively eliminate the spin index in the notations and we write $c_{1k} = c_{1k\downarrow}$ and $c_{2k} = c_{2k\uparrow}$. As previously noted, the absence of this spin degree of freedom has important ramifications for the renormalization group analysis. Were the tunnel couplings not spin polarised, as is typical in the case of a normal quantum dot, then the system's scaling would be different. The form of the $\eta_{1,2}$ operators takes into account that tunnelling between Majorana and lead can occur over two channels: by removal of an electron from the fermionic state d obtained by the superposition of $\gamma_{1,2}$ (normal tunnelling), or by splitting a Cooper pair and transferring one electron to the lead and the other electron to the d state (anomalous tunnelling) as shown in Fig. 3.2. The removal of a Cooper pair is expressed by $\mathrm{e}^{-i\phi}$, where ϕ is the superconducting phase operator, which obeys $[N_C, \mathrm{e}^{-i\phi}] = -\mathrm{e}^{-i\phi}$ for N_C the Cooper pair number operator. Andreev tunnelling processes are deliberately neglected in this analysis for two reasons. Firstly, their amplitude is proportional to t^2/Δ and so much smaller than the amplitude, t, relevant for the considered processes. Secondly, an Andreev process changes the number of charges on the nanowire by ± 2, leaving the system in an excited state that needs further relaxation, and so the Andreev processes exist only at higher orders.

The final component of the system Hamiltonian is the charging energy which is given by $H_C = E_C(2N_C + n_d - n_g)^2$, where $n_d = d^\dagger d$ and n_g is a constant controlled by the gate voltage V_g. In contrast to Ref. [121] we do not consider any Josephson coupling to a further superconductor, since this would be a more difficult setup to realise experimentally and is unlikely to lead to any significant change in our results, except in the case $E_J \gg E_C$ which essentially corresponds to a grounded TSC. We tune n_g to the value $n_g = 2n - \frac{1}{2}$, with n an integer. This results in a charging ground state degeneracy between the states $(N_C = n, n_d = 0)$ and $(N_C = n-1, n_d = 1)$, with the next excited states at $(N_C = n, n_d = 1)$ and $(N_C = n-1, n_d = 0)$ having an excitation energy $2E_C$, as shown in Fig. 3.2. Note that we have neglected any Majorana interaction energy, $H_{int} = \epsilon_\gamma (n_d - 1/2)$, which would break the ground state degeneracy. The energy ϵ_γ is proportional to the Majorana wave function overlap and can be made exponentially small by a sufficiently large system size, although this must be balanced by the requirement of maintaining a large E_C.

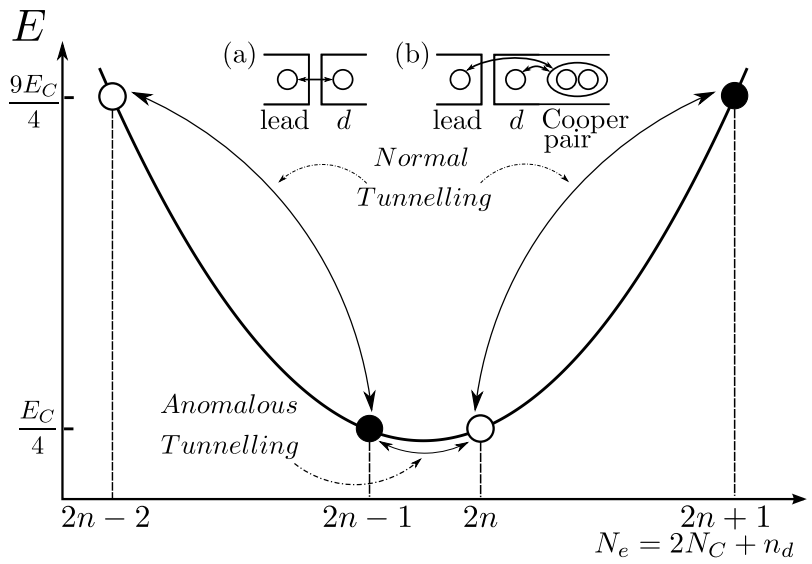

Figure 3.2: Charging energy against total number of electrons, N_e, in the nanowire for $n_g = 2n - \frac{1}{2}$. Filled (empty) circles represent states with $n_d = 1$ ($n_d = 0$). Both the ground and excited states are degenerate, with transitions between them via normal tunnelling (a) and anomalous tunnelling (b). Note that there is no process mediating transitions between the two excited states.

Ultimately, this Majorana hybridisation energy is not an issue since degeneracy can be restored by retuning n_g to $n_g = 2n - \frac{1}{2} - \frac{\epsilon_\gamma}{2E_C}$. Whilst this retuning does cause a splitting between the first excited states of $4\epsilon_\gamma$, the degeneracy of these states is inessential to our results and as long as $\epsilon_\gamma \ll E_C$ this perturbation to the excited state energy is of no consequence.

Further excited states appear only at energy $4E_C$ above the first excited states and are neglected in the present low energy description, in part because a lower order approximation is already sufficient to reveal non-trivial effects, but also because if $4E_C \lesssim \Delta_{TS}$, as stated above, then a system at energies above the first excited state will support above-gap tunnelling processes.

The resulting situation is reminiscent of the large interaction limit of the Anderson model with two-fold degenerate ground and first excited states, yet with the restriction that there is no direct scattering process connecting the two excited states because they have different total particle numbers, $2n - 2$ and $2n + 1$, as shown in Fig. 3.2. This excludes the virtual spin-flip type processes, that dominate Kondo physics, arising from the usual mapping of the Anderson model on the Kondo model, and the resulting physics for the present situation is fundamentally different. To discriminate it from the Kondo type behaviour obtained by a mutual coupling of several such Majorana wires through a common superconductor [119–127], and from the behaviour of independent Majorana states, we call the effective model

obtained from an analogous mapping the *Kondorana model* as it combines Kondo and Majorana properties on an equal footing, but exhibits exciting new physics. We note in passing that the other charging degeneracy point, $n_g = 2n + \frac{1}{2}$, also results in a many-body state similar to the one described here, due to particle-hole symmetry [126].

3.1.2 Schrieffer-Wolff Transformation

To find an effective low-energy theory of the full Hamiltonian, we carry out a Schrieffer-Wolff transformation, defined by the unitary transformation $H_{\text{eff}} = e^{W} H e^{-W}$. This transformation is chosen such that it eliminates the tunnelling processes into the high energy sector of the model and replaces them by effective low-energy processes created by virtual high energy excursions. With our choice of tuning the gate to the degenerate ground states $(N_C = n, n_d = 0)$ and $(N_C = n - 1, n_d = 1)$, the normal tunnelling terms, as shown in Fig. 3.2, provide the excitations to the high energy sector, given by the Hamiltonian,

$$H_1 = \sum_k (t_1 c_{1k}^\dagger d + i t_2 c_{2k}^\dagger d) + \text{h.c.}, \tag{3.2}$$

whereas the low energy sector is described by the lead Hamiltonian, H_{el}, the charging energy, H_{C} and the anomalous tunnelling terms indicated in Fig. 3.2,

$$H_0 = H_{el} + H_C + \sum_k (t_1 c_{1k}^\dagger \mathrm{e}^{-i\phi} d^\dagger + i t_2 c_{2k}^\dagger \mathrm{e}^{-i\phi} d^\dagger) + \text{h.c.} \tag{3.3}$$

Expanding the unitary transformation in W then leads to the effective Hamiltonian,

$$H_{\text{eff}} = H_0 + \frac{1}{2}\left[W, H_1\right], \tag{3.4}$$

in which the first order high energy excitations are absent because we require that,

$$[W, H_0] \stackrel{!}{=} -H_1. \tag{3.5}$$

To find the expression for W that satisfies (3.5), we first note that W must have the same form as H_1 and so we begin with the ansatz,

$$W = \sum_k \left\{ A_k c_{1k}^\dagger d + B_k c_{2k}^\dagger d - \text{h.c.} \right\}, \tag{3.6}$$

where the fact that W is anti-hermitian follows immediately from (3.5) and the hermitian property of H_1 and H_0. The coefficients A_k and B_k can now be found from the condition (3.5). It is necessary to calculate four commutators (one for each

of the terms in W),

$$\begin{aligned}\left[\sum_{k'} A_{k'} c_{1k'}^{\dagger} d\,,\, H_0\right] =& \sum_k A_k \left\{\epsilon_k d c_{1k}^{\dagger} + E_C\left(4N_C + 1 - 2n_g\right) c_{1k}^{\dagger} d\right\} \\ & - i \sum_{k,k'} A_{k'} t_2 c_{1k'}^{\dagger} c_{2k}^{\dagger} e^{-i\phi},\end{aligned} \tag{3.7}$$

$$\begin{aligned}\left[\sum_{k'} B_{k'} c_{2k'}^{\dagger} d\,,\, H_0\right] =& \sum_k B_k \left\{\epsilon_k d c_{2k}^{\dagger} + E_C\left(4N_C + 1 - 2n_g\right) c_{2k}^{\dagger} d\right\} \\ & + \sum_{k,k'} B_{k'} t_1 c_{1k}^{\dagger} c_{2k'}^{\dagger} e^{-i\phi},\end{aligned} \tag{3.8}$$

$$\begin{aligned}\left[-\sum_{k'} A_{k'}^{*} c_{1k'} d^{\dagger}\,,\, H_0\right] =& \sum_k A_k^{*} \left\{\epsilon_k c_{1k} d^{\dagger} + E_C\left(4N_C + 1 - 2n_g\right) d^{\dagger} c_{1k'}\right\} \\ & - i \sum_{k,k'} A_{k'}^{*} t_2 c_{1k'} c_{2k} e^{i\phi},\end{aligned} \tag{3.9}$$

$$\begin{aligned}\left[-\sum_{k'} B_{k'}^{*} d^{\dagger} c_{2k'}\,,\, H_0\right] =& \sum_k B_k^{*} \left\{\epsilon_k c_{2k} d^{\dagger} + E_C\left(4N_C + 1 - 2n_g\right) d^{\dagger} c_{2k}\right\} \\ & - \sum_{k,k'} B_{k'}^{*} t_1 c_{1k} c_{2k'} e^{i\phi}.\end{aligned} \tag{3.10}$$

We note that the above commutators generate Andreev type processes of the form $c^{\dagger}c^{\dagger}\mathrm{e}^{-i\phi}$. Such processes are indeed present at second order in tunnelling, but since they change the number of charges on the wire by 2, they always lead to high energy excitations and contribute to the low energy theory only at order $\mathcal{O}(t_j^3/E_C^2)$. These Andreev type terms can therefore safely be neglected, since we have assumed that $t_j \ll E_C$ and so we find that,

$$\begin{aligned}[W, H_0] \simeq \sum_k \Big\{ & \epsilon_k \left[A_k d c_{1k}^{\dagger} + B_k d c_{2k}^{\dagger} + A_k^{*} c_{1k} d^{\dagger} + B_k^{*} c_{2k} d^{\dagger}\right] \\ & - E_C\left(4N_C + 1 - 2n_g\right) \left[A_k d c_{1k}^{\dagger} + B_k d c_{2k}^{\dagger} + A_k^{*} c_{1k} d^{\dagger} + B_k^{*} c_{2k} d^{\dagger}\right] \Big\}.\end{aligned} \tag{3.11}$$

Imposing (3.5) gives the required expressions for A_k and B_k,

$$A_k = \frac{t_{1k}}{\epsilon_k - E_C\left(4N_C + 1 - 2n_g\right)} \qquad B_k = \frac{-i t_{2k}}{\epsilon_k - E_C\left(4N_C + 1 - 2n_g\right)}, \tag{3.12}$$

and so the Schrieffer-Wolff transform necessary to fulfil (3.5) is,

$$W = \sum_k \Xi(\epsilon_k)\left(t_1 c_{1k}^{\dagger} d - i t_2 c_{2k}^{\dagger} d\right) - \text{h.c.}, \tag{3.13}$$

where for convenience we have defined the function,

$$\Xi(\epsilon_k) = \left[\epsilon_k - E_C(4N_C + 1 - 2n_g)\right]^{-1}. \tag{3.14}$$

As noted previously this expression for W is correct only up to $\mathcal{O}(t_j^3/E_C^2)$, due to the omission of Andreev type terms in its derivation. Now, following the prescription of Eq. (3.4), we determine H_{eff} by calculating the commutator $[W, H_1]$ which, term-by-term, is,

$$\left[\sum_k A_k c_{1k}^\dagger d\,,\, H_1\right] = \sum_{k,k'} \left\{A_k t_1^* \left(c_{1k}^\dagger c_{1k'} - \delta_{k,k'} d^\dagger d\right) + i A_k t_2^* c_{1k}^\dagger c_{2k'}\right\}, \tag{3.15}$$

$$\left[\sum_k B_k c_{2k}^\dagger d\,,\, H_1\right] = \sum_{k,k'} \left\{i B_k t_2^* \left(c_{2k}^\dagger c_{2k'} - \delta_{k,k'} d^\dagger d\right) + B_k t_1^* c_{2k}^\dagger c_{1k'}\right\}, \tag{3.16}$$

$$\left[-\sum_k A_k^* d^\dagger c_{1k}\,,\, H_1\right] = \sum_{k,k'} \left\{A_k^* t_1 \left(c_{1k'}^\dagger c_{1k} - \delta_{k,k'} d^\dagger d\right) - i A_k^* t_2 c_{2k'}^\dagger c_{1k}\right\}, \tag{3.17}$$

$$\left[-\sum_k B_k^* d^\dagger c_{2k}\,,\, H_1\right] = \sum_{k,k'} \left\{i B_k^* t_2 \left(\delta_{k,k'} d^\dagger d - c_{2k'}^\dagger c_{2k}\right) + B_k^* t_1 c_{1k'}^\dagger c_{2k}\right\}. \tag{3.18}$$

If we choose to make t_1, t_2 real (which is always possible since any phase can be absorbed by shifting the phases of the lead electrons through a gauge transformation), it follows from Eq. (3.12) that $A_k = A_k^*$ and $B_k = -B_k^*$. We therefore find that the effective Hamiltonian is given by,

$$\begin{aligned}
H_{\text{eff}} &= E_C(2N_C + n_d - n_g)^2 \\
&+ \sum_k \Big[\epsilon_k\big(c_{1k}^\dagger c_{1k} + c_{2k}^\dagger c_{2k}\big) \\
&+ \big(t_1 c_{1k}^\dagger d^\dagger e^{-i\phi} + i t_2 c_{2k}^\dagger d^\dagger e^{-i\phi} + \text{h.c.}\big)\Big] \\
&+ \sum_{k,k'} \Xi(\epsilon_k)\Big[t_1^2 c_{1k}^\dagger c_{1k'} + t_2^2 c_{2k}^\dagger c_{2k'} \\
&- \delta_{k,k'}\big(t_1^2 + t_2^2\big) n_d + i t_1 t_2 \big(c_{1k}^\dagger c_{2k'} - c_{2k}^\dagger c_{1k'}\big)\Big].
\end{aligned} \tag{3.19}$$

The term with $\delta_{k,k'}$ in the last line produces an energy shift for the n_d level, similar to an overlap integral between the two Majorana wave functions. If we take $\rho(\epsilon)$ to be the density of states and D_0 to be the electronic bandwidth such that $\rho \sim 1/D_0$, we can estimate the magnitude of this term as,

$$\begin{aligned}
(t_1^2 + t_2^2) \sum_{k,k'} \delta_{k,k'} \Xi(\epsilon_k) &= (t_1^2 + t_2^2) \int d\epsilon \rho(\epsilon) \Xi(\epsilon) \\
&\sim -\frac{t_1^2 + t_2^2}{D_0} \ln\left[\frac{D_0 - E_C(4N_C + 1 - 2n_g)}{D_0 + E_C(4N_C + 1 - 2n_g)}\right],
\end{aligned} \tag{3.20}$$

where we have used the definition in Eq. (3.14) to go from the first to second line. For $E_C < D_0$ this term is on the order of $\mathcal{O}\left(t_j^2 E_C/D_0^2\right)$ and thus smaller than all other considered energies. In any case, it can always be removed by a slight adjustment

of n_g through the gate voltage since it plays the same role as the charging energy, and we shall set it to zero henceforth.

For the remaining effective theory the ϵ_k term in Eq. (3.14) is unimportant as it causes only small corrections for the low-energy properties, and we shall drop it in the following and use the approximation $\Xi(\epsilon_k) = \Xi = -[E_C(4N_C + 1 - 2n_g)]^{-1}$. It is convenient to simplify this expression further by noting that, with $n_g = 2n - 1/2$,

$$4N_C + 1 - 2n_g = \begin{cases} +2 & \text{for } (N_c = n, n_d = 0), \\ -2 & \text{for } (N_c = n-1, n_d = 1), \end{cases} \tag{3.21}$$

which allows us to write,

$$\Xi = (2n_d - 1)/2E_C, \tag{3.22}$$

for these two states. Substituting this expression for Ξ into Eq. (3.19), and omitting the term with $\delta_{k,k'}$ for the reasons stated above, we find that the effective Hamiltonian of our system is given by,

$$\begin{aligned} H_{\text{eff}} &= H_{\text{el}} + H_{\text{C}} + \sum_k \left\{ t_1 c_{1k}^\dagger d^\dagger e^{-i\phi} + i t_2 c_{2k}^\dagger d^\dagger e^{-i\phi} + h.c. \right\} \\ &+ \sum_{k,k'} \frac{(2n_d - 1)}{2E_C} \left[t_1^2 c_{1k}^\dagger c_{1k'} + t_2^2 c_{2k}^\dagger c_{2k'} + i t_1 t_2 \left(c_{1k}^\dagger c_{2k'} - c_{2k}^\dagger c_{1k'} \right) \right]. \end{aligned} \tag{3.23}$$

As indicated in Fig. 3.2, the normal particle tunnelling between leads and Majoranas generates the high energy excitations. Since there is no direct transition between both excited states, the virtual excitations into the high energy sector generate an n_d dependent scattering potential between electrons, including a teleportation type scattering across the Majorana wire $\sim c_{1k}^\dagger c_{2k'}$ [119], but do not cause any change in the Majorana parity. To facilitate comparison of the effective Hamiltonian in our, Kondorana, case with that of the typical Kondo Hamiltonian, we may also write H_{eff} in a somewhat more familiar form,

$$\begin{aligned} H_{\text{eff}} &= H_{\text{el}} + \frac{1}{\sqrt{2}} \sum_k \left[\left(J_\pm^{(1)} c_{1k}^\dagger + i J_\pm^{(2)} c_{2k}^\dagger \right) S^+ + \text{h.c.} \right] \\ &+ \sum_{k,k'} \left[J_z^{(11)} c_{1k}^\dagger c_{1k'} + J_z^{(22)} c_{2k}^\dagger c_{2k'} + i J_z^{(12)} \left(c_{1k}^\dagger c_{2k'} - c_{2k'}^\dagger c_{1k} \right) \right] S^z, \end{aligned} \tag{3.24}$$

where we have defined the pseudo-spin operators,

$$S^+ = \sqrt{2} d^\dagger \mathrm{e}^{-i\phi},\ S^- = \sqrt{2} d \mathrm{e}^{i\phi},\ S^z = 2n_d - 1, \tag{3.25}$$

and the coefficients,

$$J_\pm^{(j)} = t_j,\ J_z^{(jj')} = t_j t_{j'}/2E_C \quad \text{for } j, j' = 1, 2. \tag{3.26}$$

The Hamiltonian in Eq. (3.24) differs from the Kondo Hamiltonian in two essential ways. Firstly, it cannot be written down as a pure spin-spin interaction because it involves the tunnelling terms $J_{\pm}^{(j)}$ which create and annihilate electrons while flipping S. Secondly, the S^z term couples in parallel to an s^z and s^y electron pseudo-spin: Since the tunnelling electrons have a spin polarization locked to the lead, we can define a lead-spin pseudo-spin with projections $s \in \{s_+, s_-\} = \{(j = 1, \downarrow), (j = 2, \uparrow)\}$ and operators $s^{\alpha}_{k,k'} = c^{\dagger}_{ks}\sigma^{\alpha}_{s,s'}c_{k's'}$ for σ^{α} the Pauli matrices (with σ^0 the unit matrix). This allows us to write the S^z term as,

$$\sum_{k,k'}[\frac{1}{2}(J_z^{(11)} + J_z^{(22)})s^0_{kk'} + \frac{1}{2}(J_z^{(11)} - J_z^{(22)})s^z_{kk'} + J_z^{(12)}s^y_{kk'}]S^z. \tag{3.27}$$

This special form, mainly the appearance of the $s^y_{kk'}$ term, leads to a behaviour of the Kondorana model that is entirely different from the usual Kondo physics. Note that deviations from Eq. (3.21), such as by tuning n_g slightly away from $2n + 1/2$ due to compensation of Eq. (3.20) or because of the neglected dependence of Ξ on ϵ_k cause only corrections that either remain proportional to S^z or are independent of S^z and consist only of renormalizations of the chemical potentials in the leads. Equation (3.24) therefore represents the generic effective Hamiltonian of the system.

3.2 Renormalization

The non-Kondo behaviour of the model becomes evident if we consider a renormalization group analysis. Since H_{eff} describes free electrons that are coupled to a single localised pseudo-spin S, the Poor Man's scaling technique [103] provides a transparent approach to the physics while being perfectly accurate for our purposes. In this approach, excitations to high energy states are successively integrated out, and the bandwidth is effectively reduced, leading to modification of the coupling constants J. In the following we label with q, q' these high energy states and with k, k' the initial and final low energy states. The renormalization proceeds by directly producing corrections to the Hamiltonian. We follow a diagrammatic variant of Poor Man's scaling, as described in, for example, Ref. [100]. The first point to note is that the $J_z^{(jj')}$ couplings are invariant under scaling. The reason for this can be understood by considering Fig. 3.3, which shows the two vertex process contributing to the scaling of $J_z^{(11)}$.

Neither of the two vertices causes a change in Majorana parity, i.e. an S^z spin flip, and they therefore commute. The result is that the hole-mediated version of the depicted process will result in exact cancellation. Indeed, since only terms in the Hamiltonian proportional to $J_{\pm}^{(j)}$ change the value of S^z, and such terms constitute

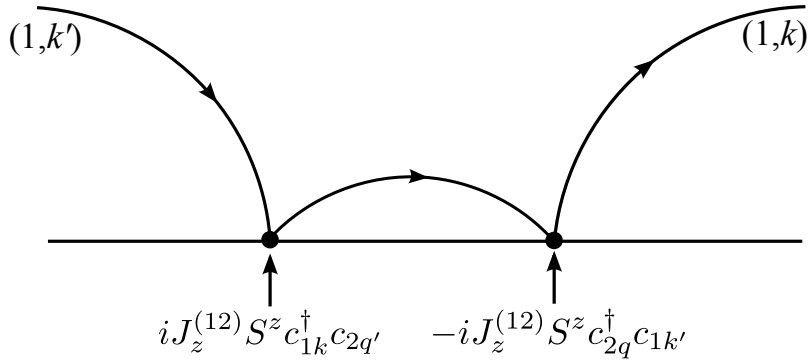

Figure 3.3: The lowest order particle mediated process contributing to the scaling of $J_z^{(11)}$. The line between the two vertices denotes a particle excited to the high energy shell. Note that the two scattering events commute, so the pathway shown here is exactly cancelled by a corresponding hole-mediated process and does not contribute to scaling.

terminal vertices, as shown in Fig. 3.4, there are no scattering diagrams, to any order, that result in scaling of $J_z^{(jj')}$. We can therefore conclude that $J_z^{(jj')}$ obeys the scaling equation,

$$\frac{d}{d\ell}J_z^{(jj')} = 0 \qquad \text{for all} \quad j, j'. \tag{3.28}$$

We now turn to the scaling of $J_\pm^{(1)}$, for which the first order scattering processes are shown in Fig. 3.4. The particle mediated channels, with excitations q, q' in an energy shell of width δD at the upper band edge, lead to the following correction of the Hamiltonian,

$$\begin{aligned}
\delta H_p &= \sum_{q,q'}\Big[J_z^{(11)}S^z c_{1k}^\dagger c_{1q'}\,(E-H_0)^{-1}\,J_\pm^{(1)}c_{1q}^\dagger\frac{1}{\sqrt{2}}S^+ \\
&+ iJ_z^{(12)}S^z c_{1k}^\dagger c_{2q'}\,(E-H_0)^{-1}\,iJ_\pm^{(2)}c_{2q}^\dagger\frac{1}{\sqrt{2}}S^+\Big] \\
&= \sum_{q,q'}\Big[J_z^{(11)}J_\pm^{(1)}c_{1k}^\dagger c_{1q'}\,(E-D)^{-1}\,c_{1q}^\dagger\frac{1}{\sqrt{2}}S^+ \\
&- J_z^{(12)}J_\pm^{(2)}c_{1k}^\dagger c_{2q'}\,(E-D)^{-1}\,c_{2q}^\dagger\frac{1}{\sqrt{2}}S^+\Big],
\end{aligned} \tag{3.29}$$

where E is the energy at which the system is probed and D is the running bandwidth of the leads. We have used the fact that $S^zS^+ = S^+$ and written $H_0c^\dagger S^+ = Dc^\dagger S^+$, since $|\delta D| \ll D$ and S^+ corresponds to zero energy excitations. Summing over the high energy interval $|\delta D|$, using the fact that $E - D \simeq -D$ and noting that far above the Fermi surface $c_{1q'}c_{1q}^\dagger = \delta_{qq'}$, we find the particle mediated contribution to the scaling is,

$$\delta H_p = -\frac{\rho|\delta D|}{D}\left[J_z^{(11)}J_\pm^{(1)} - J_z^{(12)}J_\pm^{(2)}\right]c_{1k}^\dagger\frac{1}{\sqrt{2}}S^+, \tag{3.30}$$

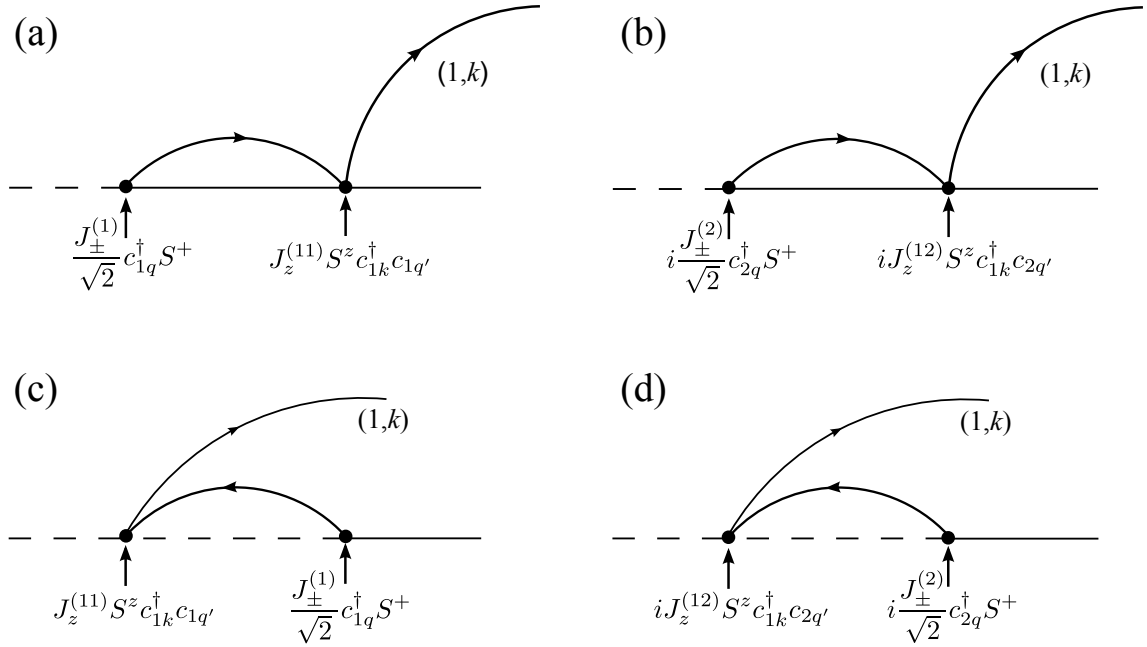

Figure 3.4: Scattering channels which contribute to renormalization of $J_\pm^{(1)}$. Diagrams (a) and (b) show particle mediated scattering via the left and right leads, respectively. Similarly, (c) and (d) depict hole mediated scattering. Curved lines represent lead electrons, whilst the straight lines correspond to the nanowire with dashed and solid lines denoting $S_z = -1$ and $S_z = +1$, respectively.

with ρ the density of states in the leads. A similar analysis for the hole mediated terms provides an identical result, so that the total Hamiltonian associated with the two vertex events corresponding to $J_\pm^{(1)}$ is therefore,

$$\delta H_{2\mathrm{v}} = -\frac{2\rho|\delta D|}{D}\left[J_z^{(11)}J_\pm^{(1)} - J_z^{(12)}J_\pm^{(2)}\right]\frac{1}{\sqrt{2}}c_{1k}^\dagger S^+. \tag{3.31}$$

Comparing this with Eq. (3.24), we see that renormalization group flow equation for $J_\pm^{(1)}$ is,

$$\frac{d}{d\ell}J_\pm^{(1)} = -2\rho\left[J_z^{(11)}J_\pm^{(1)} - J_z^{(12)}J_\pm^{(2)}\right]. \tag{3.32}$$

The derivation of the scaling for $J_\pm^{(2)}$ is essentially identical and, combining this with Eq. (3.32), we arrive at the required scaling equations,

$$\frac{d}{d\ell}\begin{pmatrix}J_\pm^{(1)}\\ J_\pm^{(2)}\end{pmatrix} = -2\rho\begin{pmatrix}J_z^{(11)} & -J_z^{(12)}\\ -J_z^{(12)} & J_z^{(22)}\end{pmatrix}\begin{pmatrix}J_\pm^{(1)}\\ J_\pm^{(2)}\end{pmatrix}, \tag{3.33}$$

where $\ell \sim -\ln(D/D_0)$ and $\rho \sim 1/D_0$, with D the running cutoff energy and D_0 the initial electron bandwidth.

The renormalization flow of $J_\pm^{(j)}$ is governed by the eigenvalues of the matrix in Eq. (3.33), which remain constant due to the invariance of the $J_z^{(jj')}$. Since

$J_z^{(jj')} = t_j t'_j/2E_C$ we find that the matrix has the eigenvalues 0 and $\lambda = J_z^{(11)} + J_z^{(22)} = (t_1^2 + t_2^2)/2E_C$, such that

$$\begin{pmatrix} J_\pm^{(1)}(\ell) \\ J_\pm^{(2)}(\ell) \end{pmatrix} = \frac{t_1^2 - t_2^2}{t_1^2 + t_2^2} \begin{pmatrix} t_1 \\ -t_2 \end{pmatrix} \mathrm{e}^{-2\rho\lambda\ell} + \frac{2t_1 t_2}{t_1^2 + t_2^2} \begin{pmatrix} t_2 \\ t_1 \end{pmatrix}. \tag{3.34}$$

The scaling therefore interpolates between the bare $J_\pm^{(j)}$ values and the fixed points $\bar{J}_\pm^{(1)} = 2t_1 t_2^2/(t_1^2 + t_2^2)$ and $\bar{J}_\pm^{(2)} = 2t_1^2 t_2/(t_1^2 + t_2^2)$, as shown in Fig. 3.5, and does not display the weak or strong coupling behaviour of a regular Kondo system. We note that this scaling only takes place in the case of asymmetric tunnel couplings, since if $|t_1| = |t_2|$ the first term in Eq. (3.34) is always zero. Although the fixed point is finite and the Hamiltonian maintains its form, the resulting state has an involved non-local, many-body structure. This is exemplified by the fact that the tunnel coupling asymmetry, $t_1 > t_2$, is reversed such that $t_1^* < t_2^*$ at the fixed point, showing that even for local coupling, the entire system including the leads is involved. Indeed, the state revealed above extends over both leads regardless of nanowire length, and is comprised of lead electrons, Majorana modes and the superconducting condensate. It is not unreasonable to suggest that such a state surpasses the threshold of being merely described as dressed and requires the many-body epithet.

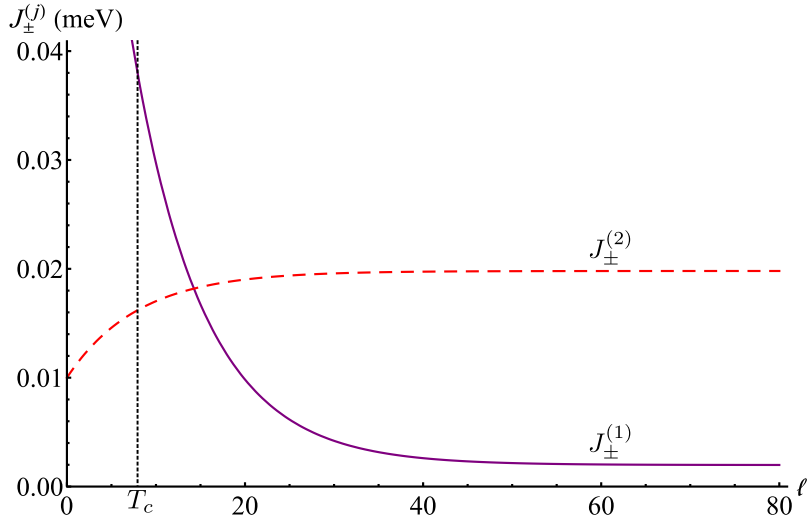

Figure 3.5: Change in anomalous tunnel couplings, $J_\pm^{(j)}$, with scaling parameter ℓ, as given by Eq. (3.34) using the system parameters in Table 3.1. The solid purple and dashed red lines show $J_\pm^{(1)}$ and $J_\pm^{(2)}$, respectively. The vertical dashed black line is the value of ℓ corresponding to the crossover temperature $T_c = 2$mK. The couplings display a rapid, exponential change from their initial values of t_1 and t_2 as ℓ increases. This high temperature sensitivity even far above T_c is due to the large ratio $t_1/t_2 = 10$.

It must be stressed that the existence of the 0 eigenvalue is a direct consequence of the $S^z s^y$ term in the Hamiltonian which incorporates the teleportation contribution

unique to the Majorana system, and that the scaling equations (3.34) would be hard to obtain in any other system. In the absence of the $S^z s^y$ term, the renormalization would flow to the regular weak coupling limit of the ferromagnetic Kondo model.

A significant consideration is whether or not the fixed point $\bar{J}_{\pm}^{(j)}$ will be reached in practice. The final value for ℓ is determined by the cutoff scale D and the renormalization stops when D becomes equal to the thermal energy $k_B T$ or any voltage bias applied to the system. The crossover scale from the bare to the renormalized values is obtained by setting $2\rho\lambda\ell \sim 1$, which resolves to

$$k_B T_c \sim D_0 \mathrm{e}^{-1/2\rho\lambda} = D_0 \mathrm{e}^{-E_C D_0/(t_1^2+t_2^2)}. \tag{3.35}$$

But, since the $J_{\pm}^{(j)}$ only renormalize for $t_1 \neq t_2$, this only makes sense for substantially different t_1 and t_2, as otherwise the changes in $J_{\pm}^{(j)}$ are small. Substituting realistic system parameters from Table 3.1, which imply $T_c = 2\mathrm{mK}$, into Eq. (3.35), we notice that the flow is very slow, and practically the fixed point is never reached. Due to this it is also of little relevance if the fixed point remains finite when further corrections beyond Poor Man's scaling are taken into account. Such corrections have an even slower renormalization flow and are always cut off before becoming important.

3.3 Transport

A straightforward verification of the behaviour predicted by Eq. (3.34) can be achieved by measuring the two terminal conductance of the topological superconductor through the Majorana states. Neglecting terms in Eq. (3.24) proportional to $J_z^{(jj')}$, which are a factor t/E_C smaller than the anomalous tunnelling processes, the effective tunnelling Hamiltonian is given by $H_T = \sum_k [J_{\pm}^{(1)} c_{1k}^\dagger f + J_{\pm}^{(2)} c_{2k}^\dagger f + \mathrm{h.c.}]$, where we define the composite fermion, $f = d^\dagger e^{-i\phi}$, and where the amplitudes $J_{\pm}^{(j)}$ are the results of the renormalization flow. This tunnelling Hamiltonian describes transitions between the two states of the system in the low energy sector, namely,

$$|\alpha\rangle = |N, 0\rangle\,, \qquad |\beta\rangle = |N-1, 1\rangle\,, \tag{3.36}$$

where we have written the states in the form $|N_C, n_d\rangle$.

3.3.1 Master Equation

To find the current through the nanowire as a result of H_T, we use a standard Master Equation approach, neglecting the influence of the excited states, since these have

been taken into account already via the Schrieffer-Wolff Transformation. We begin by considering how the probabilities of occupying $|\alpha\rangle$ and $|\beta\rangle$ change with time,

$$\begin{aligned}\dot{P}_\alpha &= \Gamma_{\beta\to\alpha}P_\beta - \Gamma_{\alpha\to\beta}P_\alpha \\ \dot{P}_\beta &= \Gamma_{\alpha\to\beta}P_\alpha - \Gamma_{\beta\to\alpha}P_\beta,\end{aligned} \tag{3.37}$$

where $\Gamma_{i\to f}$ is the scattering rate from $|i\rangle$ to $|f\rangle$ and consists of contributions from both the left and right leads i.e. $\Gamma_{i\to f} = \Gamma^l_{i\to f} + \Gamma^r_{i\to f}$. Imposing the steady-state condition $\dot{P}_\alpha = \dot{P}_\beta = 0$, along with the normalisation condition $P_\alpha + P_\beta = 1$ we find that,

$$\begin{aligned}P_\alpha &= \frac{\Gamma_{\beta\to\alpha}}{\Gamma_{\beta\to\alpha} + \Gamma_{\alpha\to\beta}} \\ P_\beta &= \frac{\Gamma_{\alpha\to\beta}}{\Gamma_{\beta\to\alpha} + \Gamma_{\alpha\to\beta}}.\end{aligned} \tag{3.38}$$

Now, the current through the device is given by,

$$I = e\left(\Gamma^l_{\beta\to\alpha}P_\beta - \Gamma^l_{\alpha\to\beta}P_\alpha\right), \tag{3.39}$$

since $|\alpha\rangle$ and $|\beta\rangle$ correspond to states with $2N$ and $2N-1$ electrons in the nanowire, respectively. Note that we have used the scattering rates arising from the left lead, but this choice is immaterial since any current through the device must be the same at both leads. Substituting (3.38) into (3.39) we find,

$$I = \frac{e}{\Gamma_{\beta\to\alpha} + \Gamma_{\alpha\to\beta}}\left[\Gamma^l_{\beta\to\alpha}\Gamma^r_{\alpha\to\beta} - \Gamma^l_{\alpha\to\beta}\Gamma^r_{\beta\to\alpha}\right], \tag{3.40}$$

where we have used the fact that $\Gamma_{i\to f} = \Gamma^l_{i\to f} + \Gamma^r_{i\to f}$ and cancelled the two $\Gamma^l_{\alpha\to\beta}\Gamma^l_{\alpha\to\beta}$ terms. The scattering rates can be found by applying Fermi's Golden Rule which, in this case, becomes,

$$\Gamma^j_{\beta\to\alpha} = \frac{2\pi}{\hbar}\sum_k |J^{(j)}_\pm|^2\delta\left(\epsilon_k + E_\beta - E - E_\alpha\right) f\left(\epsilon_k - \mu_j\right), \tag{3.41}$$

where ϵ_k is the energy of electrons in the lead, E is the energy of electrons in the nanowire, E_α is the energy of the state $|\alpha\rangle$, E_β is the energy of the state $|\beta\rangle$, f is the Fermi function and μ_j is the chemical potential of the jth lead. Since the system is in the low energy sector, $E_\alpha = E_\beta = \frac{E_C}{4}, E = 0$ and so,

$$\Gamma^j_{\beta\to\alpha} = \frac{2\pi}{\hbar}|J^{(j)}_\pm|^2 f\left(-\mu_j\right)\rho. \tag{3.42}$$

Similarly,

$$\Gamma^j_{\alpha\to\beta} = \frac{2\pi}{\hbar}|J^{(j)}_\pm|^2\left[1 - f\left(-\mu_j\right)\right]\rho, \tag{3.43}$$

with ρ the density of states in the leads. The factor of $[1 - f(-\mu_j)]$ in (3.43) accounts for the fact that there must be an unoccupied lead state for the $|\alpha\rangle \to |\beta\rangle$ transition to take place. Now, we consider applying a voltage, V to the left lead, this implies,

$$\mu_l = eV, \qquad \mu_r = 0, \tag{3.44}$$

and so the scattering rates are given by,

$$\begin{aligned} \Gamma^l_{\beta\to\alpha} &= \frac{2\pi}{\hbar}|J^{(1)}_\pm|^2 f(-eV)\,\rho, \\ \Gamma^r_{\beta\to\alpha} &= \frac{2\pi}{\hbar}|J^{(2)}_\pm|^2 f(0)\,\rho, \\ \Gamma^l_{\alpha\to\beta} &= \frac{2\pi}{\hbar}|J^{(1)}_\pm|^2 [1 - f(-eV)]\,\rho, \\ \Gamma^r_{\alpha\to\beta} &= \frac{2\pi}{\hbar}|J^{(2)}_\pm|^2 [1 - f(0)]\,\rho. \end{aligned} \tag{3.45}$$

Substituting the relations from (3.45) into Eq. (3.39), we find that,

$$I = \frac{2\pi e}{\hbar}\frac{|J^{(1)}_\pm|^2|J^{(2)}_\pm|^2}{|J^{(1)}_\pm|^2 + |J^{(2)}_\pm|^2}\,[f(-eV) - f(0)]\,\rho, \tag{3.46}$$

then using the standard expression for the Fermi function this becomes,

$$I = \frac{\pi e\rho}{\hbar}\frac{|J^{(1)}_\pm|^2|J^{(2)}_\pm|^2}{|J^{(1)}_\pm|^2 + |J^{(2)}_\pm|^2}\tanh\left(\frac{eV}{2k_BT}\right). \tag{3.47}$$

The differential conductance $G = \frac{\mathrm{d}I}{\mathrm{d}V}$ is therefore given by,

$$G = \frac{\pi e^2\rho}{2\hbar k_BT}\frac{|J^{(1)}_\pm|^2|J^{(2)}_\pm|^2}{|J^{(1)}_\pm|^2 + |J^{(2)}_\pm|^2}\left[\cosh\left(\frac{eV}{2k_BT}\right)\right]^{-2}. \tag{3.48}$$

In the $V \ll k_BT$ limit this simplifies to,

$$G \simeq K\frac{|J^{(1)}_\pm|^2|J^{(2)}_\pm|^2}{|J^{(1)}_\pm|^2 + |J^{(2)}_\pm|^2}, \tag{3.49}$$

where $K = \frac{\pi^2e^2\rho}{hk_BT}$. This result can also be obtained through the standard Green Function analysis of the resonant level model as in, for example, Ref. [145].

3.3.2 Conductance Signatures

In principle, the conductance offers two signatures of the many-body state found above. Firstly, at constant temperature, T, the variation of conductance with changing t_1, t_2 asymmetry is markedly different for $T \gg T_c$ and $T \ll T_c$. In the former case, the conductance is $G = K\frac{t_1^2t_2^2}{t_1^2+t_2^2}$, whereas, at low temperatures, we find that

$$G \simeq K\frac{2t_1^2t_2^2\left[2t_1^2t_2^2 + (t_1^2 - t_2^2)^2\,\mathrm{e}^{-\alpha}\right]}{(t_1^2 + t_2^2)^3} \text{ at } T \ll T_c, \tag{3.50}$$

where $\alpha = \frac{\ln(k_B T/D_0)}{\ln(k_B T_c/D_0)}$. However, for realistic system parameters, Eq. (3.50) implies that, even though T_c may be just about realisable in experiments, the temperature at which true fixed point behaviour is achieved is several orders of magnitude lower. For example, at a temperature of $T_c/10$ we find that $\mathrm{e}^{-\alpha} \approx 0.2$, whereas at the fixed point $\mathrm{e}^{-\alpha} = 0$.

We therefore propose a further test for the existence of a many-body state, at $T > T_c$. Fixing the system parameters, but varying T, results in a distinctive signature, as shown in Fig. 3.6. Here we plot the product of G and T, to remove the direct $1/T$ dependence in Eq. (3.49).

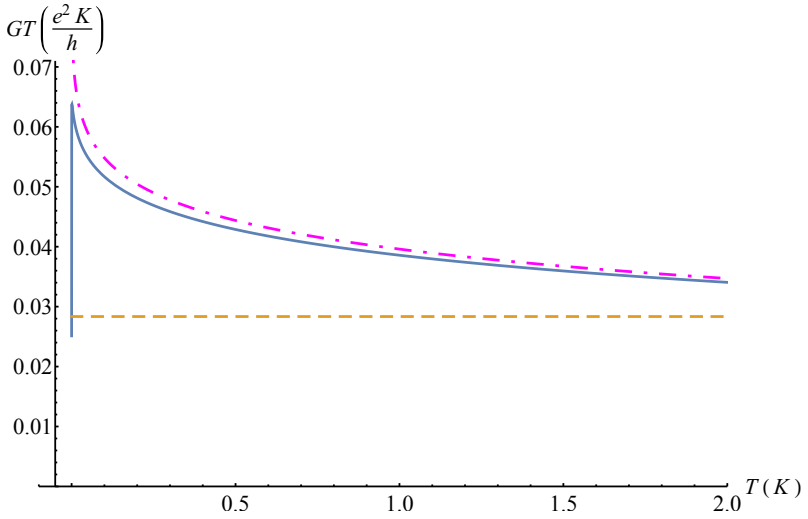

Figure 3.6: Variation of conductance amplitude with temperature, adjusted to account for generic $1/T$ dependence, as given by Eqs. (3.34) and (3.49). Note that the origin of the horizontal axis is offset for clarity. The solid blue line depicts the result for a many-body state whilst the dashed orange line corresponds to the bare tunnel couplings. The dot-dashed magenta line is a high temperature ($T \gg T_c$), high asymmetry ($t_1 \gg t_2$) approximation, $G = K t_2^2 \left(\mathrm{e}^{-2\alpha} - 4\mathrm{e}^{-\alpha} + 4\right)$, where $\alpha = \frac{\ln(k_B T/D_0)}{\ln(k_B T_c/D_0)}$. The parameters used, from Table 3.1, imply $T_c = 2\mathrm{mK}$.

It is remarkable that, even at temperatures well above T_c, there is a clear difference between the scaled result and the result found from the bare tunnel couplings. That the influence of the many-body state extends to such high temperatures is a result of the strong $J_{\pm}^{(jj')}$ dependence in both the numerator and denominator of Eq. (3.49). Observation of the characteristic behaviour shown in Fig. 3.6 appears to be within reach of current experiments and would provide compelling testament to the importance of many-body effects in this system.

3.4 Conclusions

Given the impact that the Kondo effect has had on the understanding of electron correlations in condensed matter, as well as the development of theoretical techniques to investigate those correlations, it seems plausible that some kind of topologically non-trivial analogue to the Kondo effect might be the source of deep insights into the sort of novel physics that can be facilitated by topological matter. Taking this idea as our motivation we have, in this chapter, investigated a floating topological superconductor. This setup represents a topologically non-trivial parallel to a traditional Kondo system: The Majorana modes of the superconducting condensate are analogous to magnetic impurities or quantum dots in the familiar Kondo effect, whilst the metallic leads fill the role of the electronic continuum.

One might initially expect this system to exhibit something close to conventional Kondo physics, possibly with a slight modification due to the presence of Majorana modes instead of localised topologically trivial states. However, as we have seen in this chapter, this is not the case. By using a Schrieffer-Wolff transformation to eliminate the high energy sector arising from capacitive coupling of the topological superconductor, we have found an effective Hamiltonian for the system that incorporates non-local scattering events dependent on the Majorana parity. Applying a scaling analysis to this effective Hamiltonian then reveals that the system flows to an intermediate fixed point, rather than the strong/weak coupling associated with the Kondo model. Indeed, it is clear that the existence of this intermediate scaling is directly contingent upon the presence of the Majorana Bound States.

This intermediate scaling behaviour should, in principle, be observable via a two terminal transport measurement in which we would anticipate the product of conductance and temperature, GT, displaying a distinct maximum at low temperatures.

The physics described above constitutes much more than simply a Kondo effect with Majoranas. Rather, it results from an involved interplay of Kondo and Majorana physics, motivating us to use the term *Kondorana* to describe this novel behaviour. As we shall see in the next chapter, Kondorana physics is not the only qualitatively distinct effect that can arise from electron-electron interactions in topologically non-trivial systems.

Chapter 4

Non-Equilibrium Charge Dynamics in Majorana-Josephson Devices

4.1 Introduction

In this chapter, we explore how the topologically protected Majorana bound states in a topological superconductor affect the non-equilibrium charge dynamics of a Josephson junction. The Josephson effect is one of the most prominent manifestations of superconducting phase coherence [106]. Whilst the effect owes its existence to microscopic quantum objects (Cooper Pairs), at the macroscopic level it is essentially classical in nature. There are, however, other phenomena associated with superconductors that do not admit such a classical description. As we discussed in Chapter 2, it was realised over thirty years ago [44] that the competition between charging and Josephson energies in a Josephson junction results in a system whose behaviour is directly analogous to that of an electron in a periodic potential. Just as the electron's properties depend periodically on its momentum, with period given by the reciprocal lattice vector, the observables associated with the junction are $2e$ periodic in charge, where $e > 0$ is the magnitude of the electronic charge. This periodicity is, fundamentally, contingent upon charge-phase conjugation and constitutes a macroscopic quantum phenomenon. That such a state of affairs can exist is interesting in its own right, and some experimental progress has been made in demonstrating that remarkable effects, such as Bloch Oscillations, can indeed be observed in such systems [116, 117]. However, the $2e$ periodicity acts as a barrier to interrogation of the system, since for ideal superconductors all sub-gap charge perturbations must be in multiples of $2e$ and therefore do not change the state of

the system.

By introducing a pair of MBSs into the system, we are not only able to overcome this obstacle, but also exploit the non-locality inherent to the MBSs. Taken together, the MBSs constitute a single fermionic state at zero energy which, due to interactions, persists even in rather short systems [146, 147]. The MBSs therefore allow single electrons from an external reservoir to tunnel into and out of the system, thereby permitting perturbations of the junction's electronic state in a way that is qualitatively distinct from the Cooper pair processes considered previously. Furthermore, the delocalised nature of the fermionic state corresponding to the two MBSs means that it permits current flow over an extended distance through the TSC. This non-local nature contrasts with the sub-gap quasiparticles that have been considered previously [148–152], which are believed to be due to thermal or photonic excitation and comprise a continuum of states [153]. As we shall see, it is this current through the TSC that allows controlled sub-gap perturbations of the Josephson junction. We will develop the theoretical formalism necessary to characterise such MBS mediated single-particle processes, and discuss the consequences of their existence on the charge dynamics of the Josephson junction. We will find that the system exhibits a rich variety of dynamic regimes which can be explored experimentally by varying its electrical inputs.

In Section 4.2 we will discuss the theoretical framework required to describe the dynamics of the Majorana-Josephson system. A thorough analysis of these dynamics is presented in Section 4.3, and the chapter concludes with a summary of the salient points of the Majorana-Josephson system in Section 4.4. Unless explicitly noted otherwise, the parameter values in Table 4.1 were used to produce all plots shown in this chapter. Furthermore, whenever a time average of V or I_X was carried out, the average was performed over an interval of 0.1μs.

4.2 Majorana-Josephson Hamiltonian

We consider the setup shown in Fig. 4.1, in which a one dimensional floating topological superconductor which has MBSs at its ends is coupled to three normal metal leads and connected, via a weak tunnelling junction, to a grounded s-wave superconductor. The behaviour of this system is the result of three distinct factors, namely charging energy, Josephson coupling and the MBSs. In this section we describe how we model these three components. The charging energy and Josephson coupling together give rise to quasicharge, which we discussed at length in Section 2.3

Parameter	Symbol	Value
Temperature	T	0.05K
Josephson Coupling	E_J	0.02meV
Charging Energy	E_C	0.1meV
Quasiparticle Conductance	G	e^2/h
Lead-TSC Tunnelling Coefficient	$\Gamma_{1,2}$	$10^{11}\mathrm{s}^{-1}$
Inter-Lead Voltage	$V_{1,2}$	0

Table 4.1: Representative parameters for the Majorana Josephson devices studied in this chapter. Values based in part on Refs. [86, 116, 117].

and we briefly review here in Subsection 4.2.1, whilst the evolution of quasicharge due to driving current is covered in Subsection 4.2.2. The MBSs mediate a single-particle tunnelling process between the metallic leads and TSC, which is described in Subsection 4.2.3.

4.2.1 Quasicharge and Band Structure

A setup very similar to Fig. 4.1 has previously been investigated in both theoretical [45, 119–122, 126, 133] and experimental [86] work, with the setup here being distinguished by the addition of a current biased Josephson coupling. It is therefore straightforward to write down the Hamiltonian associated with the TSC [44] (see also Ref. [148]),

$$H_{sc} = \frac{Q^2}{2C} - E_J \cos(\phi), \tag{4.1}$$

where Q is the total charge difference across the Josephson junction between the TSC and s-wave superconductor, C is the capacitance of the Josephson junction and ϕ is the phase of the TSC relative to the s-wave superconductor. As with all superconductors, the TSC obeys the charge-phase commutation relation,

$$[\phi, Q] = 2ei. \tag{4.2}$$

Using this, we rewrite (4.1) in terms of ϕ only,

$$H_{sc} = -E_C \frac{\partial^2}{\partial (\phi/2)^2} - E_J \cos(\phi), \tag{4.3}$$

where $E_C = \frac{e^2}{2C}$. Since the potential term in this Hamiltonian is periodic in ϕ, the solutions will take the familiar, periodic, Bloch form. In particular, the energies of

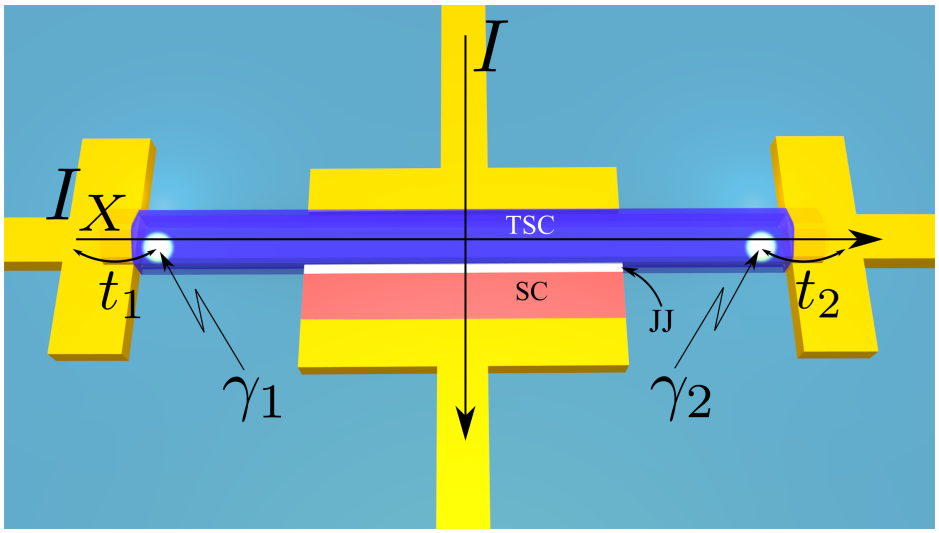

Figure 4.1: A floating topological superconductor (blue) hosting Majorana Bound States, $\gamma_{1,2}$ is coupled to normal metal leads (yellow) with tunnelling energies $\lambda_{1,2}$ and joined via an insulating weak link (white) to a grounded s-wave superconductor (red). A bias current I is passed through the Josephson junction. A transverse current I_X is established between the two metal leads, via the TSC, when there is a potential difference between them.

the Hamiltonian are given by $E_s(q)$ where s is a band index and $E_s(q) = E_s(q + 2e)$. The quasicharge, q, is directly analogous to the quasimomentum in a crystal lattice. It corresponds to the total charge on the TSC, modulo $2e$. The first two energy bands of Eq. (4.3) are shown as a function of q in Fig. 4.2. Throughout our analysis we will assume that the system is always in the lowest energy band and neglect inter-band processes. The justification for this approximation is as follows. There are two main mechanisms via which the Majorana-Josephson device might be excited to the second, or higher, energy bands in quasicharge space shown in Fig. 4.2. The first of these is straightforward thermal excitation, which has the usual probability,

$$P_T = \exp\left(-\frac{E_g}{k_B T}\right), \tag{4.4}$$

where E_g is the energy gap between the first and second bands. For the system parameters considered throughout this work, we find that, even at $q = \pm e$ where E_g takes its lowest value $E_g \approx E_J$, the excitation probability is only $P \approx 0.01$. This indicates that thermal excitation is likely to have a negligible impact and we therefore do not consider its influence in our analysis of the Majorana-Josephson device.

Of potentially greater significance for inter-band transitions is Landau-Zener

(LZ) tunnelling. The probability of this leading to an inter-band transition is [149],

$$P_Z \simeq \exp\left(-\frac{\pi e E_J^2}{\hbar E_C |I|}\right), \tag{4.5}$$

where $|I|$ is the bias current applied across the Josephson junction. Substituting in our system parameters, we find that $P_Z \approx 0.5$ for a bias current $I = 5\text{nA}$ and that P_Z is negligible only for $|I| \lesssim 0.1\text{nA}$. Hence, as we shall see, the rate of LZ tunnelling is appreciable in our system for most bias current values considered in this chapter. Despite this, we suggest that LZ tunnelling can be neglected in a description of the charge dynamics of the system. The reasoning behind this suggestion is that, whilst LZ tunnelling does mediate an inter-band transition in the vicinity of the quasicharge zone boundary, it does not change the value of the quasicharge. The effect of LZ tunnelling is just to increase the rate of Majorana tunnelling, given by Eq. (4.24) below, since the transition to a higher energy band causes subsequent Majorana tunnelling events to yield a more negative charging energy difference, δE_{ch}. However, at low temperatures, $\exp\left(\frac{\delta E_{ch}}{k_B T}\right) \simeq 0$ near the zone boundary, even in the lowest band and so the slightly enhanced tunnelling rate due to LZ transitions to the higher band is of little relevance. This point will, perhaps, be clarified by the exposition given in Subsection 4.2.3.

4.2.2 Slow Quasicharge Evolution

In addition to the charging and Josephson energies of the superconductor, the total Hamiltonian of the system also includes the current-phase interactions [111],

$$V_I = -\frac{\hbar}{2e} I(t)\,\phi, \;\; V_q = \frac{\hbar}{2e} I_q \phi, \tag{4.6}$$

in which $I(t)$ is the (possibly time dependent) bias current applied to the junction and I_q is a leakage current arising from the voltage across the Josephson junction associated with charge accumulation and carried via sub-gap quasiparticles in the superconductor, which exist independently of the MBSs. The exact origin of these quasiparticles is uncertain, indeed, they may have multiple sources, with the dominant source depending on the sample in question, but the existence of the quasiparticle current is an empirical fact [154] and so we include it in our model without overly concerning ourselves with its microscopic origin. Substituting $E_s(q)$ for the contribution to the Hamiltonian that comes solely from the superconductor, we see that the total junction Hamiltonian is given by,

$$H_{JJ} = E^{(s)}(q) - \frac{\hbar}{2e} I(t)\,\phi + \frac{\hbar}{2e} I_q \phi. \tag{4.7}$$

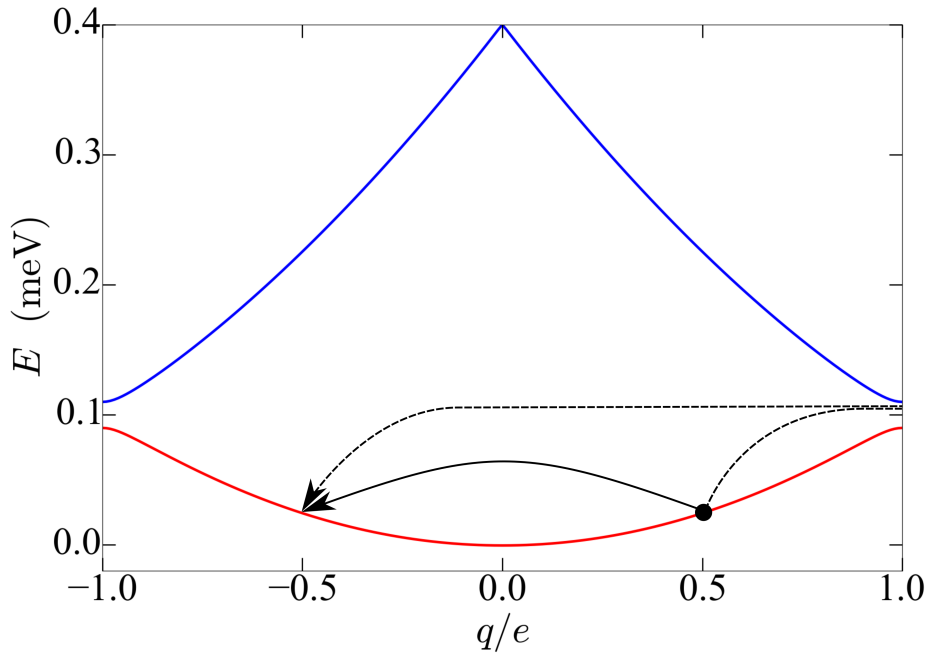

Figure 4.2: The band structure corresponding to Eq. (4.3) for $E_C = 0.1$meV and $E_J = 0.02$meV. Only the first (red) and second (blue) bands are shown. Note that the bandwidth of the first band is $\sim E_C$ whilst the band gap between the two bands is $\approx E_J$. Also shown are two Majorana tunnelling events at a typical value of $q \approx 0.5e$. The solid black line represents tunnelling of an electron from the TSC to a metallic lead, thereby reducing q by e. The dashed black line represents tunnelling of an electron from a metallic lead to the TSC, followed by a Bloch reflection in which a Cooper pair tunnels from the TSC to the s-wave superconductor, with the net result being that, once again, q is reduced by e.

As the first term in Eq. (4.7) depends only on q it is clear, from the commutation relation Eq. (4.2), that the time evolution of q depends only on the phase-current interaction terms and is given by, $\dot{q} = I(t) - I_q$. The quasiparticle current, I_q, is written formally as the product of quasiparticle mediated conductance, $G(\omega)$, and voltage, V, across the junction, $I_q = G(\omega)V$. In the single band approximation V is simply equal to $\mathrm{d}E_0/\mathrm{d}q$. Furthermore, the quasiparticle conductance is a constant $G(\omega) = G$, provided [44] $\omega \ll \frac{\Delta}{\hbar}$. Typically, $\Delta \approx 0.1\text{meV}$ and so G is constant for $\omega \ll 10^{11}\text{s}^{-1}$, which is true throughout the range of driving frequencies we study. Nevertheless, since G is a function of quasiparticle density, the exact value of G will vary depending on the superconductor and its environment [155]. Whilst this does introduce a random component to the value of G, and by extension I_q, previous work indicates that, for any given sample, G may be treated as constant over the timescales considered in this chapter [152, 154]. We therefore arrive at a Langevin-type equation for the quasicharge,

$$\dot{q} = I(t) - G\frac{\mathrm{d}E_0}{\mathrm{d}q}. \tag{4.8}$$

This evolution of the quasicharge is a result of both the bias current and the band structure resulting from the charging and Josephson energies. By analyzing Eq. (4.8) we conclude that the system exhibits two regimes. For low currents, specifically,

$$\frac{I}{G} < \max\left(\frac{\mathrm{d}E_0}{\mathrm{d}q}\right), \tag{4.9}$$

the quasicharge tends to a fixed point, q_0 where,

$$\left.\frac{\mathrm{d}E_0}{\mathrm{d}q}\right|_{q_0} = \frac{I}{G}. \tag{4.10}$$

Whilst for currents greater than those in Eq. (4.9) the quasicharge never assumes a constant value. From Eq. (4.8), $\dot{q} > 0$ at all times and so, since q is only defined modulo $2e$, the system executes Bloch oscillations with period,

$$\tau_B = \int_{-e}^{+e} \frac{\mathrm{d}q}{I - G\frac{\mathrm{d}E}{\mathrm{d}q}}. \tag{4.11}$$

We therefore define the Bloch oscillation threshold current, $I_B = G\max\left(\frac{\mathrm{d}E_0}{\mathrm{d}q}\right)$. Physically, these Bloch oscillations correspond to tunnelling of a Cooper Pair across the Josephson junction. These two cases, a static quasicharge for bias currents given by Eq. (4.9) and Bloch oscillations at larger currents, are illustrated in Fig. 4.3 (a) and (b) respectively, in the absence of Majorana tunnelling.

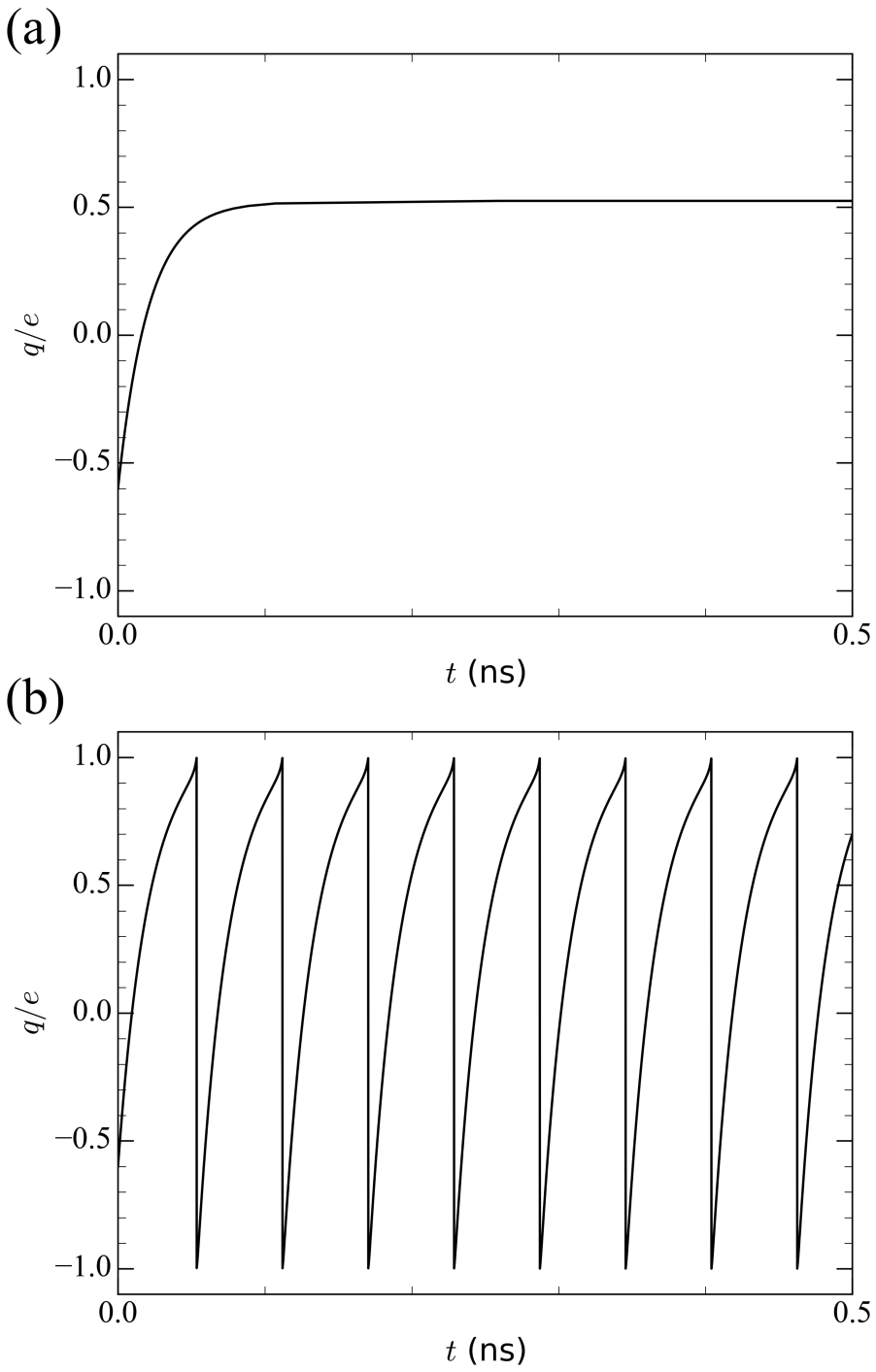

Figure 4.3: Evolution of quasicharge with time in the case of no Majorana tunnelling, with initial quasicharge $q_0 = -0.6e$. (a) A bias current of 4.0nA results in the quasicharge tending to a fixed value, $q = 0.52e$. (b) A bias current of 8.0nA gives rise to Bloch oscillations, as expected for $I_B = 6.2$nA.

4.2.3 Majorana-Mediated Single Particle Tunnelling

The results described above are a generic feature of Josephson junctions with a charging energy and do not depend upon the presence of MBSs. However, by considering the setup in Fig. 4.1 we find that the system has the potential to exhibit a much wider range of interesting phenomena when accompanied by MBSs. The presence of MBSs is notable, not only because they offer the possibility of single-particle tunnelling into the floating superconductor, below the superconducting gap, but also because their non-local nature enables transmission of current across the TSC. In this respect, the Majorana-Josephson device is essentially identical to the Kondorana setup considered in Chapter 3.

To determine the effects of the tunnelling process, we begin by finding the tunnelling rates associated with the MBS. The Hamiltonian describing tunnelling between the normal metallic leads and superconductor has been found previously by projecting the operators of the electrons in the superconductor onto an MBS manifold [66] and is given by,

$$H_T = \sum_{j,k} \lambda_j c^\dagger_{j,k} \gamma_j e^{-\frac{i\phi}{2}} + \text{h.c.}, \tag{4.12}$$

where $j = 1, 2$ indexes the two leads, λ_j are the tunnelling energies, $c_{j,k}$ is the operator for a fermion in lead j with momentum k and γ_j are the Majorana operators. Equation (4.12) is identical to Eq. (3.1), but is written in terms of Majorana operators, γ_j, rather than the fermion operators, η, with λ_j used for the tunnelling energies to avoid confusion with the time, t. The operator $e^{-\frac{i\phi}{2}}$ corresponds to annihilation of an electron in the superconductor and is required to ensure charge conservation. This factor, in concert with the charge conserving representation of γ gives rise to two tunnelling channels. Not only does the system exhibit normal tunnelling, in which electrons tunnel from the metallic leads directly to the MBSs, it also supports anomalous tunnelling, which involves splitting or forming a Cooper pair as part of the tunnelling process [45, 120, 121]. Note that we assume negligible overlap of MBS $\gamma_{1(2)}$ with lead 2(1), which is valid provided that the TSC is much longer than its coherence length. Even if this length condition were not true, a small overlap of MBS $\gamma_{1(2)}$ with lead 2(1) would not significantly affect our results. Furthermore, self-interaction effects of MBSs work against the energy splitting by the overlap and can cause a further pinning of the MBSs to zero energy [146, 147]. The absence of spin degeneracy in Eq. (4.12) is due to the spin polarisation of the MBSs [144], allowing electrons to be treated as spinless fermions for the purposes of tunnelling, despite the lead electrons being spinful. The spin polarization is inessential to the results reported in this chapter, but nonetheless is a feature of MBSs and

may have some relevance in the case of coupling to a more specialised system. The tunnelling rate corresponding to the MBSs may be calculated by applying Fermi's Golden Rule,

$$\Gamma = \frac{2\pi}{\hbar} \sum_{i,f} |\langle f| H_T |i\rangle|^2 w_i \delta (E_i - E_f), \tag{4.13}$$

where i and f label the initial and final states, respectively, w_i is a weighting factor associated with the initial states and $E_{i,f}$ are the energies of the initial and final states. We first consider the process in which an electron tunnels from the left ($j = 1$) or right ($j = 2$) metallic lead to the TSC, a process denoted by p, for particle. We may rewrite Eq. (4.13) in terms of $|i\rangle$ only, by noting that the tunnelling Hamiltonian given by Eq. (4.12) implies,

$$|f\rangle = e^{\frac{i\phi}{2}} \gamma_j c_{j,k} |i\rangle . \tag{4.14}$$

Hence, Eq. (4.13) becomes,

$$\Gamma_j^{(p)} = \frac{2\pi}{\hbar} \sum_i \left| \langle i| c_{j,k}^\dagger \gamma_j e^{-\frac{i\phi}{2}} \lambda_j e^{\frac{i\phi}{2}} \gamma_j c_{j,k} |i\rangle \right|^2 w_i \delta (E_i - E_f), \tag{4.15}$$

where we have not explicitly written out the conjugate term in H_T, since it makes no contribution. Using the identities, $\gamma_j^2 = \frac{1}{2}$ and $\left| \langle i| c_{j,k}^\dagger c_{j,k} |i\rangle \right|^2 w_i = f(\epsilon_k)$, with f the Fermi function and ϵ_k the energy of electrons in the metallic leads, we arrive at the expression,

$$\Gamma_j^{(p)} = \frac{\pi \lambda_j^2}{\hbar} \int f(\epsilon_k) \delta (E_i - E_f) \rho \, \mathrm{d}\epsilon_k, \tag{4.16}$$

in which we have used the density of states, ρ, to write the sum over the initial states as an integral over lead electron energies. Now, for tunnelling of electrons from the metallic leads to the TSC, the initial energy of the system is given by,

$$E_i = \epsilon_k - eV_j, \tag{4.17}$$

where we assume a lead bias V_j. The final energy of the system is,

$$E_f = \delta E_{ch}(q) + \epsilon_\gamma, \tag{4.18}$$

where ϵ_γ is the energy associated with occupation of the MBS pair due to hybridisation, which we neglect from now on. By $\delta E_{ch}(q)$ we denote the (quasicharge dependent) energy change on tunnelling of a single particle into or out of the TSC from the leads. We note that δE_{ch} depends on quasicharge alone, and not whether tunnelling is to or from the TSC. This is a direct consequence of the particle-hole symmetry imposed on the system by the Josephson coupling. To be more specific, the $2e$ periodicity in quasicharge mentioned above means that tunnelling of either a

particle or hole from a lead into the TSC results in the same energy change $\delta E_{ch}(q)$ in both cases, for any q, as shown by the solid and dashed arrows in Fig. 4.2. Substituting the expressions for E_i and E_f into Eq. (4.16) we find,

$$\Gamma_j^{(p)} = \frac{\pi\lambda_j^2}{\hbar}\int f(\epsilon_k)\,\delta(\epsilon_k - eV_j - \delta E_{ch})\,\rho\,\mathrm{d}\epsilon_k = \frac{\pi\rho\lambda_j^2}{\hbar} f(\delta E_{ch} + eV_j)\,. \tag{4.19}$$

The calculation is similar for the case where holes tunnel from the metallic leads to the TSC and we find that,

$$\Gamma_j^{(h)} = \frac{\pi\lambda_j^2}{\hbar}\int (1 - f(\epsilon_k))\,\delta(E_i - E_f)\,\rho\,\mathrm{d}\epsilon_k. \tag{4.20}$$

In this hole tunnelling case, the initial and final energies of the system are given by,

$$\begin{aligned} E_i &= \epsilon_\gamma \\ E_f &= \delta E_{ch}(q) + \epsilon_k - eV_j, \end{aligned} \tag{4.21}$$

and so the tunnelling rate becomes,

$$\Gamma_j^{(h)} = \frac{\pi\lambda_j^2}{\hbar}\int (1 - f(\epsilon_k))\,\delta(eV_j - \delta E_{ch} - \epsilon_k)\,\rho\,\mathrm{d}\epsilon_k, \tag{4.22}$$

where, once again, we neglect the MBS hybridisation energy, ϵ_γ. After performing the integral, and some algebraic manipulation, we find that,

$$\Gamma_j^{(h)} = \frac{\pi\rho\lambda_j^2}{\hbar}(1 - f(eV_j - \delta E_{ch})) = \frac{\pi\rho\lambda_j^2}{\hbar} f(\delta E_{ch} - eV_j)\,. \tag{4.23}$$

Combining Eqs. (4.19) and (4.23) immediately gives the total tunnelling rate between the metallic leads and TSC due the presence of MBSs,

$$\Gamma_{MBS} = \Gamma_1\zeta(\delta E_{ch}, V_1) + \Gamma_2\zeta(\delta E_{ch}, V_2)\,, \tag{4.24}$$

where $\Gamma_j = \pi\rho\lambda_j^2/\hbar$, and ζ is a combination of particle and hole Fermi functions given by,

$$\zeta(\delta E_{ch}, V) = \frac{1}{e^{\frac{\delta E_{ch}+eV}{k_B T}} + 1} + \frac{1}{e^{\frac{\delta E_{ch}-eV}{k_B T}} + 1}, \tag{4.25}$$

where T is the electron temperature and k_B is the Boltzmann constant. We have assumed that the density of states is identical in both the left (1) and right (2) leads (although this is not essential for Eq. (4.24) since any difference between the density of states can absorbed into the difference between Γ_1 and Γ_2), but that each lead has a voltage bias $V_{1,2}$. Note that the simple form of Eq. (4.24) is due, in part, to the $2e$ periodicity of q, discussed above, that is imposed by the Josephson coupling and results in identical energy changes for particle and hole tunnelling events. For an island without this $2e$ periodicity, particle and hole tunnelling events

are inequivalent and consequently have different charging energies associated with them, which results in a more complicated form for Γ_{MBS}. However, as can be seen from Eq. (4.25), the inherent particle-hole symmetry of Eq. (4.24) is broken by a finite bias voltage, $V_{1,2}$.

The impact of Eq. (4.24) on the charge dynamics of the Majorana-Josephson device can be summarised as follows. At low temperatures, $k_B T \ll |\delta E_{ch} \pm eV|$, we see from Eq. (4.25) that $\zeta \simeq 0$ when both $\delta E_{ch} + eV > 0$ and $\delta E_{ch} - eV > 0$, whilst if $\delta E_{ch} + eV < 0$ or $\delta E_{ch} - eV < 0$, or both expressions are less than zero, then ζ is of order 1 and tunnelling is likely. Since the factor $\Gamma_{1,2}$ in Eq. (4.24) is typically very large, the above observation implies that, in the low temperature limit, Γ_{MBS} transitions rapidly from zero to some very large number, as the values of δE_{ch} and eV change. From the expression for the charging energy, δE_{ch}, we find that, in the $T = 0$ limit, the tunnelling rate Γ_{MBS} is zero for $|q| < \frac{e}{2}\left(1 - \frac{eV}{E_C}\right)$ and very large otherwise. At finite temperatures the step boundary between tunnelling and non-tunnelling regimes is softened, but nonetheless we can identify an absolute value of the quasicharge above which tunnelling proceeds at a rapid rate and below which tunnelling is very slow. In particular, as the applied voltages, $V_{1,2}$, tend to zero, the threshold value of the quasicharge tends to $|q| = e/2$.

In addition to the MBSs there could be, in principle, other sub-gap quasiparticle states in the TSC [156], which may originate from thermal excitations or unintentional electromagnetic irradiation [153]. Previous experimental studies on superconducting qubits [154, 155] have found that the single-particle tunnelling rate corresponding to these quasiparticles is, $\Gamma_{QP} \sim 10^6 \mathrm{s}^{-1}$ which is much less than the typical rate associated with the MBSs, $\Gamma_{MBS} \sim 10^{11} \mathrm{s}^{-1}$, and so we safely neglect the influence of these non-topological quasiparticles. It is worth noting that, even if Γ_{QP} and Γ_{MBS} were comparable, the presence of the MBSs would give rise to qualitatively different effects from the quasiparticles. This is due to the well defined energy of the MBSs, compared with the continuum of energies adopted by the quasiparticles, which results in Γ_{MBS} being proportional to a Fermi function, whilst Γ_{QP} is proportional to a Bose function and so the two rates have qualitatively different temperature, E_C and $V_{1,2}$ dependence. Furthermore, the delocalised nature of the single particle state associated with the MBSs enables charge transport that would not necessarily be possible in the presence of non-topological quasiparticles alone.

A final point to consider in regard to tunnelling between the TSC and metallic leads is the influence of memory effects. That is to say, the impact of a given tunnelling

event on the probability of subsequent tunnelling events taking place. The most significant effect is that tunnelling changes the total charge on the TSC island, and the influence this has on future tunnelling probabilities is captured in the δE_{ch} terms that appear in Eq. (4.25). In principle there is an additional process which should be considered, in which the tunnelling event modifies the quantum state of the TSC beyond simply changing the total number of electrons. In this work we do not take into account the impact of this second consideration, for two reasons: firstly, the change in tunnelling probability associated with this process is likely to be negligible compared to the influence of macroscopic charging effects; secondly, a previous study into the relaxation of charge excitation "hotspots" in current biased superconductors [157] found that the system typically relaxed after around 50ps, which is shorter than the time scale of almost all the processes described in the rest of this chapter. This figure, 50ps, is likely to be much longer than the time scale of the processes we are neglecting, since it relates to an essentially classical excitation that is less susceptible to environmental damping. We therefore conclude that, as quantum relaxation is faster than classical relaxation, and classical relaxation takes around 50ps which is shorter than the time scales of processes studied in this chapter, we are justified in neglecting the effect of essentially quantum changes to the state of the system. Nevertheless, it is possible that the very fast "ringing" phenomena which is described later will be modified by quantum memory effects and this would be an interesting effect to study theoretically or experimentally in the future.

4.3 Device Dynamics

Several parameters influence the behaviour of the Majorana-Josephson system, such that it is impractical to simultaneously capture the effect of all of them in a single analysis. However, in the case of a static bias current, there are three main quantities of interest, namely the magnitude of the bias current, I that appears in Eq. (4.8), the tunnelling rates from the normal leads to the TSC, $\Gamma_{1,2}$, and the bias voltages, $V_{1,2}$, of the leads. By considering only the impact of variations in these three quantities, it is possible to describe the salient features of the Majorana-Josephson system's dynamics in an easily accessible manner.

We determine the dynamics of the Majorana-Josephson system by solving Eq. (4.8) with the classical Runge-Kutta algorithm and incorporate the influence of the MBSs by using a Monte Carlo approach to find the tunnelling rate given by Eq. (4.24). To appreciate the method in more detail, we first note that the dynamics of the Majorana-Josephson system can be understood with reference to the qua-

sicharge, $q(t)$, and so the numerical approach is essentially concerned with finding this quantity for a given set of system parameters and then using $q(t)$ to find any other variable desired.

The dynamics of $q(t)$ are described by Eq. (4.8) and we integrate it using the standard Runge-Kutta 4th order algorithm. To obtain $E_0(q)$, on the right hand side of Eq. (4.8), we must find the ground state energy of the Hamiltonian, H_{sc}, given by Eq. (4.3). As H_{sc} is of the Bloch form, we take as our ansatz the wave function,

$$\Psi = \sum_m a_m^{(q)} e^{i\phi\left(\frac{q}{2e}+m\right)}, \tag{4.26}$$

with $m \in \mathbb{Z}$. Substituting this into the Schrödinger equation with H_{sc} gives,

$$\begin{aligned} \sum_m \Bigg\{ & -4E_C \left(\frac{q}{2e}+m\right)^2 a_m^{(q)} e^{i\phi\left(\frac{q}{2e}+m\right)} \\ & + \frac{E_J}{2}\left(a_m^{(q)} e^{i\phi\left(\frac{q}{2e}+m+1\right)} + a_m^{(q)} e^{i\phi\left(\frac{q}{2e}+m-1\right)}\right) \\ & + E a_m^{(q)} e^{i\phi\left(\frac{q}{2e}+m\right)} \Bigg\} = 0. \end{aligned} \tag{4.27}$$

Relabelling indices as appropriate and requiring that each $e^{i\phi\left(\frac{q}{2e}+m\right)}$ vanishes, we find,

$$-4E_C \left(\frac{q}{2e}+m\right)^2 a_m^{(q)} + \frac{E_J}{2}\left(a_{m-1}^{(q)} + a_{m+1}^{(q)}\right) + E a_m^{(q)} = 0, \tag{4.28}$$

which represents an infinite set of simultaneous equations. Note that, since the potential term in H_{sc} is proportional to $\cos(\phi)$, $a_m^{(q)}$ couples only to $a_{m\pm1}^{(q)}$. It turns out that the truncation, $-3 \leq m \leq 3$ is a very good approximation for our purposes. The energy of the lowest band, $E_0(q)$, can then be found by computing the lowest eigenvalue of the 7×7 matrix corresponding to Eq. (4.28) for values of q in the range $-e < q \leq e$.

The smooth evolution of $q(t)$ by Eq. (4.8) is interrupted by the sudden charge jumps caused by the tunnelling into and out of the MBSs. We therefore supplement the equation of motion by checking for single particle tunnelling during each time step of the integration, which is done in the usual way by comparison of a random number in the interval $[0, 1]$ with $\Gamma_{MBS}\Delta t$, where Δt is the integration time step. Since tunnelling may occur through both leads simultaneously two independent checks are performed for the left and right leads. Furthermore Bloch reflections and oscillations are implemented when appropriate.

Having established $q(t)$ and $E_0(q)$, the junction voltage at any time can be found using the relation $V = dE_0/dq$, which is evaluated numerically. The transverse current I_X is calculated by a minor addition to the Runge-Kutta algorithm which counts the net flow of charge between the metallic leads through the TSC.

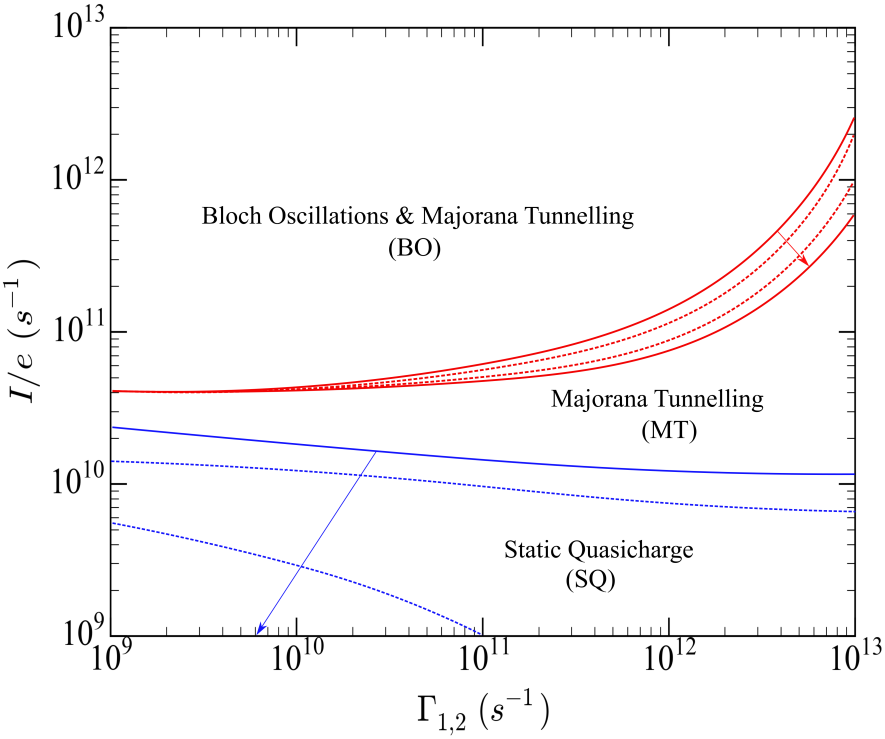

Figure 4.4: Regime diagram for the Majorana-Josephson system, plotted in terms of bias current, I, across Josephson junction and tunnelling rate $\Gamma_{1,2} = \Gamma_1 = \Gamma_2$ from normal leads to TSC. The SQ regime corresponds to a constant quasicharge with no tunnelling, in the MT regime quasicharge intermittently changes by $1e$ due to tunnelling via MBSs, whilst in the BO regime the junction exhibits both Bloch oscillations and MBS mediated tunnelling. SQ-MT and MT-BO regime boundaries are shown in blue and red, respectively. Solid lines indicate regime boundaries for bias voltages $V_2 = -V_1 = 0.0$ or 0.1mV, whilst dashed lines correspond to bias voltages of $V_2 = -V_1 = 0.03$ or 0.07mV, with arrows indicating increasing voltage magnitude. Note that at a bias voltage of 0.1mV the SQ regime is extinguished and no SQ-MT boundary is visible. The parameters $E_C = 0.1$meV and $E_J = 0.02$meV imply that $I_\theta/e = 2.4 \times 10^{10}\text{s}^{-1}$ and $I_B/e = 3.9 \times 10^{10}\text{s}^{-1}$.

4.3.1 Time Evolution of Quasicharge

Quasicharge is the most basic quantity upon which other dynamic variables depend, and so we begin by establishing a comprehensive picture of quasicharge dynamics throughout the whole of the system's parameter space. This information is presented in the regime diagram shown in Fig. 4.4.

We sort the behaviour of the system into three broad categories: Static Quasicharge (SQ), for which the bias and leakage currents in Eq. (4.8) exactly balance and the quasicharge remains at a constant value below $0.5e$; Majorana Tunnelling (MT), where the bias current, I, is not sufficiently large to drive the quasicharge to the zone boundary, but nonetheless is large enough to force the system into a regime where MBS mediated tunnelling becomes appreciable; Bloch Oscillations and Majorana Tunnelling (BO), in which tunnelling rates are appreciable, as in MT, but I is sufficiently large to drive the quasicharge to the zone boundary, resulting in Bloch oscillations. Note that whilst we denote this regime simply BO for convenience, the dynamics of the system consists primarily of Majorana tunnelling, with occasional Bloch oscillations. Examples of the different regimes are shown in Fig. 4.5. We note, in particular, the difference between Fig. 4.5c and Fig. 4.3b, which highlights the effect of the MBSs, namely enabling single particle tunnelling and consequently suppressing Bloch oscillations. It is worth emphasising that choosing to classify the Majorana-Josephson system according to these three regimes is somewhat arbitrary, particularly in the case of BO since there is little meaningful physical distinction between Bloch oscillations resulting from slow evolution of the quasicharge to the zone boundary, as in BO, and those Bloch reflections caused by Majorana tunnelling events that rapidly drive the system outside of the quasicharge Brillouin Zone, as occurs in both BO and MT. Furthermore, the stochastic nature of the system behaviour means that the position, and indeed existence, of the regime boundaries in Fig. 4.4 is not a universal property, but rather depends on the timescale over which the system is studied. In the long time limit, the SQ regime no longer exists and the MT-BO boundary is a line of constant I. Nevertheless, the classification shown in Fig. 4.4 is meaningful, in that the behaviour of the system does change significantly as its parameters change, but one should be cautious about interpreting Fig. 4.4 as a phase diagram in the usual sense of the term.

It is straightforward to understand the general form of Fig. 4.4. The bias current sets the long-time, zero-tunnelling, equilibrium quasicharge, in accordance with Eq. (4.10).

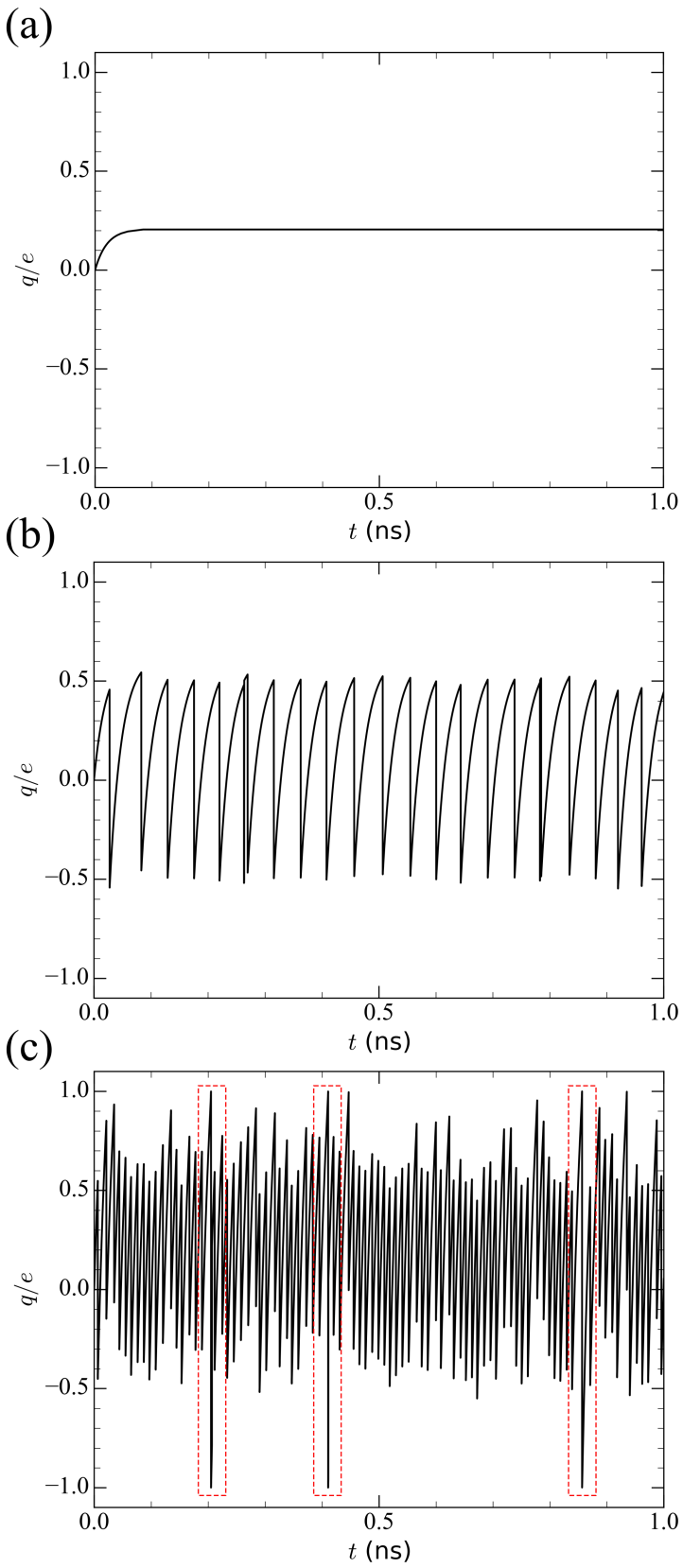

Figure 4.5: Examples of quasicharge behaviour for the three different regimes shown in Fig. 4.4. (a) Static Quasicharge, SQ ($I = 1.6$nA). (b) Majorana Tunnelling, MT ($I = 4.8$nA). (c) Bloch Oscillations, BO ($I = 16.0$nA). The red dashed outlines in (c) indicate Bloch Oscillations.

There are essentially three distinct bias current ranges:

- When the bias current is less than the threshold current for Majorana tunnelling, I_θ, we have,
$$I < I_\theta = G \left.\frac{\mathrm{d}E_0}{\mathrm{d}q}\right|_{e/2}, \tag{4.29}$$
and the system tends to a steady state with $q < e/2$.

- When the bias current is greater than I_θ, but less than the Bloch oscillation threshold current, I_B, we have $I_\theta < I < I_B = G\mathrm{max}\left(\frac{\mathrm{d}E_0}{\mathrm{d}q}\right)$ and the equilibrium quasicharge is in the range $e/2 < q < e$.

- At large bias currents, $I > I_B$, the system does not adopt a stable value of q but rather, in the zero-tunnelling limit, executes Bloch Oscillations.

Since the probability of MBS mediated tunnelling becomes very large for $q > 0.5e$ (if $T \simeq 0, V_{1,2} = 0$), for the system to be in the SQ regime, it is necessary that $I < I_\theta$, which is supported by Fig. 4.4. However, for high tunnelling rates, $\Gamma_{1,2}$, even at $q \lesssim 0.5e$ the probability of tunnelling can be appreciable and so the SQ regime persists only to lower values of bias current, as can be seen in Fig. 4.4.

Similarly, for $I < I_B$ there is no possibility of Bloch Oscillations, which is consistent with the observation that the MT-BO regime boundary does not descend below I_B in Fig. 4.4. We also see that, as the tunnelling rate increases, the MT-BO boundary shifts linearly to higher bias currents. In essence, an increase in the Majorana tunnelling rate decreases the probability that the quasicharge will evolve slowly to the zone boundary without undergoing a discrete jump due to Majorana tunnelling. A larger bias current is therefore required to more quickly drive the quasicharge towards the zone boundary. In Subsection 4.3.2 we shall discuss in more detail the role that Majorana tunnelling has to play in the promotion or suppression of Bloch oscillations.

4.3.2 Bias Voltage Dependence

Figure 4.4 also shows how the regime boundaries evolve on changing the bias voltages, $V_{1,2}$ in the left and right normal leads. The red and blue arrows indicate increasing bias voltage magnitude. We see that the SQ-MT boundary shifts to progressively lower values of bias current as $|V_{1,2}|$ increases. This is explained by examining the role of bias voltage in Eq. (4.25). For $V = 0$ and $T \simeq 0$, the exponential term in the denominator of ζ is large for $\delta E_{ch} > 0$ and so the tunnelling rate is small for values of q corresponding to $\delta E_{ch} > 0$, viz. $q < e/2$. However, if $V \neq 0$,

then even when $\delta E_{ch} > 0$ one of the two exponentials in Eq. (4.25) will be small, provided $\delta E_{ch} \pm eV < 0$ in which case the tunnelling rate will be large despite the charging energy associated with tunnelling being positive. As $|V|$ increases, progressively more positive values of δE_{ch} conform to the requirement $\delta E_{ch} \pm eV < 0$ and so the region in q-space where tunnelling rates are appreciable grows. That is to say, if $V = 0$ tunnelling is only appreciable for $|q| > e/2$, but if $V \neq 0$, then tunnelling is appreciable for $|q| > \frac{e}{2}\left(1 - \frac{V}{E_C}\right)$. The bias current, I, determines the equilibrium value of the quasicharge according to Eq. (4.10) with lower I corresponding to lower values of q_0. Consequently, as $|V|$ grows, increasing the range of quasicharge values for which tunnelling is appreciable, the SQ region, where tunnelling is negligible, corresponds to progressively lower values of the bias current.

The movement of the MT-BO regime boundary is, at first, more surprising. We previously discussed how, at high tunnelling rates, Majorana tunnelling leads to suppression of the BO region. We have also just seen how increasing bias voltage results in Majorana tunnelling in more of the quasicharge space. We might, therefore, expect increasing bias voltage to suppress the BO regime, but from Fig. 4.4 we see that the opposite is true: as bias voltage increases, the BO regime grows. To understand this result, we must fully appreciate the role that Majorana tunnelling plays in inhibiting or promoting Bloch oscillations. For a Bloch oscillation to take place, the quasicharge must evolve slowly to the zone boundary (as distinct from a Bloch reflection which occurs whenever the quasicharge reaches the zone boundary, slowly or by a sudden jump). Any processes which take the quasicharge closer to the zone boundaries therefore promote Bloch oscillations, whilst those that take q further from the zone boundaries inhibit Bloch oscillations. If tunnelling of a particle or hole takes place when $|q| > 0.5e$ then $|q|$ decreases, whilst if tunnelling takes place for $|q| < 0.5e$, $|q|$ increases, i.e. moves closer to a zone boundary. It follows that any change in the system parameters that increases the Majorana tunnelling rate for $|q| > 0.5e$ will decrease the probability of a Bloch Oscillation occurring, whilst changes that increase the tunnelling rate for $|q| < 0.5e$ will increase this probability. Recalling the preceding discussion on the SQ-MT boundary's movement with increasing bias voltage, we see that non-zero $V_{1,2}$ increases the total tunnelling rate for $|q| < 0.5e$ whilst having only a negligible impact for $|q| > 0.5e$, with the effect becoming more pronounced at larger $|V_{1,2,}|$. We therefore anticipate that the BO region will grow as $|V_{1,2}|$ increases, which we see in Fig. 4.4 is indeed the case.

4.3.3 Transverse Current Switching

We now consider the electrical properties of the Majorana-Josephson device, as shown in Fig. 4.6. Considering the transverse current, I_X, that is transmitted across the TSC between the normal leads biased at $V_{1,2}$, the system acts as a transistor controlled either by the bias current, I, across the Josephson junction, or the bias voltage, $V_{1,2}$, across the TSC. Referring back to Fig. 4.4, $I_X = 0$ when the system is in the SQ regime: no tunnelling implies no transfer of charge from the leads to the TSC and therefore no transverse current. In both the MT and BO regimes, tunnelling takes place at a high rate, resulting in an appreciable current. We note that our analysis includes only first order sequential tunnelling processes, an approximation valid in the large E_C regime where second order tunnelling processes are strongly suppressed. Since the system is not gated to a charge degeneracy point [121], but rather achieves charge degeneracy only intermittently due to the accumulation of charge caused by the bias current, I, the zero bias peak that is often regarded as a key characteristic of the MBSs does not contribute in a special way to I_X. Instead of remaining at the charge degeneracy point, the system is immediately driven away to different charging values.

Fixing the bias current and changing $V_{1,2}$ causes the SQ-MT regime boundary of the device to shift, as depicted in Fig. 4.4. Provided that the bias current and tunnelling rates are sufficiently low (such that the SQ regime is accessible in the first place) the system will cross the SQ-MT regime boundary at some finite bias voltage and transition from an insulating to conducting state, as shown in Fig. 4.6(b). The exact voltage at which this occurs depends linearly on I and exhibits a non-linear dependence on the tunnelling rate from leads to TSC. Similarly, if the bias voltage is held at a sufficiently low value for the SQ regime to have a finite size, and the bias current is increased, the system will cross the SQ-MT phase boundary and go from the insulating to conducting state. This scenario is shown in Fig. 4.6(a). In analogy with V_{switch}, the position of this crossing, I_{switch}, depends linearly on $V_{1,2}$ and also non-linearly on the tunnelling rate, $\Gamma_{1,2}$. A direct quantitative comparison between the sensitivity of $V_{switch}(I_{switch})$ to $I(V_{12})$ and V_{switch} or I_{switch} to $\Gamma_{1,2}$ is not particularly meaningful, due to the different dimensions of $V_{1,2}, I$ and $\Gamma_{1,2}$. However, from Fig. 4.4 it is possible to appreciate that, at least heuristically, the regime occupied by the Majorana-Josephson system has a rather weak dependence on $\Gamma_{1,2}$, compared to the stronger dependence on $V_{1,2}$ and I.

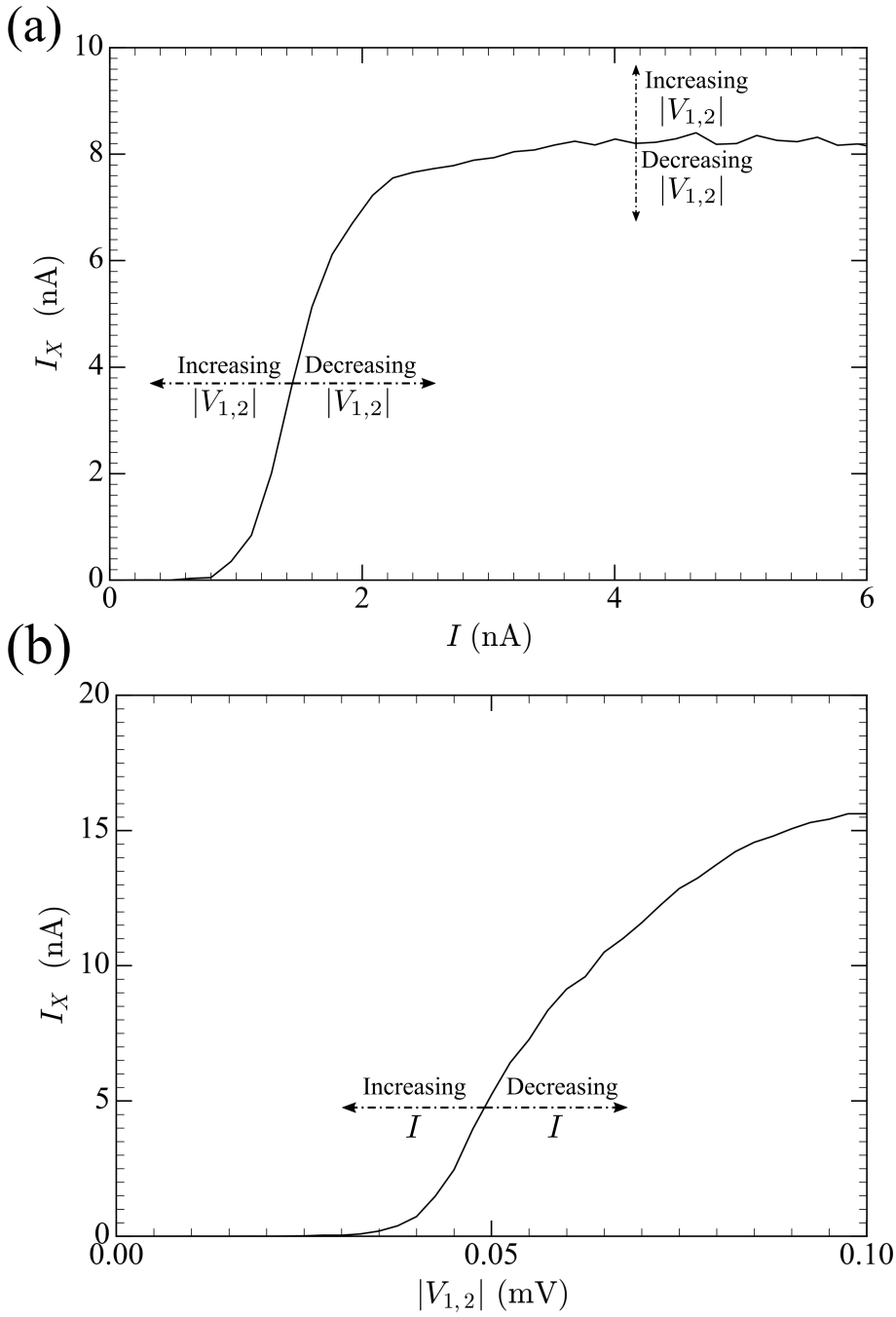

Figure 4.6: Electrical properties of the Majorana-Josephson device. (a) Time averaged I_X vs. bias current, I, across the Josephson junction. (b) Time averaged transverse current I_X vs. bias voltage, $V_2 = -V_1$, between the leads and TSC. Arrows indicate the qualitative change in (a) and (b) on changing $|V_{1,2}|$ and I, respectively. In (a), $V_2 = -V_1 = 0.05$mV whilst in (b) $I = 1.6$nA.

4.3.4 Time Dependent Driving Currents

Thus far, we have concerned ourselves only with static driving currents, but we now consider the effects of applying a time-varying bias current, $I = I(t)$. In particular, we imagine a current of the form $I = I_{DC} + I_{AC}\cos(2\pi f t)$, with $I_{DC}, I_{AC} > 0$ and study the response of the Majorana-Josephson system over a range of current amplitudes and frequencies.

There are two driving frequency-dependent quantities of interest: the voltage across the Josephson junction, $V = \frac{\mathrm{d}E_0}{\mathrm{d}q}$, and the transverse current through the TSC, I_X. We note that whilst the presence of a frequency-dependent junction voltage is a generic feature of any capacitive Josephson junction [152], the existence of a transverse current I_X is contingent upon the sub-gap Majorana bound states.

By considering the magnitudes of I_{DC} and I_{AC} relative to the current at which MBS mediated tunnelling takes place, I_θ, given by Eq. (4.29), we identify three different regimes of interest:

- The low bias regime, $I_{DC}, I_{AC} \ll I_\theta$.
- The intermediate bias regime, $I_{DC} \ll I_\theta, I_{DC} + I_{AC} \gtrsim I_\theta$.
- The high bias regime, $I_{DC} \gtrsim I_\theta, I_{AC} \neq 0$.

These three regimes originate from the behaviour of q with varying driving frequency. If driving is in the low current regime, $I_{DC}, I_{AC} \ll I_\theta$, then $I(t) < I_\theta$ for all t and so q never reaches a large enough value for Majorana tunnelling to be significant. In the intermediate current regime, $I_{DC} \ll I_\theta, I_{DC} + I_{AC} \gtrsim I_\theta$, we see that $I(t) \lesseqgtr I_\theta$, depending on the value of t. We might therefore expect Majorana tunnelling to take place at some point over one period of the bias current. However, this is not the case at high frequencies where, even though $I(t) > I_\theta$ for some values of t, there is not enough time for q to be driven to sufficiently large values for Majorana tunnelling to take place. In the high current regime, $I_{DC} \gtrsim I_\theta, I_{AC} \neq 0$, if $I_{DC} - I_{AC} > I_\theta$ then $I(t) > I_\theta$ for all t, whilst if $I_{DC} - I_{AC} < I_\theta$ then, as in the intermediate regime, $I(t) \lesseqgtr I_\theta$ depending on the value of t. The crucial difference between this and the intermediate regime is that, since $I_{DC} \gtrsim I_\theta$, even as $f \to \infty$ the quasicharge is still driven to large enough values for Majorana tunnelling to take place and so, unlike the intermediate regime, there is no cut-off frequency. Note that, whilst there are quantitative differences in the behaviour of I vs. f for the cases $I_{DC} - I_{AC} > I_\theta$ and $I_{DC} - I_{AC} < I_\theta$, there is no qualitative distinction between them and so we do not divide the high bias current regime along these lines. To reiterate, the existence of

three separate regimes is not so much a result of the value of $I(t)$ at different times, but rather the evolution of q at different frequencies.

The behaviour of the junction voltage, V, and transverse current, I_X in each of these three different regimes is shown in Fig. 4.7 and Fig. 4.8. With the exception of Fig. 4.7(a), most of the features of these plots discussed below are contingent on the presence of MBSs. The corresponding plots for the topologically trivial case are not shown, since they add very little to the discussion.

In the limit of low bias currents, $I_{DC}, I_{AC} \ll I_\theta$, the quasicharge takes a value of $q \ll e/2$ at all times and so Majorana tunnelling is negligible. This immediately implies both that the transverse current will vanish, $I_X = 0$ and that the evolution of q is determined entirely by Eq. (4.8). Furthermore, since $q \ll e$, the dispersion of the lowest energy band can be accurately modelled as $E_0 = \frac{E_C}{e^2}q^2$ and so the evolution of q is described by the equation,

$$\dot{q} = I_{DC} + I_{AC}\cos(2\pi f t) - \frac{2GE_C}{e^2}q. \tag{4.30}$$

The solution of this equation is elementary and gives $q(t)$. Then, using the fact that the voltage across the Josephson junction is given by $V = \frac{\mathrm{d}E_0}{\mathrm{d}q} \simeq \frac{2E_C}{e^2}q$, we find that,

$$\begin{aligned} V = \frac{2E_C}{e^2}\Bigg\{ & I_{AC}e^2\left[\frac{2GE_C\cos(2\pi f t) + 2\pi f e^2 \sin(2\pi f t)}{(2GE_C)^2 + (2\pi f e^2)^2}\right] \\ & + \left[q_0 - \frac{I_{DC}e^2}{2GE_C} - \frac{2I_{AC}e^2GE_C}{(2GE_C)^2 + (2\pi f e^2)^2}\right] e^{-\frac{2GE_C}{e^2}t} \\ & + \frac{I_{DC}e^2}{2GE_C}\Bigg\}, \end{aligned} \tag{4.31}$$

with the exponential term unlikely to be significant, since it decays rapidly for typical system parameters where $\frac{GE_C}{e^2} \sim 10^{10}\mathrm{s}^{-1}$. Over a long time interval (usually more than 100ns) the sinusoidal and exponential terms in Eq. (4.31) average to zero and we are left simply with the DC term,

$$\langle V \rangle_{\delta t \to \infty} \simeq \frac{I_{DC}}{G}, \tag{4.32}$$

which is independent of frequency. However, if instead we consider the variance of the average junction voltage, $\sigma_V^2 = \langle V^2 \rangle - \langle V \rangle^2$, then we find that,

$$\sigma_V^2 \simeq \frac{2\left(E_C I_{AC}\right)^2}{(2GE_C)^2 + (2\pi f e^2)^2}, \tag{4.33}$$

where we have neglected the rapidly decaying exponential terms in Eq. (4.31). We therefore see that, whilst the junction voltage itself is frequency independent, the

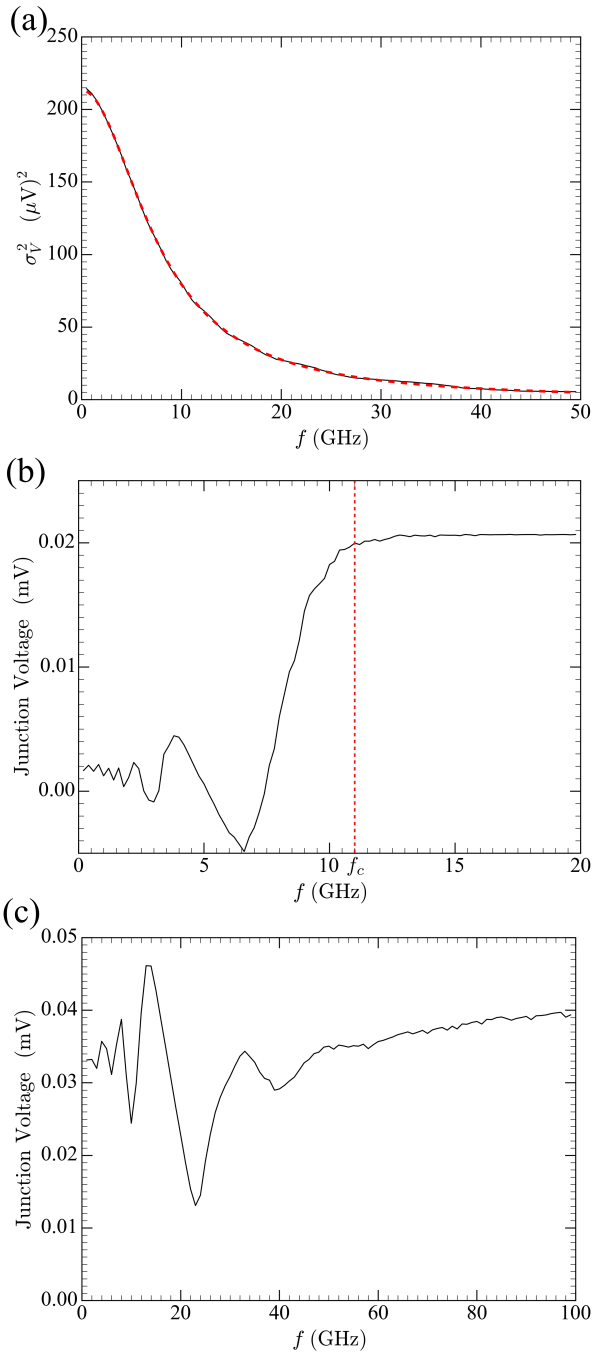

Figure 4.7: Time averaged voltage across Josephson junction, or variance of this voltage, as a function of bias current frequency for three different regimes. In all cases $I_\theta = 3.8\text{nA}$. (a) $I_{DC}, I_{AC} = 0.8\text{nA} \ll I_\theta$ and so $V(f)$ is approximated by Eq. (4.31), meaning that $\langle V \rangle_t \simeq I_{DC}/G$. We therefore plot the variance of V (solid black line) and compare it with the expected analytic result (dashed red line). (b) $I_{DC} = 0.8\text{nA} \ll I_\theta, I_{AC} + I_{DC} = 4.8\text{nA} \gtrsim I_\theta$ and $\langle V \rangle_t$ is suppressed below some cut-off frequency, f_c, marked by a dashed red line, whilst adopting a fixed value above it. (c) $I_{DC} = 4.0\text{nA} \gtrsim I_\theta, I_{AC} = 4.0\text{nA} \neq 0$ and the average junction voltage exhibits resonances at low frequencies, before increasing to a constant value at higher frequencies.

variance in the junction voltage has a driving frequency dependence which can be measured experimentally. The solid black line in Fig. 4.7(a) is a plot of σ_V^2 generated by simulation and is plotted along with the analytic result (dashed red line). As we would expect for a deterministic system, the analytic result is in excellent agreement with the simulation.

If the DC component of the bias current, I_{DC} is much less than the threshold current, I_θ, but the sum of the DC and AC components, I_{AC}, is greater than or similar to I_θ, then the total bias current applied to the Josephson junction will oscillate between values greater and less than the threshold current. By definition of I_θ, when $I > I_\theta$ the quasicharge is driven to values greater than $e/2$, whilst when $I < I_\theta$, the quasicharge tends towards a fixed value less than $e/2$. For Majorana tunnelling to take place, it is necessary that $I > I_\theta$ for long enough for the quasicharge to evolve to a value $q \gtrsim e/2$. Majorana tunnelling therefore occurs at low frequencies, but ceases above some cutoff frequency, f_c. This is clearly shown by the behaviour of I_X in Fig. 4.8(a), where $I_X = 0$ corresponds to no Majorana tunnelling. An approximate value for f_c can be calculated by considering the evolution of q according to Eq. (4.8). To find an analytic approximation for this frequency, we begin with the expression for q found by solving Eq. (4.8),

$$q \simeq \frac{I_{DC}e^2}{2GE_C} + I_{AC}e^2\left[\frac{2GE_C\cos(2\pi ft) + 2\pi fe^2\sin(2\pi ft)}{(2GE_C)^2 + (2\pi fe^2)^2}\right], \tag{4.34}$$

where we have suppressed the rapidly decaying exponential term. Now, for Majorana tunnelling to be negligible, we require that $q < q_c$ for all t, where q_c is the smallest value of the quasicharge for which tunnelling takes place at an appreciable rate. In the $T \to 0$ limit, $q_c = e/2$, but at the finite temperatures typically achieved in experiments on systems of the type we consider $q_c \approx 0.4e$. We therefore proceed by differentiating Eq. (4.34) with respect to t and finding the maximum value of q at any time, this is given straightforwardly by,

$$q_{max} = \frac{I_{AC}e^2}{\sqrt{(2GE_C)^2 + (2\pi fe^2)^2}} + \frac{I_{DC}e^2}{2GE_C}. \tag{4.35}$$

Setting $q_{max} = q_c$ and solving for f gives the required expression for the cut-off frequency in the intermediate bias regime,

$$f_c = \frac{1}{2\pi e^2}\left[\left(\frac{eI_{AC}}{\frac{q_c}{e} - \frac{eI_{DC}}{2GE_C}}\right)^2 - (2GE_C)^2\right]^{\frac{1}{2}}, \tag{4.36}$$

where q_c is the smallest magnitude of quasicharge for which Majorana tunnelling occurs at a significant rate. Taking $q_c = 0.4e$ and using the same system parame-

ters as in Fig. 4.8(a), the above formula predicts $f_c = 11\text{GHz}$, which we see is in reasonable agreement with the simulation. Note also that, just below f_c, there is a distinctive peak in I_X. With respect to the evolution of q, this can be understood as corresponding to the driving frequency which is high and so rapidly brings q to values near $e/2$, resulting in tunnelling, but is not so high as to cause cut-off. In plot (b) of Fig. 4.7 we see that, like the transverse current, the junction voltage adopts a constant value above some cut-off frequency. This behaviour can be understood in essentially the same terms as just described for I_X: at high frequencies there is no Majorana tunnelling and so, after time averaging, $\langle V \rangle = I_{DC}/G$, in accordance with Eq. (4.31); below f_c Majorana tunnelling results in an average value of q, and therefore V, of close to zero.

In the large bias current limit, $I_{DC} \gtrsim I_\theta, I_{AC} \neq 0$, there is no frequency at which Majorana tunnelling does not take place, and therefore no cutoff frequency. However, the AC component still has an effect on V and I_X, as shown in Fig. 4.7(c) and Fig. 4.8(b). Considering first the behaviour of the transverse current, we see that at high frequencies I_X adopts an approximately constant value, whilst at lower frequencies it behaves highly non-monotonically. In particular, I_X exhibits suppressions at the frequencies $f_s = \frac{n}{\tau}$, where τ is the average time between Majorana tunnelling events and n is an integer. As an aside, one can, in principle, formulate an analytical expression for τ, the stochastic nature of tunnelling means that, in practice, good agreement between the calculated and observed f_s is found only when τ is determined by numerical simulation.

To understand the origin of the suppressions of I_X at $f = \frac{n}{\tau}$, we must first appreciate what processes contribute to Majorana tunnelling and how these are affected by changes in the driving frequency. For the probability of a tunnelling event occurring to be non-negligible, q must have a sufficiently large value (typically $|q| \gtrsim \frac{e}{2}$). This value can come about in two ways: the quasicharge is driven by $I(t)$; a Majorana tunnelling event causes q to jump. Figure 4.9 is a plot of q vs. t for different driving frequencies, corresponding to the suppressions and non-suppressions seen in Fig. 4.8(b). From the plots in Fig. 4.9 it is clear that, whilst there is some variation, f has relatively little impact on τ, the time taken for q to be driven from $-e/2$ to $+e/2$. However, one should not infer from this that I_X is the same at all four frequencies since, whilst τ is relatively unchanged, there are significant differences in the number of Majorana tunnelling events that occur after q has been driven into the tunnelling regime. In plots (i) and (iii), we see that Majorana tunnelling events tend to occur singly, but in plots (ii) and (iv) there is a clustering of tunnelling events

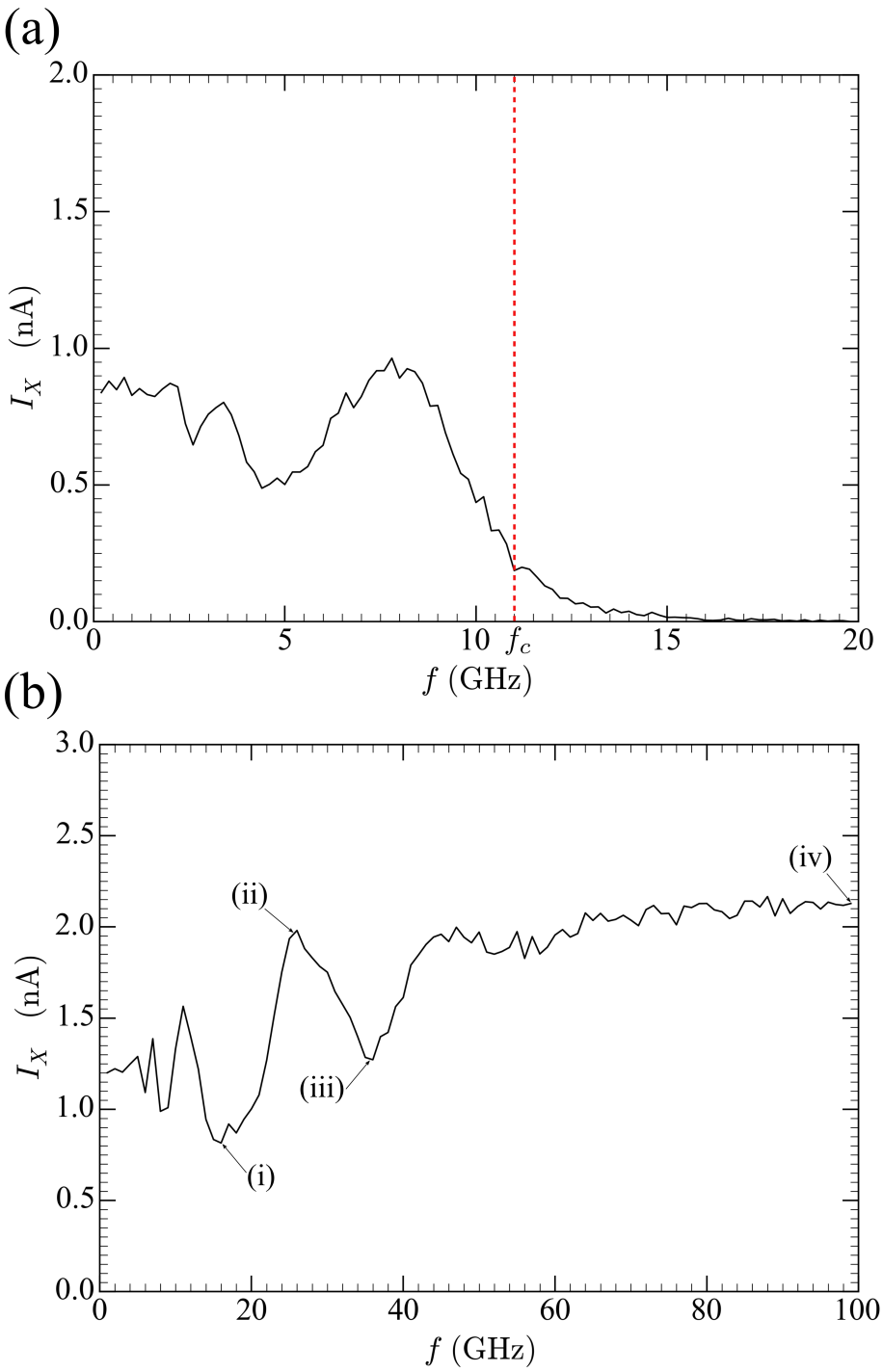

Figure 4.8: Transverse current, I_X, as a function of bias current frequency for two different regimes. In both cases $I_\theta = 3.8\text{nA}$. (a) $I_{DC} = 0.8\text{nA} \ll I_\theta, I_{DC} + I_{AC} = 4.8\text{nA} \gtrsim I_\theta$; the transverse current is finite below some threshold frequency and zero above it. (b) $I_{DC} = 4.0\text{nA} \gtrsim I_\theta, I_{AC} = 4.0\text{nA} \neq 0$ and I_X exhibits resonances at low frequencies, before increasing to a constant value at higher frequencies. Plots of q vs. t at the points (i)-(iv) are shown in Fig. 4.9. In the low bias regime, $I_{DC}, I_{AC} \ll I_\theta$, Majorana tunnelling between the leads and TSC is negligible, resulting in $I_X \simeq 0$. For both plots a bias voltage of $V_2 = -V_1 = 0.01\text{mV}$ was used.

such that, I_X is higher in both cases, compared with (i) and (iii). This "ringing" phenomenon where, instead of a single tunnelling event, several occur over a very short interval, is a result of jumps in q repeatedly causing $|q|$ to be sufficiently large for tunnelling to take place. Although the ringing phenomenon indicated by arrows in Fig. 4.9 is difficult to see, due to the very short time scale over which it takes place compared to normal tunnelling, a higher resolution comparison of ringing and single tunnelling events is shown in Fig. 4.10, where the single tunnelling events that make up the ringing are clearly visible. Note that Fig. 4.10 does not take into account possible memory effects, as described in Subsection 4.2.3, which may be of some importance, but for the reasons explained there we do not anticipate these effects making a significant qualitative difference to the results.

Ringing is suppressed if $I(t)$ rapidly drives the quasicharge to the region $|q| \ll \frac{e}{2}$ after a tunnelling event has taken place. Suppression of ringing therefore corresponds to $I(t)$ taking its maximum value immediately after a tunnelling event, i.e. we require that $\tau = \frac{n}{f_s}$, which is exactly the relation between f_s and τ observed in the simulations. In addition to $\tau = \frac{n}{f_s}$, suppression of ringing also requires a specific phase relationship between $I(t)$ and the quasicharge oscillations. However, this phase locking occurs naturally and so even if the initial phase offset for each frequency instance is randomised, as in Fig. 4.8(b), suppression of ringing, and therefore I_X, is still observed. Simulations of q vs. t for different initial phases demonstrate that the reason for the phase locking is that a positive or negative phase offset leads to a shorter or longer time τ to the next tunnel event, respectively. Thus each Majorana tunnelling reduces the offset and the latter vanishes after a few events. It follows that the observed I_X vs. f characteristics of the system are independent on the initial configurations.

It is also important to note that, even if the condition $f = \frac{n}{\tau}$ is satisfied, ringing will not be suppressed for high f, since each drive cycle will be too fast for q to be changed significantly. Quantitatively, we expect that, for $f \gg (I_{DC} + I_{AC})/e$, I_X will be approximately constant. This effect can be seen in Fig. 4.8(b). Although the suppression of ringing is the main contributor to the changes in I_X seen in Fig. 4.8(b), variation of τ also has a minor effect at some frequencies. This variation in τ is a result of $I(t)$ changing the average value of q over one quasicharge cycle and therefore affecting the average of $\dot{q}$ via the G term in Eq. (4.8). For example, comparing plots (a) and (b) in Fig. 4.9, we see that at the suppression point $f = 16.7$GHz, we obtain $\tau \approx 30$ps, whilst in between suppressions, at $f = 26.3$GHz, we obtain $\tau \approx 25$ps. From this change in τ alone, we would expect the suppressed value of I_X to be around 80% of the unsuppressed value, but since it is actually

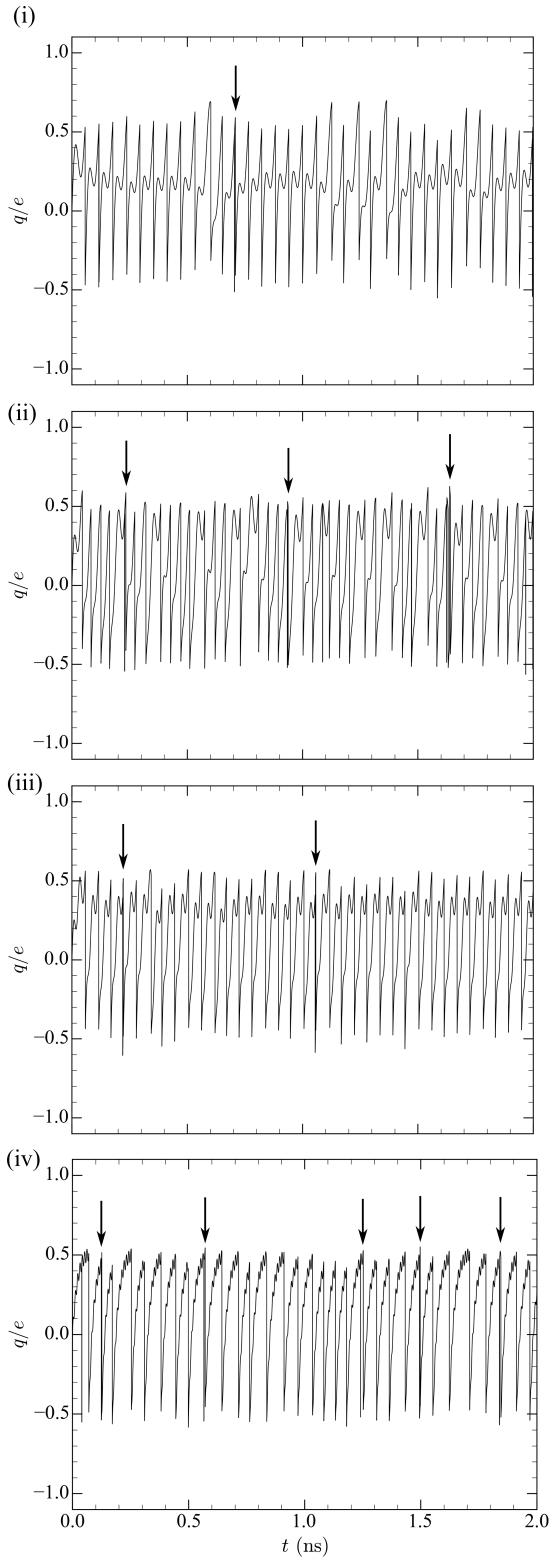

Figure 4.9: Typical plots of q vs. t at the frequencies identified in Fig. 4.8(b). Ringing events, indicated by arrows, are difficult to distinguish from normal tunnelling at this scale, but a clearer comparison is show in Fig. 4.10. Note that at the unsuppressed points, (ii) and (iv), there are more ringing events than at the suppressed points, (i) and (iii).

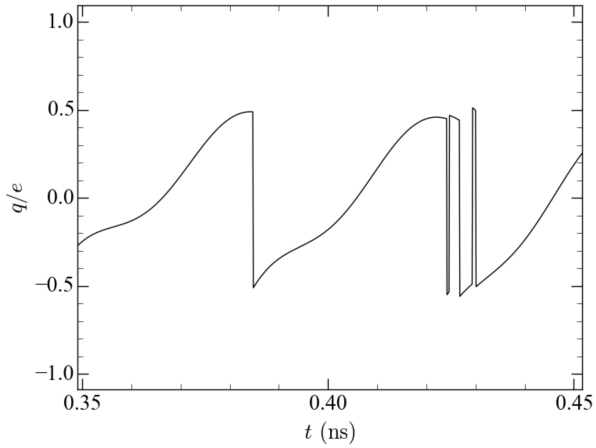

Figure 4.10: A detailed comparison of single Majorana tunnelling and ringing. A single Majorana tunnelling event takes place at $t \approx 0.38$ns, whilst a ringing event can be seen at $t \approx 0.43$ns. The ringing event constitutes five single tunnelling events over an interval of approximately 0.01ns, whilst the usual interval between single tunnelling events for the setup shown is 0.04ns. Ringing therefore has a very significant impact on the total charge transferred over a given time period, and therefore the average value of I_X.

only 40%, suppression of ringing is clearly a more important factor. Note also that, at $f = 100$GHz, we once again obtain $\tau \approx 30$ps, further emphasising that changes in τ are not as important as changes in the incidence of ringing as far as suppression of I_X is concerned. Panel (c) of Fig. 4.7 shows that the junction voltage, V, changes with f in a similar manner to I_X. The origin of this behaviour can be seen by examining a plot of q vs. t at different bias frequencies, from which it is clear that, at suppression points, q is driven rapidly from small values to the tunnelling regime, resulting in low average q, and therefore V. The mechanism which causes suppression of V is very different to the process described above that gives rise to a suppression of I_X. This is because, whilst ringing makes a major contribution to the transverse current, its effect on the average value of q, and therefore V, is very similar to that of normal Majorana tunnelling, since ringing is such a rapid process. Consequently, the values of f_s for V are not equal to the f_s for I_X.

As a final comment on the time-dependent driving phenomenology of the Majorana-Josephson system, it is worth noting that Fig. 4.7 and Fig. 4.8 depict changes in V and I_X over a frequency interval of the order of a few GHz, which may be at the limit of experimental accessibility. This is a direct consequence of the set of system parameters we have chosen to use in our simulations, in particular the values $\Gamma_{1,2} = 10^{11}\text{s}^{-1}$ and $G = e^2/h$, corresponding to what we expect for typical experimental setups. If, for example, we were to instead consider a system with

the less typical, but still experimentally achievable, parameter values of $\Gamma_{1,2} = 10^8 \mathrm{s}^{-1}$ and $G = 0.001e^2/h$, and decrease the magnitude of the bias current by a corresponding amount, then we would find that Fig. 4.7 and Fig. 4.8 were reproduced, but over a scale of MHz rather than GHz, and with the magnitude of I_X reduced by the same factor. The phenomenology, however, does not change. We therefore see that, since $\Gamma_{1,2}$ and G can be modified by careful gating of the system, the ability to measure at GHz frequencies is not required to observe the phenomena reported in this section.

4.4 Conclusions

In this chapter, we have seen how the presence of Majorana bound states in topological superconductors can enrich the behaviour of capacitive Josephson junctions. By enabling single-particle sub-gap tunnelling between the superconductor and its surroundings, MBSs allow the Josephson junction to be perturbed in a manner not consistent with the system's underlying periodicity, and thus to be excited to a non-equilibrium state. The resulting charge dynamics of the Majorana-Josephson system are dependent upon a variety of factors, but the essential parameters are the tunnelling rate between the superconductor and metallic leads and the magnitude and time dependence of the bias current applied to the Josephson junction. For a static bias current, the Majorana-Josephson system may be in one of three regimes, determined by tunnelling rate and current magnitude. If the bias current is sinusoidally varying, then the system's behaviour is a function of the current frequency in a way that depends upon the current magnitude.

The charge dynamics can be observed experimentally through measurement of the voltage across the Josephson junction, as in the non-topological case, or by studying the transverse current through the Majorana-Josephson device, the existence of which is made possible by the presence of an auxiliary fermionic state corresponding to a delocalised pair of MBSs. In either case, we have seen how experimental results can be directly linked to quasicharge behaviour.

To summarise the results of this chapter, we have seen how Majorana-Josephson devices represent an unusual arena in which to realise stochastic, non-equilibrium behaviour, made possible by the unique properties of Majorana bound states. This system provides a good example of how the interplay of topology and interactions can give rise to novel physics that can be studied both theoretically and through experiment.

Chapter 5

Summary and Outlook

Topology offers a way of understanding condensed matter systems that exhibit properties that cannot be explained purely within the paradigm of spontaneously broken symmetry. The widespread applicability of topology has become particularly apparent in the past fifteen years, as there has been a rapid increase in both theoretical and experimental exploration of this topic. Beyond simply understanding known states of matter, this research effort has led to the prediction, and subsequent observation, of novel phenomena which are not only of great physical interest in their own right, but also constitute promising tools in advanced engineering applications.

Remarkably, the successes of the topological paradigm have, in most cases, been achieved in spite of a highly idealised picture of electronic matter. In particular, many theoretical studies have used single-particle wave functions and so electron-electron interactions have been largely ignored when thinking about topologically non-trivial systems. That theoretical predictions have been so well born out by experiment, even under this severe approximation, is testament to the power of topology as a way of thinking about condensed matter systems. Nevertheless, it is desirable to go beyond a nearly-free electron type picture and consider what impact interactions might have on topological matter.

Some progress has been made in this direction already, albeit largely in the context of minimalistic toy models designed to be amenable to theoretical treatment, rather than realistic systems. There have been several studies concerned with how interactions might alter the topological classification of systems, which indicate that, depending on the specific circumstances, interactions may destroy or protect topological states. Furthermore, it has been suggested that topology is a result of long range entanglement, and therefore a manifestation of interactions [158]. However, there has previously been very little work on the question of what new physics might arise as a result of the interplay of interactions and topological states. It is this latter

question that we have attempted to answer, at least in part, over the course of this thesis.

If one hopes to observe new physics due to interactions in topological matter, it seems intuitive to draw inspiration from those non-topological systems that exhibit distinct behaviour that is directly attributable to interactions. In particular, we have looked at the Kondo effect, which is perhaps the example *par excellence* of novel physics driven by interactions, and also the case of the capacitive Josephson junction, which is possibly rather less well known, but nonetheless is an important illustration of how interactions can have a fundamental effect on the physics of condensed matter systems.

We have seen how one might go about constructing a topological extension of these two non-topological examples of interaction driven systems. For the Kondo case, the essential features are a single "impurity" state, which is in some way degenerate, with an on-site interaction energy and exchange coupled to an electron sea, which makes up a continuum of states. This scenario draws an immediate parallel with a pair of Majorana bound states, i.e. a single fermionic state, coupled to a pair of metallic leads and hosted in a floating topological superconductor. The most obvious difference between the two cases is the absence of spin in the Majorana realisation, with the degeneracy instead being a result of coupling a single fermionic state to two distinct leads. Hence, although not identical, there is a clear similarity between the Kondo system and its Majorana partner. The capacitive Josephson junction has a topological analogue of a somewhat different nature. Rather than try to realise a non-topological system with topological ingredients, we have instead seen how, by adding MBSs to the system, it can exhibit novel physics as a direct result of its new-found topology.

In Chapter 3, we considered a theoretical analysis for the Majorana analogue of the Kondo system. Beginning with a Hamiltonian comprised of lead electron, lead-TSC tunnelling and TSC charging energy terms, we carried out a Schrieffer-Wolff transformation to take into account the effect of excursions to the high energy sector on the behaviour of the system in the low energy sector. The resulting effective Hamiltonian bears some resemblance to the Kondo Hamiltonian, but is distinct in that it cannot be written as a pure spin-spin interaction and crucially there is, in addition to the $s^z S^z$ coupling present in the Kondo case, a coupling between the s^y pseudo-spin of the leads and S^z pseudo-spin associated with the MBSs, which is a direct result of the non-locality of the fermionic state associated with the MBSs.

On carrying out a Poor Man's scaling procedure to integrate out high energy processes in the leads, we find that, again in marked contrast to the Kondo case, the couplings between the metallic leads and TSC renormalize to an intermediate fixed point. The existence of this fixed point is directly contingent upon the $s^y S^z$ term in the effective Hamiltonian, which in turn depends on the non-local nature of the fermionic state formed from the two MBSs. The value of the couplings at the intermediate fixed point also demonstrates that the system plays host to a many-body state, de-localised across leads, MBSs and TSC. Perhaps the simplest experimental signature of this state would be an enhancement of the linear conductance through the system at low temperatures. The fact that the Majorana based implementation of the Kondo system exhibits behaviour that is distinct from that of the Kondo case provides motivation for the term Kondorana to describe this physics, which results from the marriage of Majorana and Kondo aspects.

The Majorana-Josephson device, discussed in Chapter 4, is a further example of novel physics, in this case arising as a result of the introduction of topological elements, the MBSs, into a system dominated by interactions, the capacitive Josephson junction. The presence of non-negligible interactions in a Josephson junction constrains the variation of the number of particles in the superconductor, taking the system outside the typical BCS regime, and necessitates treating the junction charge as a fully quantum variable. This in turn leads to an energy band structure as a function of the junction quasicharge, with an associated $2e$ periodic Brillouin Zone. The MBSs expand the phenomenology of this system for two reasons. Firstly, taken together they constitute a single-particle fermionic state within the superconducting gap, which therefore allows the system to be perturbed non-periodically. Secondly, the fermionic state is non-local and allows a transverse current to be established through the Majorana-Josephson device. By performing a numerical analysis, being careful to account for the stochastic nature of tunnelling to and from the MBSs, we can explore the consequences of these two properties. We find that the Majorana-Josephson device exhibits a rich dynamical landscape, with the behaviour of the system most strongly determined by two properties, the magnitude and time dependence of the driving current and the MBS tunnelling coefficient. For static driving currents, the system exhibits three regimes, as shown in Fig. 4.4. For a sinusoidally varying driving current, both the junction voltage and transverse current show non-monotonic behaviour as a function of the driving frequency. Both these observations can be explained by considering the time evolution of the junction quasicharge, which is characterised by intervals of slow evolution as a result of

the driving current, punctuated by rapid $1e$ jumps due to tunnelling via the MBSs. Of particular importance to the dynamics is the "ringing" phenomenon whereby the quasicharge undergoes a large number of $1e$ jumps over a very short interval. These findings illustrate how the addition of topological states to a strongly interacting system can greatly alter its behaviour beyond simple quantitative corrections.

The Kondorana and Majorana-Josephson systems are striking demonstrations of the interplay between topological matter and interactions, and the resulting physics that is qualitatively distinct from that which is present when one of the two is absent. On the one hand, for the Kondorana system, the interplay arises as a result of recreating the essential elements of a topologically trivial system, that is dominated by interactions, using MBSs. On the other hand, the Majorana-Josephson case shows how adding a topological state, the MBS, to a system with strong interactions can also result in novel physics. Taken together, these two examples offer encouraging evidence for the suggestion that, through exploiting topology and interactions in condensed matter, we may open up avenues to exciting new physics.

Over the course of this thesis, we have discussed in detail two systems in which the union of topology, or to be more specific Majorana Bound States, and electron-electron interactions results in novel physics. It seems reasonable to believe that these two cases are not unique and that there remains much research to be done and many effects to be discovered in this field. We therefore conclude by briefly considering possible extensions of the investigations described in the preceding pages. A potentially fruitful direction of research would be to extend the work presented here to topological states beyond the MBS. In particular, it would be interesting to see how the parafermions mentioned in Subsection 2.1.4 modify the behaviour of the Kondorana and Majorana-Josephson systems. Unfortunately, in contrast to Majoranas, there is no obvious representation of parafermions in terms of fermionic operators, and so the theoretical approach described here cannot be easily applied in the parafermion case, although there has been some recent progress on this point [159, 160]. A further topic worthy of investigation is the role played by the lead electrons in the Kondorana device. If the leads were to be modelled as a Luttinger liquid, this may well reveal new effects that are not apparent in the analysis presented here. A related point is the nature of the many-body state that extends across the leads and TSC in the Kondorana system, including its spin properties which are inaccessible via the Poor Man's scaling approach. The theoretical treatment of this problem is difficult, as the system appears resistant to the Bethe

Ansatz approach that is employed in the Kondo case. Nevertheless, a more thorough understanding of this point could lead to insights of importance not only for physics, but also engineering, as a device with components similar to the Kondorana setup could be expected to host this many-body state which may impact communication between the leads, or on an even larger scale.

The study of interaction effects led to profound advancements in the understanding of condensed matter during the second half of the 20th Century and topology has been an area of burgeoning interest during the early decades of the 21st. In this thesis we have seen how, at the interface of these two fields, diverse effects arise. We may justly anticipate that this interface will prove a fertile ground for new physics in the years to come.

Bibliography

[1] M. Baker and S. L. Glashow. "Spontaneous breakdown of elementary particle symmetries." *Phys. Rev.* **128**, 2462 (1962).

[2] P. W. Anderson. "Plasmons, gauge invariance, and mass." *Phys. Rev.* **130**, 439 (1963).

[3] Y. Nambu. "Nobel lecture: Spontaneous symmetry breaking in particle physics: A case of cross fertilization." *Rev. Mod. Phys.* **81**, 1015 (2009).

[4] P. W. Anderson and P. Morel. "Generalized Bardeen-Cooper-Schrieffer states and the proposed low-temperature phase of liquid He^3." *Phys. Rev.* **123**, 1911 (1961).

[5] D. D. Osheroff, R. C. Richardson and D. M. Lee. "Evidence for a new phase of solid He^3." *Phys. Rev. Lett.* **28**, 885 (1972).

[6] A. Leggett. *Quantum Liquids: Bose condensation and Cooper pairing in condensed-matter systems.* Oxford University Press, United States (2008).

[7] V. L. Berezinskiĭ. "Destruction of long-range order in one-dimensional and two-dimensional systems having a continuous symmetry group I. classical systems." *Sov. Phys. JETP* **32**, 493 (1971).

[8] J. M. Kosterlitz and D. J. Thouless. "Ordering, metastability and phase transitions in two-dimensional systems." *J. Phys. C* **6**, 1181 (1973).

[9] K. von Klitzing, G. Dorda and M. Pepper. "New method for high-accuracy determination of the fine-structure constant based on quantized Hall resistance." *Phys. Rev. Lett.* **45**, 494 (1980).

[10] R. B. Laughlin. "Quantized Hall conductivity in two dimensions." *Phys. Rev. B* **23**, 5632 (1981).

[11] D. C. Tsui, H. L. Stormer and A. C. Gossard. "Two-dimensional magnetotransport in the extreme quantum limit." *Phys. Rev. Lett.* **48**, 1559 (1982).

[12] D. J. Thouless, M. Kohmoto, M. P. Nightingale and M. den Nijs. "Quantized Hall conductance in a two-dimensional periodic potential." *Phys. Rev. Lett.* **49**, 405 (1982).

[13] M. Stone. *Quantum Hall Effect*. World Scientific (1992).

[14] D. J. Thouless. *Topological quantum numbers in nonrelativistic physics*. World Scientific, Singapore (1998).

[15] C. L. Kane and E. J. Mele. "$\mathbb{Z}_2$ topological order and the quantum spin Hall effect." *Phys. Rev. Lett.* **95**, 146802 (2005).

[16] B. A. Bernevig, T. L. Hughes and S.-C. Zhang. "Quantum spin Hall effect and topological phase transition in HgTe quantum wells." *Science* **314**, 1757 (2006).

[17] M. König, S. Wiedmann, C. Brüne, A. Roth, H. Buhmann, L. W. Molenkamp, X.-L. Qi and S.-C. Zhang. "Quantum spin Hall insulator state in HgTe quantum wells." *Science* **318**, 766 (2007).

[18] A. Kitaev. "Unpaired Majorana fermions in quantum wires." *Usp. Fiz. Nauk.* **131** (2001).

[19] A. P. Schnyder, S. Ryu, A. Furusaki and A. W. W. Ludwig. "Classification of topological insulators and superconductors in three spatial dimensions." *Phys. Rev. B* **78**, 195125 (2008).

[20] L. Fu and C. L. Kane. "Superconducting proximity effect and Majorana fermions at the surface of a topological insulator." *Phys. Rev. Lett.* **100**, 096407 (2008).

[21] V. Mourik, K. Zuo, S. M. Frolov, S. R. Plissard, E. P. A. M. Bakkers and L. P. Kouwenhoven. "Signatures of Majorana fermions in hybrid superconductor-semiconductor nanowire devices." *Science* **336**, 1003 (2012).

[22] G. Xu, H. Weng, Z. Wang, X. Dai and Z. Fang. "Chern semimetal and the quantized anomalous Hall effect in $HgCr_2Se_4$." *Phys. Rev. Lett.* **107**, 186806 (2011).

[23] X. Wan, A. M. Turner, A. Vishwanath and S. Y. Savrasov. "Topological semimetal and fermi-arc surface states in the electronic structure of pyrochlore iridates." *Phys. Rev. B* **83**, 205101 (2011).

[24] S.-Y. Xu, I. Belopolski, N. Alidoust, M. Neupane, G. Bian, C. Zhang, R. Sankar, G. Chang, Z. Yuan, C.-C. Lee, S.-M. Huang, H. Zheng, J. Ma, D. S. Sanchez, B. Wang, A. Bansil, F. Chou, P. P. Shibayev, H. Lin, S. Jia and M. Z. Hasan. "Discovery of a Weyl fermion semimetal and topological Fermi arcs." *Science* **349**, 613 (2015).

[25] C. Nayak, S. H. Simon, A. Stern, M. Freedman and S. Das Sarma. "Non-abelian anyons and topological quantum computation." *Rev. Mod. Phys.* **80**, 1083 (2008).

[26] F. D. M. Haldane. "Nobel lecture: Topological quantum matter." *Rev. Mod. Phys.* **89**, 040502 (2017).

[27] C. W. J. Beenakker. "Search for Majorana fermions in superconductors." *Annu. Rev. Condens. Matter Phys.* **4**, 113 (2013).

[28] E. Majorana. "Teoria simmetrica dell'elettrone e del positrone." *Il Nuovo Cimento* **14**, 171 (1937).

[29] A. S. Eddington. "A symmetrical treatment of the wave equation." *Proc. R. Soc. A* **121**, 524 (1928).

[30] J. Alicea. "New directions in the pursuit of Majorana fermions in solid state systems." *Rep. Prog. Phys.* **75**, 076501 (2012).

[31] S. Das Sarma, M. Freedman and C. Nayak. "Majorana zero modes and topological quantum computation." *npj Quantum Inf.* **1**, 15001 (2015).

[32] A. Y. Kitaev. "Fault-tolerant quantum computation by anyons." *Ann. Phys.* **303**, 2 (2003).

[33] D. A. Ivanov. "Non-Abelian statistics of half-quantum vortices in p-wave superconductors." *Phys. Rev. Lett.* **86**, 268 (2001).

[34] G. Castagnoli and M. Rasetti. "The notions of symmetry and computational feedback in the paradigm of steady, simultaneous quantum computation." *Int. J. Theor. Phys.* **32**, 2335 (1993).

[35] M. H. Freedman, M. Larsen and Z. Wang. "A modular functor which is universal for quantum computation." *Comm. Math Phys.* **227**, 605 (2002).

[36] K. Law, P. Lee and T. Ng. "Majorana fermion induced resonant Andreev reflection." *Phys. Rev. Lett.* **103**, 237001 (2009).

[37] P. W. Anderson. "Localized magnetic states in metals." *Phys. Rev.* **124**, 41 (1961).

[38] J. Kondo. "Resistance Minimum in Dilute Magnetic Alloys." *Prog. Theor. Phys.* **32**, 37 (1964).

[39] P. Nozières and A. Blandin. "Kondo effect in real metals." *J. Phys. France* **41**, 193 (1980).

[40] W. J. de Haas, J. de Boer and G. J. van dën Berg. "The electrical resistance of gold, copper and lead at low temperatures." *Physica* **1**, 1115 (1934).

[41] K. Le Hur. "Condensed-matter physics: Quantum dots and the Kondo effect." *Nature* **526**, 203 (2015).

[42] L. Kouwenhoven and L. Glazman. "Revival of the Kondo effect." *Physics World* **14**, 33 (2001).

[43] J. R. Schrieffer and P. A. Wolff. "Relation between the Anderson and Kondo Hamiltonians." *Phys. Rev.* **149**, 491 (1966).

[44] K. K. Likharev and A. B. Zorin. "Theory of the Bloch-wave oscillations in small Josephson junctions." *J. Low Temp. Phys.* **59**, 347 (1985).

[45] I. J. van Beek and B. Braunecker. "Non-Kondo many-body physics in a Majorana-based Kondo type system." *Phys. Rev. B* **94**, 115416 (2016).

[46] I. J. van Beek, A. Levy Yeyati and B. Braunecker. "Nonequilibrium charge dynamics in majorana-josephson devices." *Phys. Rev. B* **98**, 224502 (2018).

[47] C. Xu and J. E. Moore. "Stability of the quantum spin Hall effect: Effects of interactions, disorder, and $\mathbb{Z}_2$ topology." *Phys. Rev. B* **73**, 045322 (2006).

[48] J. C. Budich and B. Trauzettel. "From the adiabatic theorem of quantum mechanics to topological states of matter." *physica status solidi (RRL)* **7**, 109 (2013).

[49] Z. Wang and B. Yan. "Topological Hamiltonian as an exact tool for topological invariants." *J. Phys. Cond. Matt.* **25**, 155601 (2013).

[50] Z. Wang and S.-C. Zhang. "Topological invariants and ground-state wave functions of topological insulators on a torus." *Phys. Rev. X* **4**, 011006 (2014).

[51] S. Rachel. "Interacting topological insulators: a review." *Rep. Prog. Phys.* **81**, 116501 (2018).

[52] N. N. Bogoljubov, V. V. Tolmachov and D. V. Širkov. "A new method in the theory of superconductivity." *Fortschritte der Physik* **6**, 605 (1958).

[53] A. Altland and M. R. Zirnbauer. "Nonstandard symmetry classes in mesoscopic normal-superconducting hybrid structures." *Phys. Rev. B* **55**, 1142 (1997).

[54] C. Caroli, P. D. Gennes and J. Matricon. "Bound fermion states on a vortex line in a type II superconductor." *Phys. Lett.* **9**, 307 (1964).

[55] N. B. Kopnin and M. M. Salomaa. "Mutual friction in superfluid ^{3}He: Effects of bound states in the vortex core." *Phys. Rev. B* **44**, 9667 (1991).

[56] G. Volovik. "Fermion zero modes on vortices in chiral superconductors." *JETP Lett.* **70**, 609 (1999).

[57] N. Read and D. Green. "Paired states of fermions in two dimensions with breaking of parity and time-reversal symmetries and the fractional quantum Hall effect." *Phys. Rev. B* **61**, 10267 (2000).

[58] K. Ishida, H. Mukuda, Y. Kitaoka, K. Asayama, Z.Q. Mao, Y. Mori and Y. Maeno. "Spin-triplet superconductivity in Sr_2Ruo_4 identified by ^{17}O Knight shift." *Nature* **396**, 658 (1998).

[59] H. Tou, Y. Kitaoka, K. Asayama, N. Kimura, Y. Ōnuki, E. Yamamoto and K. Maezawa. "Odd-parity superconductivity with parallel spin pairing in UPt_3: Evidence from ^{195}Pt knight shift study." *Phys. Rev. Lett.* **77**, 1374 (1996).

[60] C. Kallin. "Chiral p-wave order in Sr_2RuO_4." *Rep. Prog. Phys.* **75**, 042501 (2012).

[61] E. Lieb, T. Schultz and D. Mattis. "Two soluble models of an antiferromagnetic chain." *Ann. Phys.* **16**, 407 (1961).

[62] W. Shockley. "On the surface states associated with a periodic potential." *Phys. Rev.* **56**, 317 (1939).

[63] M. Wimmer, A. R. Akhmerov, M. V. Medvedyeva, J. Tworzydło and C. W. J. Beenakker. "Majorana bound states without vortices in topological superconductors with electrostatic defects." *Phys. Rev. Lett.* **105**, 046803 (2010).

[64] Y. Oreg, G. Refael and F. von Oppen. "Helical liquids and Majorana bound states in quantum wires." *Phys. Rev. Lett.* **105**, 177002 (2010).

[65] R. M. Lutchyn, J. D. Sau and S. Das Sarma. "Majorana fermions and a topological phase transition in semiconductor-superconductor heterostructures." *Phys. Rev. Lett.* **105**, 1 (2010).

[66] K. Flensberg. "Tunneling characteristics of a chain ofMajorana bound states." *Phys. Rev. B* **82**, 180516 (2010).

[67] G. E. Blonder, M. Tinkham and T. M. Klapwijk. "Transition from metallic to tunneling regimes in superconducting microconstrictions: Excess current, charge imbalance, and supercurrent conversion." *Phys. Rev. B* **25**, 4515 (1982).

[68] A. Das, Y. Ronen, Y. Most, Y. Oreg, M. Heiblum and H. Shtrikman. "Zero-bias peaks and splitting in an Al–InAs nanowire topological superconductor as a signature of Majorana fermions." *Nat. Phys.* **8**, 887 (2012).

[69] M. T. Deng, C. L. Yu, G. Y. Huang, M. Larsson, P. Caroff and H. Q. Xu. "Anomalous zero-bias conductance peak in a Nb-InSb nanowire-Nb hybrid device." *Nano Lett.* **12**, 6414 (2012).

[70] H. O. H. Churchill, V. Fatemi, K. Grove-Rasmussen, M. T. Deng, P. Caroff, H. Q. Xu and C. M. Marcus. "Superconductor-nanowire devices from tunneling to the multichannel regime: Zero-bias oscillations and magnetoconductance crossover." *Phys. Rev. B* **87**, 1 (2013).

[71] S. Nadj-Perge, I. K. Drozdov, J. Li, H. Chen, S. Jeon, J. Seo, A. H. MacDonald, B. A. Bernevig and A. Yazdani. "Observation of Majorana fermions in ferromagnetic atomic chains on a superconductor - Supplementary Material." *Science* (2014).

[72] R. Pawlak, M. Kisiel, J. Klinovaja, T. Meier, S. Kawai, T. Glatzel, D. Loss and E. Meyer. "Probing atomic structure and Majorana wavefunctions in mono-atomic Fe chains on superconducting Pb surface." *npj Quantum Inf.* **2**, 16035 (2016).

[73] H. Kim, A. Palacio-Morales, T. Posske, L. Rózsa, K. Palotás, L. Szunyogh, M. Thorwart and R. Wiesendanger. "Toward tailoring Majorana bound states in artificially constructed magnetic atom chains on elemental superconductors." *Sci. Adv.* **4**, eaar5251 (2018).

[74] R. Heid, K.-P. Bohnen, I. Y. Sklyadneva and E. V. Chulkov. "Effect of spin-orbit coupling on the electron-phonon interaction of the superconductors Pb and Tl." *Phys. Rev. B* **81**, 174527 (2010).

[75] A. C. Potter and P. A. Lee. "Topological superconductivity and Majorana fermions in metallic surface states." *Phys. Rev. B* **85**, 094516 (2012).

[76] B. Braunecker and P. Simon. "Interplay between classical magnetic moments and superconductivity in quantum one-dimensional conductors: Toward a self-sustained topological Majorana phase." *Phys. Rev. Lett.* **111**, 147202 (2013).

[77] P. A. Lee. "Seeking out Majorana under the microscope." *Science* **346**, 545 (2014).

[78] Y. Peng, F. Pientka, L. I. Glazman and F. von Oppen. "Strong localization of Majorana end states in chains of magnetic adatoms." *Phys. Rev. Lett.* **114**, 106801 (2015).

[79] E. Dumitrescu, B. Roberts, S. Tewari, J. D. Sau and S. Das Sarma. "Majorana fermions in chiral topological ferromagnetic nanowires." *Phys. Rev. B* **91**, 094505 (2015).

[80] D. I. Pikulin, J. P. Dahlhaus, M. Wimmer, H. Schomerus and C. W. J. Beenakker. "A zero-voltage conductance peak from weak antilocalization in a Majorana nanowire." *New J. Phys.* **14**, 125011 (2012).

[81] K. J. Thomas, J. T. Nicholls, M. Y. Simmons, M. Pepper, D. R. Mace and D. A. Ritchie. "Possible spin polarization in a one-dimensional electron gas." *Phys. Rev. Lett.* **77**, 135 (1996).

[82] Y. Meir, K. Hirose and N. S. Wingreen. "Kondo model for the "0.7 anomaly" in transport through a quantum point contact." *Phys. Rev. Lett.* **89**, 196802 (2002).

[83] S. M. Cronenwett, H. J. Lynch, D. Goldhaber-Gordon, L. P. Kouwenhoven, C. M. Marcus, K. Hirose, N. S. Wingreen and V. Umansky. "Low-temperature fate of the 0.7 structure in a point contact: A Kondo-like correlated state in an open system." *Phys. Rev. Lett.* **88**, 226805 (2002).

[84] S. Takei, B. M. Fregoso, H.-Y. Hui, A. M. Lobos and S. Das Sarma. "Soft superconducting gap in semiconductor Majorana nanowires." *Phys. Rev. Lett.* **110**, 186803 (2013).

[85] E. J. H. Lee, X. Jiang, R. Aguado, G. Katsaros, C. M. Lieber and S. De Franceschi. "Zero-bias anomaly in a nanowire quantum dot coupled to superconductors." *Phys. Rev. Lett.* **109**, 186802 (2012).

[86] S. M. Albrecht, A. P. Higginbotham, M. Madsen, F. Kuemmeth, T. S. Jespersen, J. Nygård, P. Krogstrup and C. M. Marcus. "Exponential protection of zero modes in Majorana islands." *Nature* **531**, 206 (2016).

[87] P. San-Jose, E. Prada and R. Aguado. "AC Josephson effect in finite-length nanowire junctions with Majorana modes." *Phys. Rev. Lett.* **108**, 257001 (2012).

[88] J. Alicea. "Superconductors: Exponential boost for quantum information." *Nature* **531**, 177 (2016).

[89] E. Fradkin and L. P. Kadanoff. "Disorder variables and para-fermions in two-dimensional statistical mechanics." *Nucl. Phys. B* **170**, 1 (1980).

[90] N. H. Lindner, E. Berg, G. Refael and A. Stern. "Fractionalizing Majorana fermions: Non-abelian statistics on the edges of abelian quantum Hall states." *Phys. Rev. X* **2**, 041002 (2012).

[91] D. J. Clarke, J. Alicea and K. Shtengel. "Exotic non-abelian anyons from conventional fractional quantum Hall states." *Nat. Commun.* **4**, 1348 (2013).

[92] M. Barkeshli and X.-L. Qi. "Synthetic topological qubits in conventional bilayer quantum Hall systems." *Phys. Rev. X* **4**, 041035 (2014).

[93] F. Zhang and C. L. Kane. "Time-reversal-invariant $\mathbb{Z}_4$ fractional Josephson effect." *Phys. Rev. Lett.* **113**, 036401 (2014).

[94] C. P. Orth, R. P. Tiwari, T. Meng and T. L. Schmidt. "Non-abelian parafermions in time-reversal-invariant interacting helical systems." *Phys. Rev. B* **91**, 081406 (2015).

[95] J. Alicea and P. Fendley. "Topological phases with parafermions: Theory and blueprints." *Annu. Rev. Cond. Matt. Phys.* **7**, 119 (2016).

[96] D. K. C. Macdonald, W. B. Pearson and I. M. Templeton. "Thermo-electricity at low temperatures. IX. The transition metals as solute and solvent." *Proc. R. Soc. A* **266**, 161 (1962).

[97] M. P. Sarachik, E. Corenzwit and L. D. Longinotti. "Resistivity of Mo-Nb and Mo-Re Alloys containing 1 % Fe." *Phys. Rev.* **135**, A1041 (1964).

[98] O. S. Lutes and J. L. Schmit. "Low-temperature magnetic transitions in dilute Au-based alloys with Cr, Mn, and Fe." *Phys. Rev.* **134**, A676 (1964).

[99] G. J. van den Berg. "Anomalies in dilute metallic solutions of transition elements." In C. J. Gorter (editor), "Prog. Low Temp. Phys.", vol. 4, 194 (1964).

[100] P. Phillips. *Advanced Solid State Physics.* 2nd edn. Cambridge University Press (2012).

[101] Y. Nagaoka. "Self-consistent treatment of Kondo's effect in dilute alloys." *Phys. Rev.* **138**, A1112 (1965).

[102] A. A. Abrikosov. "Electron scattering on magnetic impurities in metals and anomalous resistivity effects." *Physics Physique Fizika* **2**, 5 (1965).

[103] P. W. Anderson. "A Poor man's derivation of scaling laws for the Kondo problem." *J. Phys. C* **3**, 2436 (1970).

[104] K. G. Wilson and J. Kogut. "The renormalization group and the ϵ expansion." *Phys. Rep.* **12**, 75 (1974).

[105] K. G. Wilson. "The renormalization group: Critical phenomena and the Kondo problem." *Rev. Mod. Phys.* **47**, 773 (1975).

[106] B. D. Josephson. "Possible new effects in superconductive tunnelling." *Phys. Lett.* **1**, 251 (1962).

[107] P. W. Anderson and J. M. Rowell. "Probable observation of the Josephson superconducting tunneling effect." *Phys. Rev. Lett.* **10**, 230 (1963).

[108] S. Shapiro. "Josephson currents in superconducting tunneling: The effect of microwaves and other observations." *Phys. Rev. Lett.* **11**, 80 (1963).

[109] P. Anderson. "Special effects in superconductivity." In "Lectures on the Many-body Problems," 113 – 135. Academic Press (1964).

[110] J. Bardeen, L. N. Cooper and J. R. Schrieffer. "Theory of superconductivity." *Phys. Rev.* **108**, 1175 (1957).

[111] A. I. Larkin, K. K. Likharev and Y. N. Ovchinnikov. "Secondary quantum macrpscopic effects in weak superconductivity." *Physica B+C* **126**, 414 (1984).

[112] F. Bloch. "Über die Quantenmechanik der Elektronen in Kristallgittern." *Zeitschrift fur Physik* **52**, 555 (1929).

[113] W. Zwerger, A. T. Dorsey and M. P. A. Fisher. "Effects of the phase periodicity on the quantum dynamics of a resistively shunted Josephson junction." *Phys. Rev. B* **34**, 6518 (1986).

[114] Y. N. Ovchinnikov and B. I. Ivlev. "Dissipative quantum mechanics of a particle in the washboard potential: Application to the Josephson junction." *Phys. Rev. B* **39**, 9000 (1989).

[115] B. I. Ivlev and Y. N. Ovchinnikov. "Interference of the Bloch oscillations in the Josephson junctions." *J. Low Temp. Phys.* **76**, 75 (1989).

[116] L. S. Kuzmin and D. B. Haviland. "Observation of the Bloch oscillations in an ultrasmall Josephson junction." *Phys. Rev. Lett.* **67**, 2890 (1991).

[117] F. Nguyen, N. Boulant, G. Ithier, P. Bertet, H. Pothier, D. Vion and D. Esteve. "Current to frequency conversion in a Josephson circuit." *Phys. Rev. Lett.* **99**, 187005 (2007).

[118] M. Sato and S. Fujimoto. "Topological phases of noncentrosymmetric superconductors: Edge states, Majorana fermions, and non-abelian statistics." *Phys. Rev. B* **79**, 094504 (2009).

[119] L. Fu. "Electron teleportation via Majorana bound states in a mesoscopic superconductor." *Phys. Rev. Lett.* **104**, 056402 (2010).

[120] A. Zazunov, A. Levy Yeyati and R. Egger. "Coulomb blockade of Majorana-fermion-induced transport." *Phys. Rev. B* **84**, 1 (2011).

[121] R. Hützen, A. Zazunov, B. Braunecker, A. Levy Yeyati and R. Egger. "Majorana single-charge transistor." *Phys. Rev. Lett.* **109**, 166403 (2012).

[122] A. Zazunov and R. Egger. "Supercurrent blockade in Josephson junctions with a Majorana wire." *Phys. Rev. B* **85**, 104514 (2012).

[123] Y. H. Wang, H. Steinberg, P. Jarillo-Herrero and N. Gedik. "Observation of Floquet-Bloch states on the surface of a topological insulator." *Science* **342**, 453 (2013).

[124] J. Ulrich and F. Hassler. "Majorana-assisted nonlocal electron transport through a floating topological superconductor." *Phys. Rev. B* **92**, 075443 (2015).

[125] J. D. Sau, B. Swingle and S. Tewari. "Proposal to probe quantum nonlocality of Majorana fermions in tunneling experiments." *Phys. Rev. B* **92**, 020511 (2015).

[126] S. Plugge, A. Zazunov, P. Sodano and R. Egger. "Majorana entanglement bridge." *Phys. Rev. B* **91**, 214507 (2015).

[127] S. Plugge, A. Zazunov, E. Eriksson, A. M. Tsvelik and R. Egger. "Kondo physics from quasiparticle poisoning in Majorana devices." *Phys. Rev. B* **93**, 104524 (2016).

[128] B. Béri and N. R. Cooper. "Topological Kondo effect with Majorana fermions." *Phys. Rev. Lett.* **109**, 156803 (2012).

[129] A. Altland and R. Egger. "Multiterminal Coulomb-Majorana junction." *Phys. Rev. Lett.* **110**, 196401 (2013).

[130] B. Béri. "Majorana-Klein hybridization in topological superconductor junctions." *Phys. Rev. Lett.* **110**, 216803 (2013).

[131] M. R. Galpin, A. K. Mitchell, J. Temaismithi, D. E. Logan, B. Béri and N. R. Cooper. "Conductance fingerprint of Majorana fermions in the topological Kondo effect." *Phys. Rev. B* **89**, 045143 (2014).

[132] A. Zazunov, A. Altland and R. Egger. "Transport properties of the Coulomb-Majorana junction." *New J. Phys.* **16**, 015010 (2014).

[133] A. Altland, B. Béri, R. Egger and A. M. Tsvelik. "Multichannel Kondo impurity dynamics in a Majorana device." *Phys. Rev. Lett.* **113**, 076401 (2014).

[134] A. Altland, B. Béri, R. Egger and A. M. Tsvelik. "Bethe ansatz solution of the topological Kondo model." *J. Phys. A* **47**, 265001 (2014).

[135] O. Kashuba and C. Timm. "Topological Kondo effect in transport through a superconducting wire with multiple Majorana end states." *Phys. Rev. Lett.* **114**, 116801 (2015).

[136] F. Buccheri, H. Babujian, V. E. Korepin, P. Sodano and A. Trombettoni. "Thermodynamics of the topological Kondo model." *Nucl. Phys. B* **896**, 52 (2015).

[137] M. Lee, J. S. Lim and R. López. "Kondo effect in a quantum dot side-coupled to a topological superconductor." *Phys. Rev. B* **87**, 241402 (2013).

[138] R. Chirla, I. V. Dinu, V. Moldoveanu and C. P. Moca. "Transport in a hybrid normal metal/topological superconductor Kondo model." *Phys. Rev. B* **90**, 195108 (2014).

[139] M. Cheng, M. Becker, B. Bauer and R. M. Lutchyn. "Interplay between Kondo and Majorana interactions in quantum dots." *Phys. Rev. X* **4**, 031051 (2014).

[140] D. A. Ruiz-Tijerina, E. Vernek, L. G. G. V. Dias da Silva and J. C. Egues. "Interaction effects on a Majorana zero mode leaking into a quantum dot." *Phys. Rev. B* **91**, 115435 (2015).

[141] P. Coleman, L. B. Ioffe and A. M. Tsvelik. "Simple formulation of the two-channel Kondo model." *Phys. Rev. B* **52**, 6611 (1995).

[142] V. J. Emery and S. Kivelson. "Mapping of the two-channel Kondo problem to a resonant-level model." *Phys. Rev. B* **46**, 10812 (1992).

[143] Z.-Q. Bao and F. Zhang. "Topological Majorana two-channel Kondo effect." *Phys. Rev. Lett.* **119**, 187701 (2017).

[144] D. Sticlet, C. Bena and P. Simon. "Spin and Majorana polarization in topological superconducting wires." *Phys. Rev. Lett.* **108**, 096802 (2012).

[145] H. Haug and A. P. Jauho. *Quantum Kinetics in Transport and Optics of Semiconductors*. Springer-Verlag Berlin Heidelberg (1996).

[146] F. Domínguez, J. Cayao, P. San-Jose, R. Aguado, A. L. Yeyati and E. Prada. "Zero-energy pinning from interactions in Majorana nanowires." *npj Quantum Mater.* **2**, 13 (2017).

[147] S. D. Escribano, A. Levy Yeyati and E. Prada. "Interaction-induced zero-energy pinning and quantum dot formation in Majorana nanowires." *Beilstein J. Nanotechnol.* **9**, 2171 (2017).

[148] M. Büttiker. "Zero-current persistent potential drop across small-capacitance Josephson junctions." *Phys. Rev. B* **36**, 3548 (1987).

[149] U. Geigenmüller and G. Schön. "Single electron effects and Bloch oscillations in normal and superconducting tunnel junctions." *Physica B Cond. Matt.* **152**, 186 (1988).

[150] K. Mullen, E. Ben-Jacob and Z. Schuss. "Combined effect of Zener and quasiparticle transitions on the dynamics of mesoscopic Josephson junctions." *Phys. Rev. Lett.* **60**, 1097 (1988).

[151] T. A. Fulton, P. L. Gammel, D. J. Bishop, L. N. Dunkleberger and G. J. Dolan. "Observation of combined Josephson and charging effects in small tunnel junction circuits." *Phys. Rev. Lett.* **63**, 1307 (1989).

[152] H. Vora, R. L. Kautz, S. W. Nam and J. Aumentado. "Modeling Bloch oscillations in nanoscale Josephson junctions." *Phys. Rev. B* **96**, 054505 (2017).

[153] J. Aumentado, M. W. Keller, J. M. Martinis and M. H. Devoret. "Nonequilibrium quasiparticles and 2e periodicity in single-Cooper-pair transistors." *Phys. Rev. Lett.* **92**, 066802 (2004).

[154] J. M. Martinis, M. Ansmann and J. Aumentado. "Energy decay in superconducting Josephson-junction qubits from nonequilibrium quasiparticle excitations." *Phys. Rev. Lett.* **103**, 097002 (2009).

[155] L. Sun, L. DiCarlo, M. D. Reed, G. Catelani, L. S. Bishop, D. I. Schuster, B. R. Johnson, G. A. Yang, L. Frunzio, L. Glazman, M. H. Devoret and R. J. Schoelkopf. "Measurements of quasiparticle tunneling dynamics in a band-gap-engineered transmon qubit." *Phys. Rev. Lett.* **108**, 230509 (2012).

[156] F. Guinea and G. Schön. "Coherent charge oscillations in tunnel junctions." *EPL (Europhys. Lett.)* **1**, 585 (1986).

[157] F. Marsili, M. J. Stevens, A. Kozorezov, V. B. Verma, C. Lambert, J. A. Stern, R. D. Horansky, S. Dyer, S. Duff, D. P. Pappas, A. E. Lita, M. D. Shaw, R. P. Mirin and S. W. Nam. "Hotspot relaxation dynamics in a current-carrying superconductor." *Phys. Rev. B* **93**, 094518 (2016).

[158] B. Zeng, X. Chen, D.-L. Zhou and X.-G. Wen. *Quantum Information Meets Quantum Matter*. Springer-Verlag New York (2019).

[159] E. Cobanera and G. Ortiz. "Fock parafermions and self-dual representations of the braid group." *Phys. Rev. A* **89**, 012328 (2014).

[160] A. Calzona, T. Meng, M. Sassetti and T. L. Schmidt. "$\mathbb{Z}_4$ parafermions in one-dimensional fermionic lattices." *Phys. Rev. B* **98**, 201110 (2018).